Morphologic analysis of the apicoplast formation in Plasmodium falciparum

Linzke, Marleen

DOI:
10.33612/diss.107482905

Morphologic Analysis of the Apicoplast Formation in *Plasmodium falciparum*

Marleen Linzke

rijksuniversiteit groningen

Universidade de São Paulo

Morphologic Analysis of the Apicoplast Formation in *Plasmodium falciparum*
Marleen Linzke

PhD Thesis
University of Groningen, The Netherlands
University of São Paulo, Brazil
December 2019

The research described in this thesis was carried out at the Unit for Drug Discovery, Department of Parasitology, Institute of Biomedical Sciences at the University of São Paulo, Brazil and at the Structural Biology Unit, Department of Drug Design, Groningen Research Institute of Pharmacy at the University of Groningen, The Netherlands and was financially supported by an Ubbo Emmius and a FAPESP (project number 2014/23330-9) fellowship, further by the CAPES/Nuffic MALAR-ASP network and Marie Sklodowska-Curie grant Agreement No. 675555, Acelerated Early stage drug discovery (AEGIS).

Printing of this thesis was financially supported by the University Library and the Graduate School of Science, Faculty of Science and Engineering, University of Groningen, The Netherlands.

Printing: Ridderprint BV

ISBN: 978-94-034-2164-3 (Printed version)
ISBN: 978-94-034-2163-6 (Electronic version)

Layout: Marleen Linzke
Cover design: Marleen Linzke. The image was taken from Pixabay (https://www.pixabay.com).

university of groningen

Morphologic Analysis of the Apicoplast Formation in *Plasmodium falciparum*

Phd thesis

to obtain the degree of PhD of the
University of Groningen
on the authority of the
Rector Magnificus Prof. C. Wijmenga
and in accordance with
the decision by the College of Deans

and

to obtain the degree of PhD of the
University of São Paulo
on the authority of the
Rector Prof. Dr. V. Agopyan
and in the accordance with
the decision by the College of Deans

Double PhD degree

This thesis will be defended in public on

Friday 20 December 2019 at 09.00 hours

by

Marleen Linzke

born on 17 January 1991
in Grevesmühlen, Germany

Supervisors

Prof. A.S.S. Dömling
Prof. C. Wrenger

Co-supervisor

Prof. M.R. Groves

Assessment Committee

Prof. M. Schmidt
Prof. W.J. Quax
Prof. G. Wunderlich
Prof. P.H. Elsinga

Paranymph(s)

Rick Oerlemans, MSc
Wiebke Queißer, MSc

This thesis is dedicated to my mother which always believed in me even when I was not believeing in myself anymore. For all the support and love which made me the person I am today.

Diese Arbeit is meiner Mutter gewidmet, dafür, dass du immer an mich geglaubt hast, auch wenn ich das selbst nicht mehr konnte. Für all deine Unterstützung und deine Liebe, die mich zur der Person gemacht haben, die ich heute bin.

CONTENTS

Abstract (Dutch)

LINZKE, M. **Morfologische analyse van de Apicoplast-vorming in *Plasmodium falciparum*** 2019. 109p. Promovendus (Parasitologie) -Instituut van biomedische wetenschappen, Universiteit van São Paulo en Universiteit van Groningen, São Paulo, 2019.

Malaria, veroorzaakt door *Plasmodium spp.*, is jaarlijks met meer dan 400.000 sterfgevallen een van de dodelijkste ziektes wereldwijd. De toename van resistentie tegen huidige medicijnen vormt een grote bedreiging voor de bestrijding en uitroeiing van de ziekte, waardoor nieuwe doelwitten voor geneesmiddelen hard nodig zijn. De apicoplast, een chloroplast-achtig organel van de *Plasmodium* parasiet, is aangetoond essentieel te zijn voor overleving van de parasiet, wat het een interessant te onderzoeken doelwit maakt. Hoe de parasiet dit essentiële organel deelt tijdens de aseksuele replicatie is tot nu toe een open vraag geweest. De voorouders van de apicoplast, namelijk de chloropast en bacteriën, realiseren hun distributie met behulp van eiwitten uit de Min-familie, welke nog niet zijn geïdentificeerd in *Plasmodium spp*. Door intensief BLAST-onderzoek werd een mogelijk ortholoog van een lid van de Min-familie, MinD, geïdentificeerd voor *P. falciparum*. Het ortholoog vertoont de karakteristieke domeinen voor de functie van ATPase die is beschreven voor MinD, en het wordt voorspeld, dat deze gericht is op de apicoplast van de parasiet. Analyse van het recombinante eiwit toont het vermogen aan om het substraat ATP te binden, gevolgd door polymerisatie. Deze effecten zijn afhankelijk en worden versterkt door toevoeging van tweewaardige metalen. Lokalisatiestudies in *P. falciparum* toonden de apicoplast als doelwit aan. Bovendien vertoonde overexpressie van het ortholoog in transgene parasietlijnen een remmend effect op de proliferatie van de parasiet. Met behulp van een referentielijn voor de visualisatie van de apicoplast, zijn technieken voor het visualiseren en analyseren van de apicoplast, door middel van levende cel fluorescentie beeldopnames tijdens het erytrocytische stadium, vastgesteld en geverifieerd voor de analyse van de apicoplast morfologie onder invloed van het mogelijke MinD ortholoog.

Tefwoorden: *Plasmodium falciparum*, apicoplast, live cell imaging, geneesmiddeldoen validatie.

Abstract (English)

LINZKE, M. **Morphologic Analysis of the Apicoplast Formation in *Plasmodium falciparum*** 2019. 109p. Ph.D. (Parasitology) -Institute of Biomedical Sciences, University of São Paulo and University of Groningen, São Paulo, 2019.

Malaria, caused by *Plasmodium spp*., remains with more than 400.000 deaths per year one of the most severe diseases worldwide. Increasing drug resistance against the available antimalarial drugs poses a great threat in combating and eradication of this disease and new drug targets are greatly needed. The apicoplast, a chloroplast-like organelle of the *Plasmodium* parasite has been shown to be essential for the parasite survival and offers a new drug target to exploit. How the parasite distributes this essential organelle during the asexual replication has been an open question up to this point. The ancestor of the apicoplast, namely the chloroplast and bacteria accomplish their distribution by the aid of proteins from the Min family that has not been identified in *Plasmodium spp.* yet. Through intensive BLAST research, one possible orthologue of one member of the Min family, MinD, was identified for *P. falciparum*. The orthologue displays the characteristic domains for the function of an ATPase described for MinD and is predicted to be targeted to the apicoplast of the parasite. Analysis of the recombinant protein demonstrated its ability to bind to the substrate ATP and to polymerise upon addition of the substrate. This effect is dependent and enhanced by addition of divalent metals. Localisation studies in *P. falciparum* demonstrated the targeting to the apicoplast. Furthermore, overexpression of the orthologue in transgenic parasite lines displayed an inhibitory effect on the proliferation of the parasite. With the help of a reference line for visualisation of the apicoplast, techniques to visualise and analyse the apicoplast by live cell fluorescence imaging during the erythrocytic stage have been established and verified for the analysis of the apicoplast morphology under influence of the possible MinD orthologue.

Keywords: *Plasmodium falciparum*, apicoplast, live cell imaging, Drug target validation.

Resumo

LINZKE, M. **Análise morfológica da formação de apicoplasto em *Plasmodium falciparum*** 2019. 109f. Tese (Doutorado em Parasitologia) - Instituto de Ciências Biomédicas, Universidade de São Paulo e Universidade de Groningen, São Paulo, 2019.

A malária, causada por *Plasmodium spp*., permanece como uma das doenças infecciosas mais importantes do mundo, sendo responsável por mais de 400,000 mortes por ano. O aumento da resistência aos medicamentos antimaláricos disponíveis representa uma grande ameaça ao combate e a erradicação desta doença e a descoberta de novos alvos são necessários. O apicoplasto dos parasitas *Plasmodium*, uma organela semelhante ao cloroplasto, demonstrou ser essencial para a sobrevivência do parasita e oferece um novo alvo a ser explorado. Como o parasita distribui essa organela essencial durante a replicação assexuada tem sido uma questão em aberto até o momento. Ancestrais do apicoplasto, como cloroplasto e bactérias, realizam sua distribuição com o auxílio de proteínas da família Min que ainda não foram identificadas em *Plasmodium spp*. Através de intensa pesquisa BLAST, um possível ortólogo de um membro da família Min, MinD, foi identificado em *P. falciparum*. O ortólogo exibe os domínios característicos da função de ATPase descrita para MinD e prevê-se que seja direcionada ao apicoplasto do parasita. A análise da proteína recombinante demonstrou sua capacidade de se ligar ao substrato ATP e polimerizar após adição do substrato. Este efeito é dependente e aprimorado pela adição de metais divalentes. Estudos de localização em *P. falciparum* demonstraram o direcionamento para o apicoplasto. Além disso, a superexpressão do ortólogo nas linhagens de parasitas transgênicos causou um efeito inibitório na proliferação do parasita. Com a ajuda de uma linhagem de referência para visualização do apicoplasto, técnicas de visualização e análise do apicoplasto por imagem de fluorescência de células vivas durante o estágio eritrocítico foram estabelecidas e verificadas, possibilitando a análise da morfologia do apicoplasto sob influência do possível ortólogo de MinD.

Palavras-chave: *Plasmodium falciparum*, apicoplasto, imagens de células vivas, alvo terapêutico.

INTRODUCTION

1.1. A burden for humanity – the disease malaria

No other parasitic disease had such a powerful impact on humanity then malaria. It is a burden on human health, society and economics and has shaped our evolution for a long time. First references of what supposedly describes the disease malaria date back to ancient China in about 2700 BC, Mesopotamia in 2000 BC and Egypt in 1570 BC. More clear reports emerged from the early Greeks, including Homer in about 850 BC and Hippocrates in about 400 BC, describing the poor health, periodic fevers and enlarged spleens of inhabitants of marshy area, a common characteristic of malaria (1).

The word malaria originates from the Italian word for bad or spoiled air, mal´aria, and represents the belief that the malaria fevers were caused by miasmas rising from swamps, which persisted for over 2500 years. Just in the year 1880 with the discovery of its causative agent, the research to demystify malaria and to understand its complex pathogenesis and biology began.

Malaria is a mosquito-borne infectious disease caused by the protozoan parasite *Plasmodium spp*. It is most common in tropical and subtropical areas (Figure 1). In the year 2017, about 219 million cases of malaria occurred leading to around 435 thousand deaths worldwide. More than 90% of the deaths related to malaria occurred in Sub-Saharan Africa and mostly affects children under the age of five (2). Six species of *Plasmodium* are responsible for malaria in human, *P. falciparum*, *P. malariae*, *P. ovale*, *P. vivax*, *P. knowlesi* and the newly reported *P. cynomolgi* (3). The species *P. vivax* and *P. falciparum* are the most widespread and responsible for most malaria cases worldwide. The most severe species is *P. falciparum* which is responsible for most deaths by malaria and can lead to severe malaria in human. However, new evidence suggests a bigger impact of *vivax* malaria which can also lead to severe malaria and seems to have a higher indirect mortality rate than previously thought (4,5).

The World Health Organization (WHO) already implemented twice a plan for eradication of malaria by use of antimalarial drugs and vector control. The first plan in the year 1955 succeeded in eliminating malaria in Europe, North America, the Caribbean and parts of Asia and South-Central America but failed in Africa which has over 80% of today´s malaria burden (6). In 2007, the eradication of malaria came back on the agenda of the WHO (7). From the years 2000-2017 the global malaria burden has been drastically reduced.

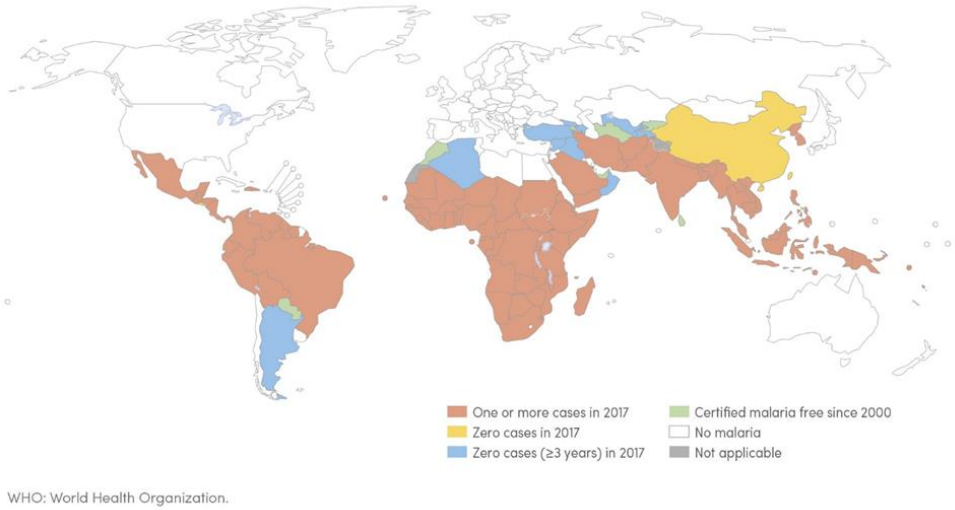

Figure 1: Global Distribution of malaria. The worldwide case distribution between the year 2000 until 2017 is shown. Red indicates the region which are endemic for malaria up to the year 2017 while yellow and blue shows region with no malaria cases in the year 2017. Green regions belonged once to the endemic area for malaria but were declared malaria free in the year 2000. In the white regions malaria is not endemic. Changed from (2).

However, in the recent years the number of malaria cases remained at a constant level due to increasing resistance against antimalarial drugs and insecticides. Past attempts to eradicate malaria taught us that this recent decrease might not last and malaria can easily emerge more devastating than before. Understanding the parasite biology and its interaction between its two host is from utmost importance to combat this disease and to reach the goal of eradication of bmalaria.

1.1.1. The complex life cycle of *Plasmodium*

The life cycle of *Plasmodium spp.* is a complex one alternating between two different forms of replication in two different host. While the life cycle shows differences depending on the species studied, their common ground is that sexual replication takes place in the mosquito host, a female *Anopheles* mosquito, while the asexual replication occurs in the vertebrate host. This description of the life cycle will focus on *P. falciparum* but will show important differences to the other human malaria parasites (Figure 2).

The life cycle starts with the bite of an infected female *Anopheles* mosquito. The *Plasmodium* sporozoites, located inside the salivary glands of the mosquito, are injected into the human dermis during the blood meal of the mosquito (8,9). The sporozoites rapidly leave the infection site by a gliding motility and enter the bloodstream of the host. There, they quickly access the liver by a process called cell traversal which includes crossing the sinusoidal barrier (10,11). Upon infection of hepatocytes in the liver, the sporozoite transforms into the liver stage form over the course of the following 2-10 days. There, they go through a multiplication process termed schizogony, producing up to 40.000 merozoites per infected hepatocyte which are released into the bloodstream by budding of parasite-filled vesicles, the merosomes (12). While *P. falciparum* directly enters schizogony in the liver, *P. vivax* is able to form a long-lived dormant stage in the liver called hypnozoite. This stage can survive in the liver for years and leads to the recurring infections characteristic for *vivax* malaria (13).

The free merozoites quickly interact, invade and establish the invasion of the red blood cells (RBCs) within two minutes of being released from the merosome (14). The initial contact between merozoites and erythrocytes is crucial, as the parasite must distinguish between erythrocytes compatible for invasion and other cell types. The merozoite attaches to the erythrocytes, repositioning itself with the apical end facing the erythrocytes and entering the cell by an actin-myosin motor driven process (15). As the parasite enters the red blood cells, it engulfs itself in the cell membrane of the erythrocytes and forms the parasitophorous vacuole that separates the parasite from the cytosol of the host cell and establishes a favourable environment for the parasite to grow in. The invasion process is followed by echinocytosis which causes the erythrocyte to shrink and form spiky protrusions (16). Which type of red blood cell is invaded differs for *P. falciparum* and *P. vivax*. While the first can invade a large percentage of RBCs, *P. vivax* is limited almost excusively to Duffy blood group positive red blood cells and reticulocytes (17,18).

After erythrocyte invasion, the parasite undergoes schizogony which results in the development of 16-32 merozoites. Inside the erythrocyte, the merozoites grows into the ring stage followed by the trophozoite and schizont stage which are called the erythrocytic stages. The schizont undergoes repeated cycles of asexual replication to form new

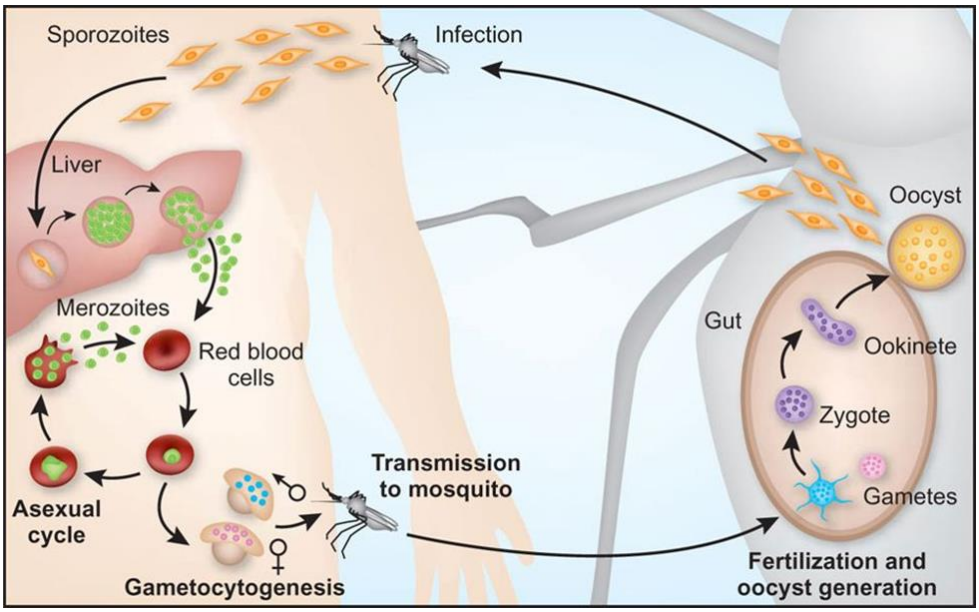

Figure 2: Life cycle of *Plasmodium falciparum*. Malaria is transmitted by the bite of an infected female *Anopheles* mosquito, which injects the sporozoites into the skin of persons. From there, the sporozoites migrate into the liver where they undergo one cycle of asexual replication called schizogony. The produced merozoites are released into the blood stream where they invade the red blood cells. During this stage, the parasite undergoes repeated step of schizogony. At some point inside the asexual stage, the merozoites mature into gametocytes which can be taken up into the mosquito during a blood meal. Inside the mosquito gut, the gametocytes merge into the zygote which further develops into the ookinete, which penetrates the mid-gut wall and develops into the oocyst. The oocyst undergoes sporogony to produce sporozoites, which then migrate into the salivary glands of the mosquito where their further development is stalled until transmission to a new host.

merozoites. When the replication is completed, the merozoites egress from the parasitophorous vacuole and erythrocyte and this leads to the release of non-motile merozoites into the bloodstream where they can infect new erythrocytes. The erythrocytic cycle corresponds with the periodic fever characteristic for malaria and its duration depends on the species. *P. falciparum* and *P. vivax* undergo the cycle in 48 hours' while *P. malariae* needs 72 hours to complete the erythrocytic cycle.

During schizogony, some parasites undergo a developmental switch to commit to sexual development to form male microgametocytes and female macrogametocytes (gametocytosis). The molecular events leading to the developmental switch are not fully understood yet, but the depletion of lyso-phosphatidyl serine is associated with increased

development of gametocytes which indicates that the parasite can sense its environment (19,20). The development of mature gametocytes lasts 11 days where they remain sequestered inside the bone marrow to avoid splenic clearance (21). Upon maturation, the gametocytes emerge in the peripheral blood circulation to be taken up by a mosquito during its next blood meal. Here, the strategies of *P. falciparum* and *P. vivax* are different. While *P. falciparum* shifts towards sexual development normally after several asexual erythrocytic cycles and the manifestation of clinical symptoms, *P. vivax* develops gametocytes shortly after the release of merozoites from the liver and thus, can be transmitted before the clinical symptoms of malaria manifest (16).

The sexual replication is completed in the midgut of the mosquito vector (sporogonic cyle). The gametocytes taken up by the blood meal merge and form the zygote. The zygote develops into the motile form, the ookinete, which penetrates the midgut wall of the mosquito where it develops into the oocyst. This form undergoes a cycle of sporogony to produce sporozoites. Upon maturation, the oocysts lyse to release the sporozoites which then migrate to the salivary glands of the mosquito. There, the sporozoites are waiting to be injected into the next human host during a blood meal of the mosquito and thus, starting the cycle again.

1.1.2. What makes malaria so deadly?

Malaria is endemic in tropical and subtropical areas of the world, limited by the environmental conditions on the mosquito vector, in general the temperature to fulfil the sexual life cycle of the parasite (22). In these endemic areas, the transmission rate of malaria can be categorised as stable and unstable transmission and vary from many hundred to less than one infectious bite per year. Depending on the transmission rate, previous exposure and acquired immunity, the symptoms and clinical outcome of malaria can vary considerably.

Infection of a naïve subject almost always leads to a febrile illness with flu-like symptoms. The additional symptoms vary between the individuals and can include rigors, headache, nausea and muscle pain. If not treated at this point, uncomplicated malaria can develop into severe malaria which may ultimately lead to death. In high transmission areas like Africa,

severe malaria mostly occurs in children and displays three dominating symptoms, respiratory distress, severe anaemia and cerebral malaria which can either occur separately or in combination (23,24). Severe malaria in older subjects is rare and the intensity of the febrile episodes of uncomplicated malaria decline with age because the subject can develop a certain degree of immunity through the reoccurring infections with the parasite (25).

In unstable transmission areas including Asia and Latin America, severe malaria can develop in all ages. However, the symptoms differ for what we observe in young children in Africa. Although cerebral malaria is also existing, severe malaria presents itself as a multi-system disorder with renal and hepatic dysfunction (26).

The biological features that lead to the symptoms and the mortality of malaria are multifactorial. Exponential growth of the parasite, destruction of infected and also uninfected RBCs, initiation of the host inflammatory response and microvascular obstruction play important roles (27). The last one is the central factor for severe malaria and is established through sequestration of the parasite to receptors on endothelial cells in deep venules. During maturation of the parasite inside the erythrocyte, it remodels the host cell to bind to endothelial cells. Through sequestration, the parasite removes itself from the blood circulation and avoids clearance through the spleen. The most intensively studied surface protein is *P. falciparum* erythrocyte membrane protein 1 (*Pf*EMP1) which allows the parasite to bind to a variety of receptors (28–30). *Pf*EMP1 is encoded by the *var* gene family which is also responsible for the clonal antigenic variation of the parasite (31–33). The parasite expresses and presents a single *var* gene out of a repertoire of 60 possibilities in its genome. Each variant can bind another type of receptor. Also, the parasite can avoid the immune system of the host by changing the transcription of the *var* genes (34,35). It is believed that protective immunity in stable transmission regions is acquired to repeated infection of *P. falciparum* strains presenting different variants of *var* genes. Thus, the individual acquires a repertoire of antibodies against different strains, decreasing cytoadherence and sequestration.

The parasite can sequestrate in any organ, however, sequestration inside the brain or placenta of pregnant woman leads to the most severe forms of malaria. Cerebral malaria is defined as the presence of a coma caused by *falciparum* malaria which however, can also be achieved through sequestration in other organs and their side effects (36,37). Malaria in

pregnancy can lead to stillbirth and miscarriage, as well as low birth weight and anaemia in the mother. Placental malaria can also affect primigravid with already acquired immunity against blood stage malaria, most likely because the placenta presents a new site for sequestration for the parasite. However, protective immunity is developed quickly with better outcomes and protection for following pregnancies (38,39).

1.1.3. How to combat malaria

The World Health Organization issued recommendations for prevention, diagnosis and treatment of malaria. The main objectives to combat malaria are vector control by targeting the *Anopheles* vector and effective case management of malaria-infected patients. Prevention is mostly focused on vector control and prophylaxis with certain antimalarial drugs. Intensive investments into control of the *Anopheles* vector led to eradication of malaria in wide parts of the world (40). Focus is thereby the prevention of the contact between mosquito and men by either mechanical barriers or insect repellent. Application of insecticides is the primary tool of vector control programs worldwide (41). Indoor residual spray (IRS) and insecticide-treated mosquito nets (ITNs) are widely used and have proven to reduce vector density and contact to men (42). The discovery of dichlorodiphenyltrichlorethane (DDT) as the first synthetic organic insecticide lead to great success in vector control (43). However, DTT has toxic environmental effects and its use was banned in several countries. The decision to recommend DTT in malaria endemic countries under restriction is controversial, but relatable due to no safer and cheaper alternatives (44).

Recent development of resistance of the mosquito vectors against most common insecticides complicates the efforts made in vector control and pushes the field towards new approaches and techniques. In addition, vector control may have reached its limits in eradication of malaria.

Effective case management implies the fast and correct diagnosis of malaria and the responsible *Plasmodium* parasite and the correct and effective treatment of the disease. Antimalarial drugs have been reported to be responsible for a 40% reduction of global

malaria cases and deaths. However, they are not sufficient to control and reduce malaria completely until 2020 like planned by the WHO (2).

Most antimalarial drugs target the asexual stages of the parasite and focus on the two metabolic pathways of haemoglobin degradation and nucleic acid synthesis (45). They can be categorised by their chemical composition into amino alcohols (quinine, mefloquine), 4-aminoquinolines (chloroquine), 8-aminoquinolines (primaquine), naphtoquinone (atovaquone), antifolates (sulfadoxine, proguanil), endoperoxides (artemisinin and its derivates) and antibiotics (tetracycline, doxycycline).

Quinine is the first antimalarial drug which was approved for prophylaxis. First used as powder made from bark of the cinchona tree in the 1630s and then as direct isolate in 1820, it was widely administered against malaria (46,47). The drug targets the haem polymerisation and disposal within the digestive vacuole, but it was also associated with inhibition of other processes (48,49). When demand of the quinine rose during World War I and II, the production of quinine was not sufficient. Thus, two synthetic analogues, namely chloroquine and mefloquine, have been developed as alternatives for quinine (46).

In comparison to quinine, chloroquine was an effective drug which displays low risk of side effects and was fast and cheap to produce. It rapidly became the preferred treatment and chemoprophylaxis against uncomplicated *falciparum* and *vivax* malaria. It also targets the haemoglobin digestions by accumulating inside the digestive vacuole of the parasite where it binds and forms complex with the free haem and hinders the formation of non-toxic hemozoin (50,51). The chloroquine-haem complexes have been shown to be more toxic for the parasite than free haem (51). However, if the interference of the haem polymerisation is the main target for chloroquine has been up to debate.

Resistance to chloroquine has developed after 20 years of successful administration against *P. falciparum* and *P. vivax* in South-East Asia and South America followed by resistance reported in Africa as well (50–52). Mutations in multiple genes such as *Pfcrt* (chloroquine resistance transporter gene), *Pfmdr1* (multidrug resistance gene) and *Pfmrp* (multidrug resistance-associated protein) have been reported to induce resistance in *P. falciparum* (50,51,53), while in *P. vivax* the *Pvmdr1* gene was associated with chloroquine resistance (54). The direct effects of the reported mutations are not completely understood yet, but they are thought to inhibit the transport and accumulation of chloroquine inside the digestive

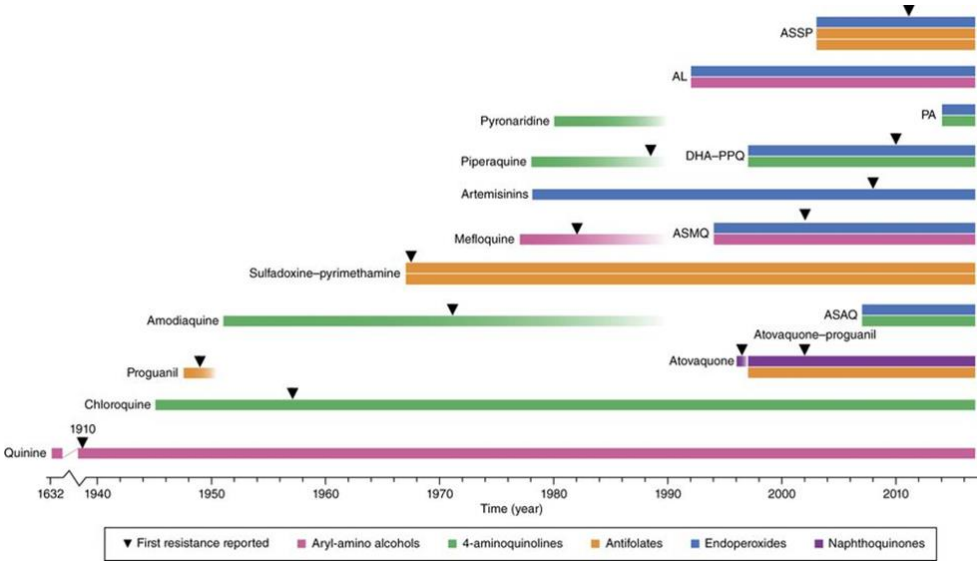

Figure 3: Available antimalarial drugs and their first reported resistance. Shown are the different antimalarial drugs currently on the market, their years of use for treatment of malaria and their first reported resistance.

vacuole (53). Mutations in the *Pfmdr1* gene are also responsible for resistance against other amino alcohol drugs like quinine, mefloquine and lumefantrine.

The current first-line treatment for *falciparum* malaria in all endemic countries is the artemisinin combination therapy (ACTs) (2). Artemisinin is a natural antimalarial drug extracted from the Chinese medicinal herb *Artemisia annua* and targets almost all the asexual and sexual stages of the parasite (50,53,55–57). Artemisinin and its derivates artesunate and artemether showed rapid clearance of parasitemia and can be used for treatment of uncomplicated and severe malaria (58). The ACT combines the fast acting artemisinin or one of its derivates which rapidly clears the parasitemia with a slow acting partner drug with different pharmacological properties like amino alcohols or 4-aminoquinoline compounds which clears the remaining parasites (59).

Unfortunately, partial artemisinin resistance was reported in the Greater Mekong Subregion in the year 2008 – 2009 which resulted in a slower clearance of parasitemia after artemisinin monotherapy or ACT (60,61). The target of artemisinin is the phosphatidylinositol-3-kinase (*Pf*PI3K) which handles the export form essential proteins from the endoplasmic reticulum of the parasite to the host erythrocytes at the early ring stage of the asexual cycle through proteolysis of *Pf*PI3K through the Kelch13 protein (62,63). The term partial resistance

implies that the ring stage of the parasite shows increased artemisinin resistance and thus, the clearance of the parasite is delayed. Mutations of the Kelch13 protein are associated with the development of the partial resistance and several mutations have been identified (64–68). Luckily, there are no reports of full artemisinin resistance yet and partial resistance is limited to the Greater Mekong Subregion (2).

Growing resistance against antimalarial drugs is a great threat on our way to fight and eradicate this deadly disease. With the exception of Artemisinin, *P. falciparum* straines have developed partial or full resistance against all available antimalarial drugs and deployment of new drugs is not expected before 2020 (66) (Figure 3). No highly effective vaccines against malaria are available yet. The most advanced vaccine candidate RTS,S/AS01 is currently undergoing a large-scale pilot implementation in Malawi, Kenya and Ghana, but four repeated doses are needed to achieve a partial resistance and a malaria incidence reduction of 39% (69). Thus, new drug targets are currently needed. High-throughput screening of new compounds are underway to identify new drugs. But also, new possible drug targets are urgently needed which can be utilised in combination with the already available drugs on the market. To find these new possible targets, research has to step back from compound screening and take a deeper look to understand the biology of the parasite.

1.2. A relict from the past - the apicoplast

Plasmodium spp. belongs to the Phylum Apicomplexan which includes other important protozoan parasites like *Toxoplasma* or *Babesia* that pose a health burden for livestock and other animals. Members of this Phylum received their name from the apical complex which consists of three organelles (rhoptry, micronems and conoids) important for the invasion of the targeted host cell. Additionally, all members except for *Cryptosporidium* possess a relict plastid, the apicoplast.

First evidences for the apicoplast were found in the year 1975 where images of the malaria parasite *P. lophurae* showed a circular, extrachromosomal DNA molecule (70). Researchers first thought they found the mitochondrion of the parasite (70–72). However, this was challenged by the discovery of a circular DNA molecule of 6kb which encoded classical mitochondrial genes (73–76). Sequence analyses of the 35kb circular genome of *P.*

falciparum showed that the genome had prokaryotic ancestry but surprisingly from plastids of plants and algae (77–79). Complete sequencing of the circular genome confirmed its plastid origin with typical genes but missing the genes for photosynthesis (80). In-situ hybridisation analysis using electron microscopy in *Toxoplasma gondii* was able to localise the genome to a four-membrane organelle, the apicoplast (81).

1.2.1. What makes the apicoplast essential to the parasite?

The apicoplast is a non-photosynthetic organelle which possess four membranes marking it as a secondary endosymbiont (82). Debates about the origin of the apicoplast came to the conclusion that the apicoplast derived from red alga by finding the photosynthetic ancestor of the apicomplexan lineage, *Chromera velia,* which lives as a symbiont in corals (83). The 35 kb genome of the apicoplast has been highly reduced in size and encodes for less than 50 proteins mainly functioning for self-maintenance of the apicoplast in processes such as DNA replication, transcription and translation (80,84). Perturbation of these basic housekeeping processes by antibiotics which target the prokaryotic machinery of the apicoplast lead to the interesting phenome of the "delayed death" response (85). The parasite does not display an inhibitory effect upon destruction of the apicoplast but rather fails to establish infection in the following generation. So, researchers were baffled why the parasite kept a non-photosynthetic plastid and what it does to be essential to the parasite.

Typical for endosymbionts, most of the genes for apicoplast function are encoded in the nuclear genome and the corresponding proteins have to be transported to the apicoplast. Trafficking to the apicoplast is mediated by the bi-partite leader at the N-terminus of proteins (86,87). The leader sequence consists of two parts, a signal peptide which mediates transport into the endomembrane system of the endoplasmic reticulum (ER) and a transit peptide which controls the transport into the apicoplast. However, the path how the transported protein reaches the apicoplast from the ER is not completely solved yet. The transit peptide displays no conserved sequence or secondary structure but positive charges of the transit peptide have been shown to be important for successful transit in the apicoplast (88–90).

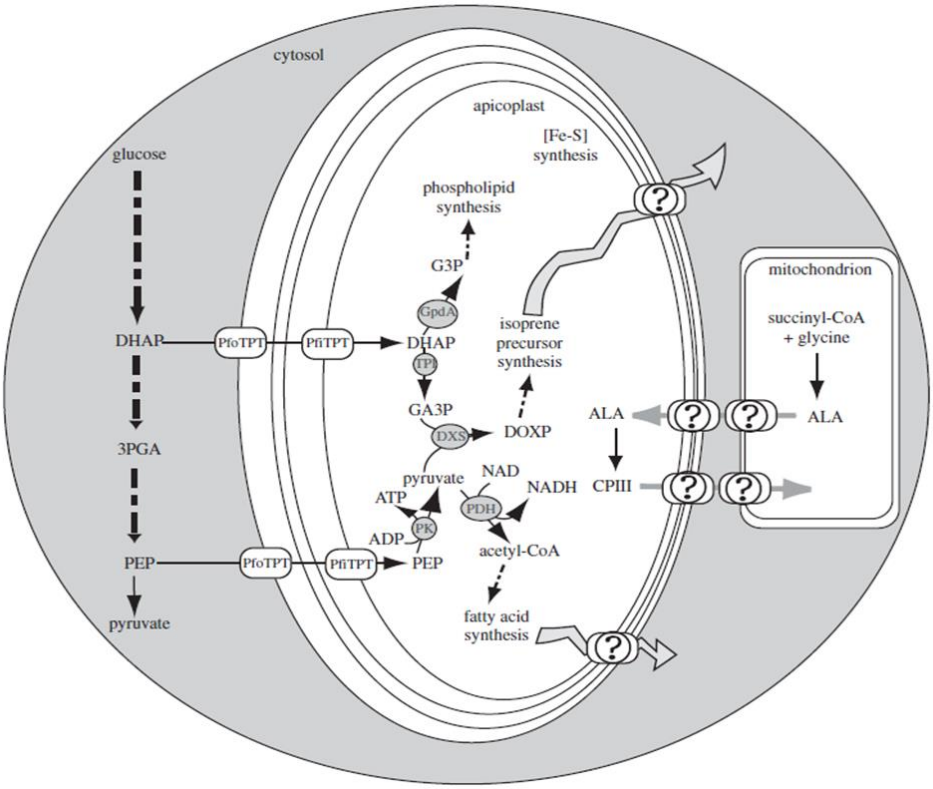

Figure 4: Metabolic map of the apicoplast in *Plasmodium*. Shown are the four pathways which are localised inside the apicoplast, namely the biosynthesis of fatty acid, isoprenoids, iron-sulphur cluster and haem. Only the biosynthesis of isoprenoids is essential in the blood stage while biosynthesis of fatty acid and haem are essential in other stages of the life cycle. The pathway for haem is shared between the cytosol, mitochondrion and apicoplast of *Plasmodium* (114).

Identification of the bi-partite leader sequence enabled the use of bioinformatics tools to predict proteins targeted to the apicoplast and get a better picture of its function (88,91). The putative pathways of the biosynthesis of fatty acid, isoprenoids, iron-sulphur cluster and haem could be linked to the apicoplast (92) (Figure 4). The exact mechanism or metabolites produced by these pathways are not fully understood yet but inhibition of the pathways lead to the death of the parasite. Although dispensable for some stages of the life cycle, these pathways are essential for the survival of the parasite.

The best characterised pathway in the apicoplast is the type II fatty acid synthesis (FASII) pathway. Gene deletions studies in murine *Plasmodium* parasites revealed that the pathway

is expressed during all stages of the life cycle but is essential only in late liver stage (93–97). Schizogony in the liver stage gives rise to up to 40000 merozoites per infected liver cell and the parasite is likely not able to scavenge the necessary amount of fatty acid from the host cell (93,94). Why the pathway is expressed in blood stage although not essential is not clear yet but it is supposed that it provides antioxidants against the oxidative stress produced by haemoglobin digestion (98).

Additionally, to the FASII pathway, the pathways for biosynthesis of iron-sulphur clusters (Fe-S) and haem were also shown to be dispensable for blood stage parasite. Biosynthesis of iron-sulphur clusters is believed to be for self-maintenance of the apicoplast by generation of reducing equivalents (92,99) while the cellular requirements of Fe-S clusters are met by the *de novo* Fe-S pathway of the mitochondrion. The pathway for haem synthesis is spanned over the cytosol, mitochondrion and apicoplast of the parasite and contains parts of prokaryotic and eukaryotic ancestors (92,100). The pathway has been shown to be essential for the development of oocysts but is not required for the blood stage (101–103). During the erythrocytic cycle, the parasite invades the red blood cells and scavenge the haem from digestion of the haemoglobin and hence, does not require an additional supply of haem. In fact, the parasite has developed a way to detoxify the excessive haem by polymerising it to non-toxic hemozoin crystals inside the food vacuole (104).

This just leaves the biosynthesis of the precursors of isoprenoids as the essential pathway of the apicoplast. Indeed, *Plasmodium* parasites without the apicoplast can survive and replicate when IPP, the end product of the isoprenoid biosynthesis, is added to the growth media (105). Similar to its prokaryotic ancestors, the apicoplast utilises the non-mevalonate/2-C-methyl-D erythritol 4-phosphate (MEP)/1-deoxy-D-xylulose-5-phosphate (DOXP) pathway for isoprenoid synthesis compared to the canonical mevalonate pathway in eukaryotes (92,106). The two pathways differ considerable and hence, the DOXP pathway is a prominent source for new drug targets. One example is Fosmidomycin, a herbicide and known inhibitor of the DOXP pathway, which was already tested in several clinical trials (107–110).

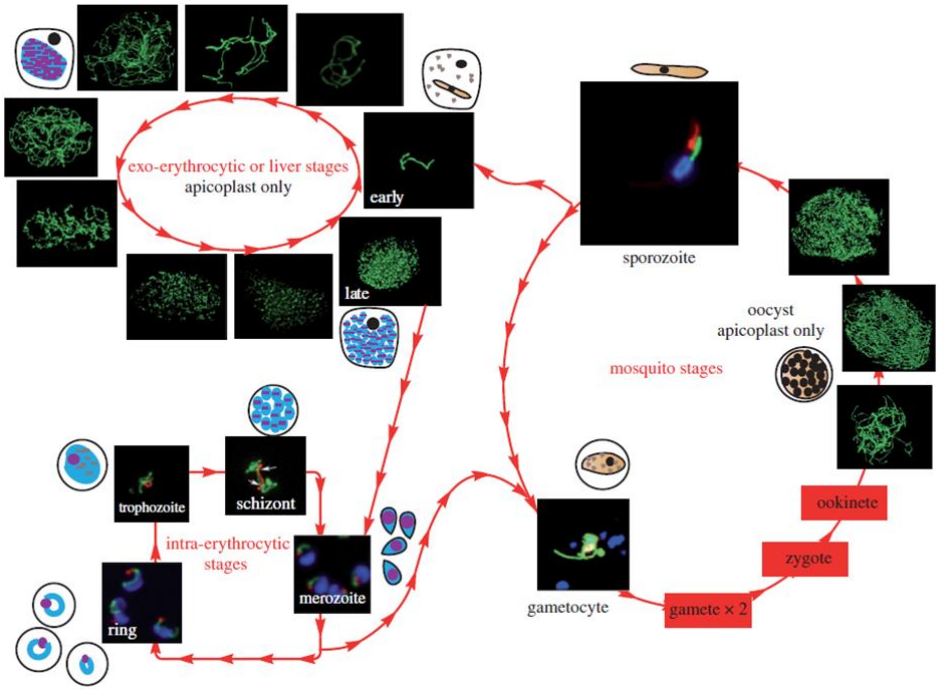

Figure 5: Visualisation of the apicoplast during the life cycle of *Plasmodium*. The morphology of the apicoplast is shown by fluorescence microscopy targeting fluorescent proteins to the apicoplast. In most stages the apicoplast appears as a small, round organelle. But in the erythrocytic stage, the organelle undergoes a dramatic morphological change. At ring stage, the apicoplast still appears at small round structure which quickly starts to expand and branch extensively all while keeping close contact with the mitochondrion (114).

1.2.2. The apicoplast during the life cycle of *Plasmodium*

Since the apicoplast cannot be formed *de novo*, the parasite has to properly divide and distribute the organelle during schizogony to the newly formed daughter cells. Advances in fluorescence microscopy and gene manipulation enabled the visualisation of the apicoplast during all stages of the life cycle of *Plasmodium* (111–114) (Figure 5).

Throughout the various stages of the life cycle, the apicoplast is always in close proximity to the mitochondrion and shares at least one contact point with the other organelle (112,113). This might be due to metabolite dependency between the two organelles, given that they share the haem pathway between each other (92,113). The apicoplast appears as a small round organelle. During gametocytosis, the apicoplast does not change or grow in

shape. Also, only the female gametocyte carries the apicoplast and mitochondrion which is consistent with the maternal inheritance of the organelles (111,112,115,116). During the erythrocytic stage, the apicoplast passes through a remarkable change in morphology. Starting from a relatively round organelle, the apicoplast quickly starts to elongate and branch extensively into a complex structure which then gets divided into the daughter cells, leaving each newly formed merozoite with a small round apicoplast. The parasite first undergoes repeated steps of nucleus division followed by the division of the apicoplast and lastly the mitochondrion (113). However, how exactly the apicoplast is divided onto the next generation is unknown. Its ancestor, chloroplast of higher plants and bacteria have developed a complex system to successfully divide into equal daughter cells or organelles. If the parasite has inherited these mechanisms of its ancestors or if it has developed new mechanisms to ensure a successful division is still an open question in malaria research.

1.3. A look in the past – the ancestral Min system for cell and plastid division

Bacteria and chloroplast divide by binary fission to produce two equally sized daughter cells or organelles. Intensive studies in *Escherichia coli* have identified the molecular mechanism behind the binary fission and thus, research was able to create a detailed picture of what is happening during the division (reviewed in (117)).

In *E. coli*, division is realised by the multi-protein machinery called divisome which has as the main component the FtsZ (Filamenting temperature-sensitive mutant Z) protein (118,119). FtsZ is a conserved tubulin homologue, which shows no sequence conservation but high structural similarity to tubulin of eukaryotes. FtsZ is the first protein to arrive at the future division site and recruits additional proteins to form the divisome and perform the divison. FtsZ is a GTPase which can bind to GTP in its monomeric form. Upon interaction with GTP, FtsZ starts to dimerise and the active site of the GTPase function is formed the junction of two FtsZ monomers (120). In the GTP-bound state, the protein starts to form linear protofilaments which ultimately build the Z-ring, a contractile ring which is the driving force of the fission. The Z-ring does not consist of one very long protofilament but rather clusters of short and overlapping protofilaments which align horizontal to the

long axis of the cell (121). These clusters of short protofilaments are then further stabilised by additional proteins, namely ZapA, ZapB, ZapC, ZapD, FtsA and ZipA which are recruited during the assembly of the protofilaments of FtsZ. While ZapA, ZapC and ZapD can directly bind to FtsZ, crosslinking the protofilaments and inhibiting the GTPase activity (122–127), ZapB interacts and crosslinks ZapA but not directly FtsZ (128). FtsA and ZipA are responsible for anchoring the Z-ring to the cytoplasmic membrane by forming a functional cytokinetic ring (129,130). FtsA has also been shown to modulate and change the phospholipids at the division site upon interaction with ATP which leads to the contraction of the membrane (131). When division starts, the protofilaments condense and with the help of this additional proteins form a tight structure called the divisome (132,133). The divisome then interacts with the Prostagladin (PG) synthases and binds directly to the chromosomes to fulfil the division of the cell to produce two equally sized daughter cells (134,135).

But how does the bacteria cell define its mid cell point during division? Two systems have been proposed which restricts the formation of the divisome towards the mid cell point, the nucleoid occlusion (NO) system where nucleoid-associated SlmA inhibits the Z-ring construction over the chromosomes (136) and the Min system.

The Min system was discovered through a mutation of its gene locus *minB* which resulted in the formation of miniature, anucleate cells (137,138). These minicells gave the gene locus its name, Min. Three proteins are encoded by the *minB* locus, namely MinC, MinD and MinE and their interactions restrict the division site to the midpoint of the cell (139) (Figure 6). MinC is the effector protein of the system which directly interacts and inhibit the assembly of the FtsZ protofilament and thus, destroying the Z-ring at unwanted position within the cell. However, MinD and MinE are the driving forces which decide the exact position of the divisome by their specific oscillatory behaviour. MinD is a Walker A ATPase which undergoes a conformational change upon binding to ATP from a monomeric form into a dimer (140,141). In the ATP-bound form, the C-terminus will be exposed which contains membrane-targeting sequence (MTS) which directs the dimer towards the inner cell membrane. The MTS of MinD was shown to have weak affinity to the membrane and has to be present in two or more copies to enable the binding to the membrane (142,143).

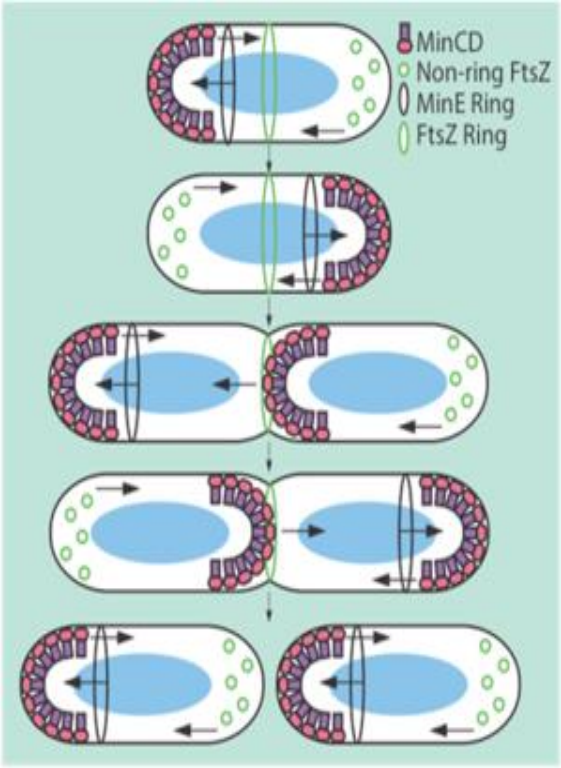

Figure 6: The Min system in *E. coli*. Correct placement of the divisome is regulated by the Min family consisting of MinC, MinD and MinE. MinD and MinC form a complex upon binding of MinD with ATP and association to the inner cell membrane. There, the complex moves from the cell pole to the midpoint of the cell, inhibiting possible Z-ring formation by interaction of MinC with the protofilaments of FtsZ. At the midpoint, the complex comes in contact with MinE which competes for binding to MinD, enhances its ATPase activity and thus, the disassociation from the membrane. While doing so, MinE can jump from one complex to another until it reaches the starting cell pole. The MinCD complex can form again at the other cell pole where the process starts anew. The oscillation between MinD and MinE restricts the formation of the Z-ring to the midpoint of the cell.

The MinD dimer then recruits MinC to the cell membrane, building a complex which spreads on the membrane towards the midpoint of the cells and inhibiting possible Z-rings on its way. Upon reaching the midpoint of the cell, the MinCD complex comes in contact with MinE which destroys the complex by interacting with MinD. MinE competes with MinC for the binding site of MinD and removes MinC from the complex (144). Then, it stimulates the ATPase activity of MinD and enhancing it greatly. Thus, MinD converts the bound ATP and changes back into its monomeric form which can no longer be retained at the cell membrane. MinE then jumps to the next MinCD complex, and repeating the process while moving towards the cell pole. MinE was shown to remain for some time at the cell membrane to inhibit MinD to directly bind to the membrane again and just dissolves from the membrane when no interaction partner is in proximity (145,146).

Thus, MinD is forced to integrate to the other cell pole to avoid MinE and the dynamic process starts over. MinC is only a passive passenger in this dynamic process of oscillation between MinD and MinE being carried along by binding to the activated MinD. The

oscillation keeps the concentration of MinC lowest at the cell midpoint and thus, allows the construction of the Z-ring at this point.

The ratio of these proteins can greatly infect the Z-ring placement since overexpression or deletion of one or more of them greatly changes the morphology of the resulting daughter cells. Complete absence of the *minB* locus results in the formation of mini cells because the Z-ring can form in random places within the cell which lead to asymmetric division and anucleated cells (139). Deletion of MinC or MinD results in the same phenotype since both are responsible for inhibition of Z-ring construction at the cell poles (139). Deletion of MinE result in a failure of division with enlarged filamentous cells because the MinCD complex can spread over the entirety of the cell and hence, the Z-ring cannot form at all (147,148). The same phenotype occurs upon overexpression of MinD or its mutation to be unable to hydrolyse ATP (140,141,149).

How exactly MinC inhibits the polymerisation of FtsZ is not clear. Surprisingly, MinC does not influence the GTPase activity of FtsZ but the hydrolysis of GTP plays a critical role since FtsZ bound to the non-hydrolysable GTP analogue GMPCPP cannot be disassemble by MinC (150–154). Also, the inhibitory effect of MinC has been shown to be greatly enhanced by MinD (155–157). Upon interaction with MinD, MinC is recruited to the membrane and thus its local concentration at the inner membrane is increased where it interacts with the FtsZ protofilaments. Fusion constructs of MinC with the MTS of either MinD or ZipA which target the protein to the cell membrane have been shown to successfully inhibit the Z-ring construction. However, co-expression of this fusion construct with MinD leads to an even greater inhibitions and MinD seems to activate MinC in an additional different manner (143,158).

Like its ancestors, the chloroplast also utilises the Min system for its correct organelle division. While the basic components and the oscillatory behaviour of the Min system and Z-ring are similar, new additional proteins are recruited into this process. In the plant Arabidopsis thaliana, the Z- ring is formed by two orthologues of the FtsZ protein, FtsZ1 and FtsZ2. Furthermore, MinD and MinE are present and are both stromal chloroplast division components (159,160). The role of the Arabidopsis proteins in plastid division site selection was clearly demonstrated by the observation that decreased levels of functional *At*MinD1 (159,161) or elevated levels of *At*MinE1 (160) result in asymmetric chloroplast

division events. Until now, no MinC orthologue was found in the chloroplast. But, a similar effect on the Z-ring as MinC was demonstrated for a protein belonging to the ARC (Accumulation and replication of chloroplast) family, ARC3 (162).

The Min system can be found in several species of bacteria and in the chloroplast of higher plants and its basic functions are and components are highly conserved with MinD being found in most species. If the apicoplast which descended from the chloroplast is handling its division through the Min system or another mechanism has been one of the open question of the malaria research.

JUSTIFICATION AND OBJECTIVES

Malaria, caused by *Plasmodium spp*., remains with more than 200 million cases and more than 400.000 deaths per year one of the most severe diseases worldwide. The steady decrease of malaria cases has stalled in recent years, with stable numbers in the past five years. No highly efficient vaccine is available so far and just a few antimalarial drugs are available on the market. Spreading drug resistance against almost all available drugs has rendered them ineffective in combating the disease. New drugs are urgently needed to prevent a new rise of this severe disease. The apicoplast, a relict plastid of secondary endosymbiosis, is a promising source for new drug targets due to its prokaryotic ancestry and its absence in the mammalian host. The plastid has been shown to be essential to the survival of the *Plasmodium* parasite. Understanding its biology further will lead to the discovery of novel drug targets which can be exploited for drug discovery in the future.
This work is focusing on the mode of replication of the apicoplast of *P. falciparum* during its erythrocytic life cycle. We focus on the Min system utilised during the division of the apicoplast`s ancestry, the chloroplast. We could identify a possible homologue of one of the main components of this system, the division inhibitor MinD, in the plasmodial genome. To further characterise and prove that this protein is a key part of apicoplast division during replication of the *Plasmodium* parasite this work had the following objectives:

- Cloning of the open reading frame of *Pf*MinD into the expression vector pASK-IBA3 and the transfection vector pARL 1a+
- Analysis of the activity and oligomerisation of the recombinant protein including substrate profiling
- Mutagenic analysis of important domains by site-directed mutagenesis
- Generation of transgenic *P. falciparum* parasite overexpressing MinD or a mutated version of MinD
- Localisation of the protein within *P. falciparum* using GFP chimeras
- Evaluation of the overexpression of MinD on the viability of *P. falciparum* via transgenic parasites
- Mutagenic analysis of the protein by co-transfection to GFP-tagged reference proteins in order to study apicoplast morphology

MATERIALS AND METHODS

3.1. Working with recombinant protein in *E. coli*

3.1.1. Database searches and sequence analyses

The gene apparently encoding *minD* was identified in the *Plasmodium* genome database PlasmoDB (http://PlasmoDB.org) (163) by performing blastp searches using the protein sequences from *E. coli* (accession number P0AEZ3) and *Arabidposis thaliana* (accession number Q9MBA2). Prediction of N-terminal targeting sequences was performed using signalP (http://www.cbs.dtu.dk/services/SignalP/) (164) and PlasmoAP (http://www.PlasmoDB.org/restricted/PlasmoAPcgi.shtml) (88). Protein sequence alignment was performed using ClustalW (165) and T-coffee (166).

3.1.2. Cloning and Mutagenesis of the constructs for recombinant expression of *Pf*MinD

The open reading frame (ORF) of the plasmodial *minD* was determined by BLAST searches against the plasmodial genome database PlasmoDB. The apicoplast targeting sequence was predicted by the bioinformatics tool PlasmoAP and was cut off for the expression construct. The ORF was amplified by polymerase chain reaction (PCR) using the Platinum Supermix High Fidelity (Invitrogen, USA) using the primers MinD-short-IBA-S and MinD-IBA-AS (Table 1) and genomic deoxyribonucleic acid (gDNA) from unsynchronised 3D7 culture as template. The primers contain the restriction site for *BsaI* for cloning into the expression vector pASK-IBA3 (IBA Lifesciences, Germany) (Figure 7). The vector contains a C-terminal Strep-Tag for later protein purification. The purified PCR product and the vector were both digested with the restriction enzyme BsaI, ligated using the T4 DNA Ligase (NEB, USA) and transformed into *E. coli* DH10β strain. Obtained clones were verified by automated DNA sequencing.

3.1.3. Cloning of the synthetic MinD construct into the expression vector pASK-IBA3

Due to the high AT content of the plasmodial *minD* gene a codon-optimised construct was purchased from Genscript, USA. The construct was delivered in the pUC cloning vector

Table 1: Listed of used primers for cloning of the expression constructs into the pASK-IBA3 vector.

MinD-IBA-S	GCGCGCGGTCTCGAATGAATGTATTCACAAAAAGAAGC
MinD-IBA-AS	GCGCGCGGTCTCAGCGCTTTCTTTTTTCTCCTCAAGAAACGG
MinD-short-IBA-S	GCGCGCGGTCTCGAATGAATAACAGTATACCTGACGAATGC
MinD-K131A-S	GGTAAAGGAGGAGTAGGCGCCTCAACAGTGGCTGCACAATTAG
MinD-K131-AS	CTAATTGTGCAGCCACTGTTGAGGCGCCTACTCCTCCTTTACC
MinD-L348G-S	GAAAGAATTATATCATGGATGTAGTATTCTTATACAGG
MinD-L348G-AS	GCTGTATAAGAATACTACATCCATGATATAATTCTTTC
M13-S	GTTTTCCCAGTCACGAC
M13-AS	CAGGAAACAGCTATGAC
MinD-syn-K131A-S	GGCAAGGGTGGCGTGGGCGCCAGCACCGTTGCGGCGCAGC
MinD-syn-K131A-AS	GCTGCGCCGCAACGGTGCTGGCGCCCACGCCACCCTTGCC
MinD-syn-L348G-S	GCAAGGAGCTGTATCACGGATGCAGCATCCTGATTCAGC
MinD-syn-L348G-AS	GCTGAATCAGGATGCTGCATCCGTGATACAGCTCCTTGC
IBA3-Seq-S	AGAGTTATTTTACCACTCCCT
IBA3-Seq-AS	GACGCAGTAGCGGTAAACG

and contained a C-terminal 6xHis-Tag. The gene was amplified by PCR as described above using the primers M13-S and M13-AS and utilizing the delivered construct as template. The purified PCR product and the pASK-IBA3 vector were digested with the restriction enzymes XhoI and HindIII, ligated using the T4 DNA Ligase (NEB, USA) and transformed via heat shock into *E. coli* DH10β strain. Obtained clones were verified by automated DNA sequencing.

3.1.4. Site directed Mutagenesis

For the introduction of the desired point mutation into the ORF of *minD* a whole plasmid mutagenesis PCR was performed. Overlapping mutagenesis primers containing the point mutation were used (Table 1) and as template served the beforehand cloned and verified MinD construct in the pASK-IBA3 vector. The PCR reaction was performed with the Pfu polymerase (NEB, USA). The PCR product was digested with DpnI restriction enzyme to remove the template DNA and transformed via heat shock into *E. coli* DH10β strain. Obtained clones were verified by automated DNA sequencing.

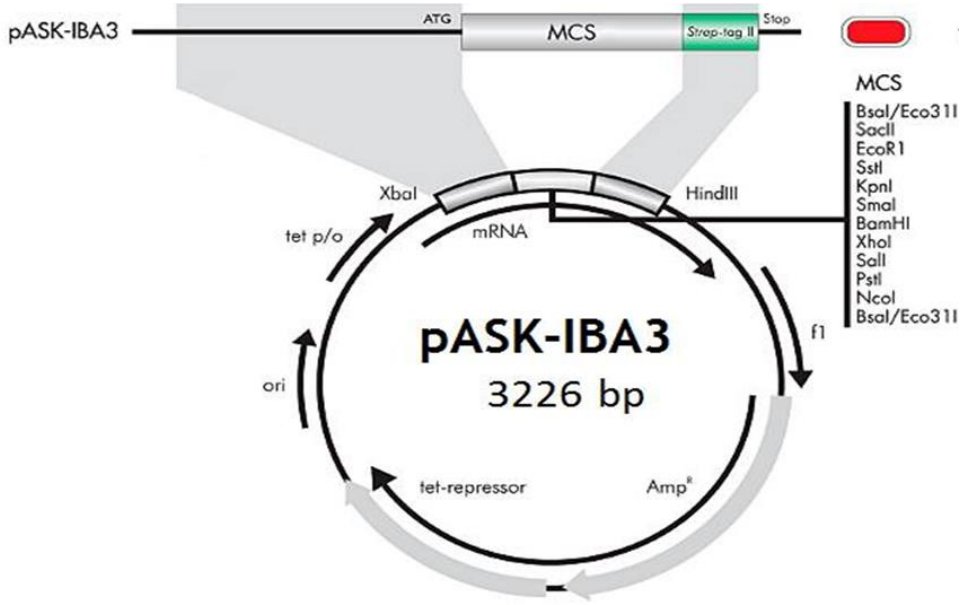

Figure 7: Vector map of the expression vector pASK-IBA 3. For expression of the recombinant protein, the truncated ORF of MinD was cloned into the pASK-IBA3 vector using hte BsaI restrcition sites.

3.1.5. Expression of *Pf*MinD

The recombinant plasmodial MinD protein was expressed in *E. coli* BLR(DE3) expression strain (Novagen, India). An overnight culture of LB complemented with 10mg/ml Ampicillin (Amp) was inoculated with a single colony of a freshly transformed LB-Agar plate containing the expression constructs. The culture was diluted 1:100 into the main expression culture containing LB and Amp. The main culture was grown at 37°C until it reached an OD_{600} of around 0.5. The culture was induced by 200ng/ml anhydrotetracycline (AHT) and grown at 37°C for additional 4 hours. The cells were harvested by centrifugation at 4°C, 5000rpm for 15min and stored at -20°C until further use.

3.1.6. Strep-purification

Purification of *Pf*MinD by Strep-Tag was performed by gravity flow using the Strep-Tactin Sepharose (IBA Lifescience, Germany) according to manufacturer´s instructions. The cell

pellet was resuspended in Buffer W (100mM Tris, 150mM NaCl, 1mM EDTA, pH 8) and the cells were pre-lysed in the presence of lysozyme for 20 min on ice followed broken sonification for 2min with a pulse for 1 second and a break of 5 seconds and an amplitude of 50% (Branson Digital Sonifier, Germany). To avoid protein degradation 1mM PMSF was added right before sonification. The broken cells were centrifuged for 1h at 15000rpm and 4°C. The clear cell lysate was then applied to the beforehand washed and with Buffer W equilibrated Strep-Tactin beads 3 times via gravity flow. After the cell lysate passed through, the beads were washed twice with Buffer W and the protein was eluted with Buffer E (Buffer W + 2.5mM desthiobiotin). Samples from all steps were collected to check purity and yield in an SDS-PAGE. The protein was stored at 4°C until further use. The beads were then washed with Buffer W complemented with 1mM HABA (hydroxy-azophenyl-benzoic acid) until the beads were dyed red followed by an intensive wash with water. The clean beads were then stored at 4°C in 20% Ethanol until next use.

3.1.7. His-purification

Purification of *Pf*MinD via 6xHis-Tag was performed by gravity flow using the Ni-NTA beads (Iba Lifescience, Germany). The cell pellet was resuspended in Buffer His (50mM Tris, 300mM NaCl, 5% Glycerol, pH 8) containing 20mM Imidazole. The cells were opened and centrifuged like described above. The clear cell lysate was then incubated for 30 min with the Ni-NTA beads which were washed with water and equilibrated with Buffer His beforehand. The cell lysate was removed from the beads by gravity flow and the beads were washed intensively with Buffer His containing 20mM Imidazole. The protein was eluted from the beads by Buffer His containing 500mM Imidazole. Directly after elution, 1mM EDTA pH 8 and 10mM DTT were added and the protein was kept at 4°C until further use. The beads were washed with water and with 6M Guanidine-HCl to erase possible protein precipitation. The Ni^{2+} were stripped from the membrane by wash with 100mM EDTA followed by another wash with water. The beads were recharged with 100mM $NiSO_4$ and kept in 20% Ethanol at 4°C.

3.1.8. Anion Exchange Chromatography

Anion Exchange chromatography (AEX) is a purification technique which separates molecules by their charge. The stationary phase is coated with positively charged cations and thus can bind to negatively charged molecules. With an isoelectric point pI of 5.5 the MinD protein could bound to an anion exchanger column being in a buffer solution with a pH of higher than 7.

The technique was performed via the Äkta pure chromatography system using the HiTrap Q HP 1ml column (GE Healthcare, USA) using a salt gradient to elute the protein. The column was connected to the system and washed with 20 column volume (CV) water, followed by first equilibration of 10CV of AEX Buffer B (50mM HEPES, 5% Glycerol, 10mM DTT, 1M NaCl, pH 7.5) and a second equilibration with AEX Buffer A (50mM HEPES, 5% Glycerol, 10mM DTT, pH 7.5) using a flow rate of 1ml/min. The sample after His-purification has been diluted with AEX Buffer A to a salt concentration of 40mM NaCl and applied to the column. The column was then washed for 5CV with AEX Buffer A, followed by a second wash of 20CV of 5% AEX Buffer B. The protein has been eluted by a gradient from 5% to 60% AEX Buffer B over 30CV. The elution was followed by a wash of 5CV 60% AEX Buffer B and a second wash of 10CV 100% AEX Buffer B. The UV signal at 280nm as well as the conductivity (mS/cm) and percentage of AEX Buffer B was measured during the whole run and all fractions have been collected. Peak fractions have been loaded onto an SDS-PAGE to verify content and purity of the sample. The column was washed after use with water and 20% Ethanol and the protein was stored at 4°C until further use.

3.1.9. Size Exclusion Chromatography

Size Exclusion chromatography (SEC, also called gel filtration chromatography) is a purification method which separates molecules by their size. The molecules have to pass a stationary phase composed of agarose where the smaller molecules can enter the bead matrix and the bigger molecules are excluded, hence passing faster through the column and eluting from it earlier.

The technique was performed via the Äkta pure chromatography system using the HiLoad 16/600 Superdex 200 pg column (GE Healthcare, USA). The column was connected to the system, washed with water and equilibrated with SEC buffer (50mM MES, 100mM NaCl, 5% Glycerol, 10mM DTT, pH 6,5) using a flow rate of 1ml/min. After equilibration the sample was applied in a 1ml loop to the column and the elution was performed in the SEC Buffer and same flow rate. The UV signal at 280nm as well as the conductivity (mS/cm) was measured during the whole run and all fractions were collected. Peak fractions were loaded onto an SDS-PAGE to verify content and purity of the sample. The column was washed after use with water and 20% Ethanol and eluted proteins were stored at 4°C until further use.

3.1.10. Western Blot

The recombinant protein expression was verified by Western Blot analysis using antibodies against the protein tags Strep and 6xHis, respectively. The purified protein was resuspended in 5x SDS-PAGE sample buffer and boiled for 5 min. The supernatant was separated by 10% SDS-PAGE. The proteins were transferred to a nitrocellulose membrane (BioRad, Germany) as described in (167) using the Trans-Blot SD Semi-Dry Transfer Cell (BioRad, Germany). The expressed proteins were detected via their Strep- or 6xHis-Tag by using a monoclonal anti Strep- (1:1000 dilution; IBA, Germany) or anti His-antibody (1:1000 dilution; Pierce, USA) and a secondary anti-mouse horseradish peroxidase (HRP)-labelled antibody (1:7500 dilution; Pierce, USA) and visualized on X-ray films using the SuperSignal West Pico detection system (Thermo Scientific, USA).

3.1.11. Buffer Screening by differential scanning fluorimetry

The search for optimal buffer conditions for the stability of the protein was performed by differential scanning fluorimetry (DSF), also called fluorescence-based thermal shift assay (Thermofluor) (168). Thereby, the tested protein is incubated at a rising temperature in the presence of a hydrophobic fluorophore which allows to distinguish between folded and unfolded protein. Upon denaturation of the protein, the fluorophore interacts with the

hydrophobic core of the protein and emits a fluorescence signal. The denaturation temperature varies depending on the stability of the protein in the tested buffer conditions. The purified MinD protein was concentrated to 2mg/ml and incubated with 2µl of Sypro Orange protein stain and distributed to a 96well plate screening for different pH, salt conditions and additives. The temperature was increased in 1K steps each 2 minutes. Fluorescence was detected by CFX96 Real-Time system (BioRad, Germany).

3.1.12. Polymerisation Studies using Dynamic Light Scattering

Dynamic Light Scattering (DLS) is a technique to determine the size distribution of molecules in solution. It measures the diffraction pattern of these molecules by applying consecutive

shots of a laser. Due to the Brownian motion of the molecules in solution, the diffraction pattern changes with each consecutive measurement and the size of the molecules can be calculated.

For analysis of the oligomeric state of the recombinant protein DLS measurements using the Zetasizer µV (Malvern Panalytical) were performed. The recombinant protein was centrifuged before at 13000 rpm and 4°C for 10 min to pellet possible interferences. Then, the protein was applied to the cuvette in a concentration of 0.5mg/ml and measured for 3 times with each measurement consisting of 10 runs of 10 seconds. To study the effect of ATP and its dependency on divalent metal ions, the protein was incubated with $MgCl_2$, $CaCl_2$, $MnCl_2$ and different concentrations of ATP (100µM, 1mM and 10mM). As controls for the dependency of metal ions, the reaction was also carried out without any added metal present and with 10mM EDTA to quench possible metal contamination. As further control, the reaction was also carried out without ATP to see effects caused by the added metal ions alone. The mixture was measured in the DLS during a time period of 20 min, by equilibrating the solution and chamber to 22°C before measurement and then 20 measurements consisting of 6 run each of 10 seconds. The Zetasizer software monitors the size and distribution of the protein during this time. The size was then plotted against the time in the Graphpad Prism 5 program.

3.1.13. Malachite Green Assay as detection method for free inorganic phosphate

The Malachite Green Assay is a colorimetric assay to detect free inorganic phosphate. Under acidic conditions the malachite green forms a complex with molybdate and free phosphate which promotes a colour change from yellow to green which can be measured at an absorbance at 640nm.

The assay was performed in a 96 well plate with a reaction volume of 100µl containing 1µM of recombinant MinD protein, 5mM metal solution ($MgCl_2$, $CaCl_2$, $MnCl_2$) or 5mM EDTA and either 100µM ATP or 1mM ATP. As controls for spontaneous hydrolysis of ATP the reaction was also carried out with all the components except for the protein. The reaction was incubated for 30 min at 37°C and stopped by addition of 50µl of 4.5M H_2SO_4 containing 100mM ammonium molybdate. After 5 min of incubation 100µl of the freshly prepared Malachite Green reagent (0.5µM malachite green and 0.1% polyvinyl alcohol) was added and incubated in the dark at room temperature for further 30 min. Absorbance was measured at 640nm in the CLARIOstar Microplate Reader (BGM Labtech, Germany). Free phosphate concentration was calculated by the beforehand performed standard curve using KH_2PO_4 as standard and plotted in Graphpad Prism 5 program.

3.1.14. ATP-Glo Assay as detection for ATP concentration

For detection of ATP concentration in the reaction the ATP-Glo Bioluminometric Cell Viability Assay from Biotium was used. The assay is made for detection of ATP levels in viable cells by coupling the ATP to a luciferase reaction which uses the ATP to oxidize D-Luciferin leading to the production of light which correspond to the amount of ATP available.

The ATP hydrolysis of MinD was carried out in a 96 well plate in a volume 100µl at 37°C for 30 min containing 5µM protein, 5mM $MgCl_2$, $CaCl_2$ or $MnCl_2$ or 10mM EDTA as well as 10µM ATP. As negative control served the reaction mixture without the recombinant MinD protein. After 30 min, the EDTA concentration of all reactions was fitted to 10mM EDTA as final concentration. The reaction was stopped for 5 min at 95°C for heat denaturation of the protein and then cooled on ice back to room temperature. The luciferase

cocktail was prepared as described in the manufacturer´s instruction. In short, 1mg D-Luciferin was dissolved in 2.5ml of ATP-Glo Assay Buffer and 25µl of Firefly Luciferase was added. Additionally, 12mM $MgCl_2$ was added to the cocktail to compensate for the EDTA in the reaction mixture. 100µl of the Luciferase cocktail was added to each reaction and the luminescence signal was measured constantly for 15 min in the CLARIOstar Microplate Reader (BGM Labtech, Germany). The values were the calculated for the conversion of ATP in percentage based on the ATP only control. The values were then plotted in Graphpad Prism 5 program.

3.2. Working with transgenic parasites

3.2.1. Cloning of the plasmodial MinD into the transfection vector pARL 1a+

For transfection into the *P. falciparum* parasite a full length and truncated version of *Pf*MinD were cloned into the transfection vector pARL 1a+ (169,170) (Figure 8). Both the full length ORF and the truncated version were amplified by polymerase chain reaction (PCR) using the Platinum Supermix High Fidelity (Invitrogen, USA) using gDNA from unsynchronised 3D7 culture as template. Amplification of the full-length construct was down by the primer pair MinD-pARL-S and MinD-pARL-AS where the antisense primer contains a C-terminal myc-tag and ends with a stop codon. The truncated version for was amplified by using the primers MinD-pARL-S and MinD-short-pARL-AS where the antisense primer contains no stop codon so that the construct expresses the C-terminal GFP-tag present in the pARL1a+ vector (Table 2). The obtained PCR products and the transfection vector were digested using the restriction enzymes KpnI and AvrII, ligated using the T4 DNA Ligase (NEB, USA) and transformed by heat shock into chemo-competent *E. coli* DH10β. Obtained clones were verified by automated DNA sequencing.

3.2.2. Culture Conditions of *Plasmodium falciparum*

All *P. falciparum* strains were maintained in continuous culture as originally described by Trager and Jansen (171) with modifications from Das Gupta et al., 2005 (172). The parasites were cultured in RPMI 1640 media (AppliChem Panreac, Germany) complemented with

Table 2: List of used primers for cloning into the vector pARL 1a+ for transfection into the *Plasmodium* parasite.

MinD-pARL-S	GAGAGGTACCATGAATGTATTCACAAAAAGAAGC
MinD-short-pARL-AS	GAGACCTAGGTTTTCCTACTCCTCCTTTACCTG
MinD-pARL-AS	GAGACCTAGGTTCTTTTTTCTCCTCAAGAAACGG
MinD-kpnMut-S	GTATGAATGGATGGGTTCCAATTTATAAAAAT
MinD-kpnMut-AS	ATTTTTATAAATTGGAACCCATCCATTCATAC
pARL-Seq-S	ATATCCGTTAATAATAAATACACGC
pARL-Seq-AS	TTTCATATGATCTGGGTATCTCGC

2g D-Glucose, 1g Sodium bicarbonate, 30mg Hypoxantine, 20mg Gentamycin and 5g Albumax per liter at a temperature of 37 °C in an atmosphere of 90% N_2, 5% O_2 and 5% CO_2. The culture was kept at 4% haematocrit in O-positive blood provided by ProSangue, Brazil. Transgenic cell lines were additionally cultured under drug pressure of 5nM WR99210 or 1ug/ml blasticidine to maintain the episomal plasmid. Every 2 to 3 days, the parasitemia of the culture was observed by Giemsa stained blood smear and diluted accordingly. To maintain the parasite in the same stage of the life cycle, the cultures were synchronized for the ring stage using Sorbitol (173). Therefore, the whole culture was pelleted, incubated with 5 pellet volume of pre-warmed 5% Sorbitol for 10 min, washed once and further cultivated in fresh RPMI media. The cultures were regularly checked for mycoplasma contamination.

3.2.3. Maxi Preparation

For transfection into *P. falciparum* parasite a high amount of plasmid DNA was needed. To obtain this a maxi preparation of the desired cloned transfection vector was performed. Therefore, a LB culture of 800ml complemented with 10mg/ml Ampicillin was inoculated from a freshly transformed LB-Agar plate of *E. coli* DH10β strain carrying the desired plasmid. The cells were grown for 16h at 37°C. The cells were pelleted and the Maxi preparation was performed via the Qiagen Maxi Preparation Kit according to the manufacturer's instructions. After precipitation of the plasmid DNA the pellet was resuspended in 400µl of TE buffer. Concentrations were determined by Nanodrop (ThermoScientific, USA) and aliquots of 120µg of DNA were prepared and supplemented

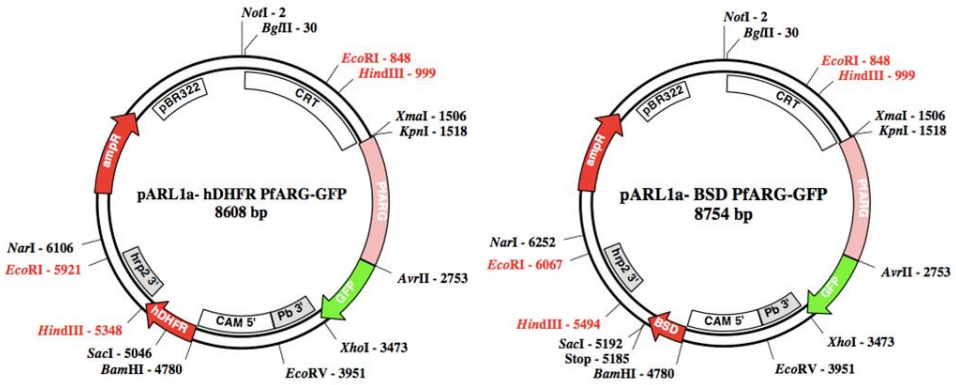

Figure 8: Vector map of the transfection vector pARL1a+. Two different vectors were used for transfection into *P. falciparum* which differ by their resistance cassetes, namely *hDFR* and *bsd*.

with 1/10 volume of 3M Sodium acetate pH 4.8 and 2.5 volume of ice-cold absolute Ethanol. The aliquots were stored at -20°C until further use.

3.2.4. Transfection

The desired constructs were transfected into the *P. falciparum* parasite via electroporation into the ring stage of the parasite (167). The plasmid DNA was centrifuged at 14000rpm, at 4°C for 30 min, the supernatant was discarded and the pellet was resuspended in 50µl of sterile Tris-EDTA Buffer (10 mM Tris-HCl; 1 mM EDTA; pH 7.5) and 200µl of cytomix (174). For transfection, a parasite culture (either 3D7 wildtype or a transgenic cell line, see Table 3) of a parasitemia of more than 2% ring stage parasite was centrifuged for 10min at 1200rpm and 4°C. The supernatant was removed and 200 µL of infected red blood cells (iRBC) were added to the resuspended plasmid and subsequently transferred to an electroporation cuvette (BioRad, Germany) and electroporated using the BioRad X-cell total system (BioRad, Germany) at 0.31 kV and 900 mF. After electroporation, the iRBC were washed once with fresh RPMI media and then transferred into new culture flask containing fresh RPMI media and 200µl of fresh RBCs for culturing at the above described conditions. Parasites were grown for 24 hours without drug selection before the medium was supplemented with 5nM of WR99210 or 1ug/ml of Blasticidin, where parasites were maintained in continuous culture for selection. First parasite showed up after 3 to 4 weeks after transfection.

Table 3: List of transfection events.

Name of Construct	Cell type used	Time (ms)	Voltage (V)
MinD GFP pARL 1a+ WR	3D7	12.6	307
MinD myc pARL 1a+ BSD	3D7	14.0	306
MinD K131A myc pARL 1a+ BSD	3D7	15.0	307
MinD L348G myc pARL 1a+ BSD	3D7	21.9	307
PDH E1a GFP pARL 1a+ WR	3D7	14.0	307
MinD myc pARL 1a+ BSD	PDH E1a GFP pARL 1a+ WR	14.7	307
MinD K131A myc pARL 1a+ BSD	PDH E1a GFP pARL 1a+ WR	15.1	305
MinD L348G myc pARL 1a+ BSD	PDH E1a GFP pARL 1a+ WR	14.3	307
mock pARL 1a+ BSD	PDH E1a GFP pARL 1a+ WR	17.8	306

3.2.5. Western Blot Analysis

The protein expression of the transgenic cell lines was verified via western blot analysis. Therefore, an asynchronous culture of transgenic parasites was isolated via saponin lysis (175). The tagged protein was purified by its C-terminal myc-Tag or GFP-Tag using the µMACS c-myc Isolation Kit or µMACS GFP Isolation Kit (Miltenyi Biotec, Germany) according to the manufacturer´s instructions. The purified sample was separated by 10% SDS-PAGE and trasnferred to a nitrocellulose membrane (BioRad, Germany) by the Trans-Blot SD Wet Transfer Cell (BioRad, Germany) using the protocol described in (167). The expressed proteins were detected via their myc- or GFP-tag by using a monoclonal anti myc- (1:1000 dilution) or anti GFP-antibody (1:1000 dilution; Pierce, USA) and a secondary anti-mouse horseradish peroxidase (HRP)-labelled antibody (1:7500 dilution; Pierce, USA) and visualized on X-ray films using the SuperSignal West Pico detection system (Thermo Scientific, USA).

3.2.6. Quantitative real-time polymerase chain reaction

To analyse the overexpression of the transfected cell lines on the transcriptional level a quantitative real-time PCR (qRT-PCR) was performed. Infected erythrocytes were saponin lysed and total RNA was extracted using TRIZOL (Invitrogen) according to the manufacturer's instruction. Total cDNA was obtained by using a random primer (0.5 pmol/µL) in a RT-PCR using 50ng of RNA. After this qRT-PCR with the specific primers using 5x HOT FIREPol EvaGreen qPCR Supermix (Solis BioDyne, Estonia) was performed in the Realplex2 Mastercycler EpGradient S (Eppendorf, Germany). The obtained results were analysed via the $2^{-\Delta CT}$ method normalising the results with the plasmodial housekeeping gene *Pf*Aldolase (176). The experiments were performed in triplicate through three independent experiments.

3.2.7. Growth Assay by flow cytometry

To analyse the effects of overexpression of MinD, the growth of the transgenic parasites was observed over the course of 10 days. The assay was performed at 2% haematocrit and started at a parasitemia of 0.5% and cultivated under normal culture conditions. Medium was changed daily to ensure optimal growth. A sample was taken daily in PBS to measure the parasitemia by flow cytometry using the Guava EasyCyte equipped with the CytoSoft 4.2.1 software. Therefore, the sample was incubated with 2µg/ml Ethidium bromide for 15 min in the dark and subsequently washed two times with PBS. After the last wash step, the sample was resuspended in PBS and parasitemia was measured by flow cytometry. 5000 events were counted, and the events were sorted for the shape of intact erythrocytes by forward and site scatter, followed by detection of the red fluorescence by ethidium bromide. Using these gates, the parasitemia can be calculated and was plotted in the Graphpad Prism 5 software.

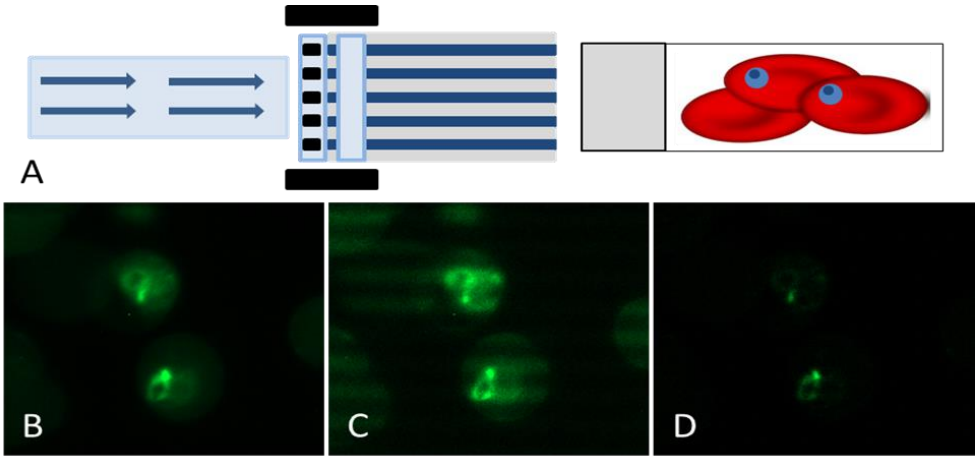

Figure 9: The Apotome.2 technique. The Zeiss Observer Z1 is equipped with the Apotome.2 device for fluorescence microscopy. The Apotome.2 technique can highly increase the resolution of the fluorescence signal byreducing the background signal. (A) For the calculation, a grid is placed in front of the specimen. Because of this grid, some parts of the specimen are being illuminated while other parts are not. A lens behind the grid moves then into at least 3 different positions to change the illumination pattern on the specimen. The Zeiss Zen Software can analyse the created pattern and reduce the background to enhance the resolution. (B-D) Fluorescence images of GFP chimera target to the Apicoplast of *P. falciparum*. (B) Image taken by conventional fluorescence microscopy. (C) Raw data produced by the Apotome.2 (D) Apotome.2 analysed fluorescence picture with highly reduced background signal.

3.2.8. Localisation Studies using Fluorescence Microscopy

Parasites were analysed by live cell fluorescent microscopy using an Axio Observer Z1 microscope (Zeiss, Germany) equipped with an AxioCam HRC digital camera (Zeiss, Germany). Infected RBCs were incubated with 10 µg/ml of HOECHST 33342 (Invitrogen, USA) for 5 min for nucleus staining. For co-localisation of the mitochondrion and the endoplasmic reticulum, the stains MitoTracker Red CMX Ros and ER-Tracker Red were used. Both stains were added to the iRBCs in final concentration of 50nM and incubated for 5min at 37°C. The images were analysed with the Zeiss Zen Blue 2.6 software.

3.2.9. 3D Images with higher resolution – Z-stack and Apotome technique

For observation of the morphological changes in the apicoplast formation during the erythrocytic life cycles 3D images of the apicoplast during different stages were taken for

subsequent calculation of the apicoplast volume and form. The 3D images were taken by live cell fluorescent microscopy using an Axio Observer Z1 microscope (Zeiss, Germany) equipped with an AxioCam HRC digital camera (Zeiss, Germany) and the Apotome.2 technique to increase the resolution of the fluorescence signal (Figure 9). Asynchronous transgenic parasite targeting GFP to the apicoplast were stained as described above by HOECHST 33342 and/or MitoTracker Red CMX Ros and loaded onto a microscope slide for analysis with fluorescence microscopy. The Z-stack was chosen to span 8µm to cover the whole length of the erythrocyte with each stack being 0.31µm apart. At each stack 5 pictures were taken by the Apotome.2 device. The images were analysed with the Zeiss Zen Blue 2.6 software.

RESULTS

4.1. The search for a possible MinD homologue in *P. falciparum*

For studying the Min system in *P. falciparum*, the members of the system have to be identified. Blast research in the *Plasmodium* database (PlasmoDB) for all the members of the Min family was performed (MinC or ARC3, MinD and MinE), but there were no matches for MinC and MinE. However, by utilizing the protein sequences of *At*MinD1, the MinD orthologue of *Arabidospis thaliana*, a possible match in the database was found. Sequences alignment using T-coffee against *At*MinD1 and *Ec*MinD analysed a sequence homology of just 25% between the protein sequences but the characteristic domains seemed to be conserved between all three proteins (Figure 10). The Walker A motif for binding and hydrolysing the ATP is highly conserved as well as the C-terminal loop which is responsible for polymerisation of MinD and association to the membrane. The identified match is described in PlasmoDB as putative cytosolic Fe-S cluster assembly factor NBP35 (accession number PF3D7_0910800). Although the protein is described as cytosolic factor, sequence analysis with PlasmoAP identified the bi-partite targeting sequences for localisation into the apicoplast. The found protein shows promising features to be a possible MinD orthologue, thus we focused to describe its function on recombinant protein level and its effect on the *P. falciparum* parasites biology. The protein will hereby be referred to as *Pf*MinD.

4.2. Purification of recombinant *Pf*MinD

To evaluate the function and activity of *Pf*MinD, the gene was cloned into the expression vector pASK-IBA 3 and recombinant expressed in *E. coli* BLR(DE3) cells and purified via its C-terminal strep-tag.

Bioinformatic analysis showed that the protein contains the bi-partite leader sequence for targeting into the apicoplast which had to be truncated for expression in *E. coli*. Three truncated versions were cloned from gDNA into the expression vector pASK-IBA3. Two truncations were decided by BLAST searches against other *Plasmodium spp.* ($MinD_{29-447}$ and $MinD_{63-447}$) while the third one was decided by the bioinformatics tools PlasmoAP ($MinD_{58-447}$). The first two constructs failed to express soluble protein while the latter one expressed protein which could be purified via Strep-Tag purification (Figure 11A). Analysis

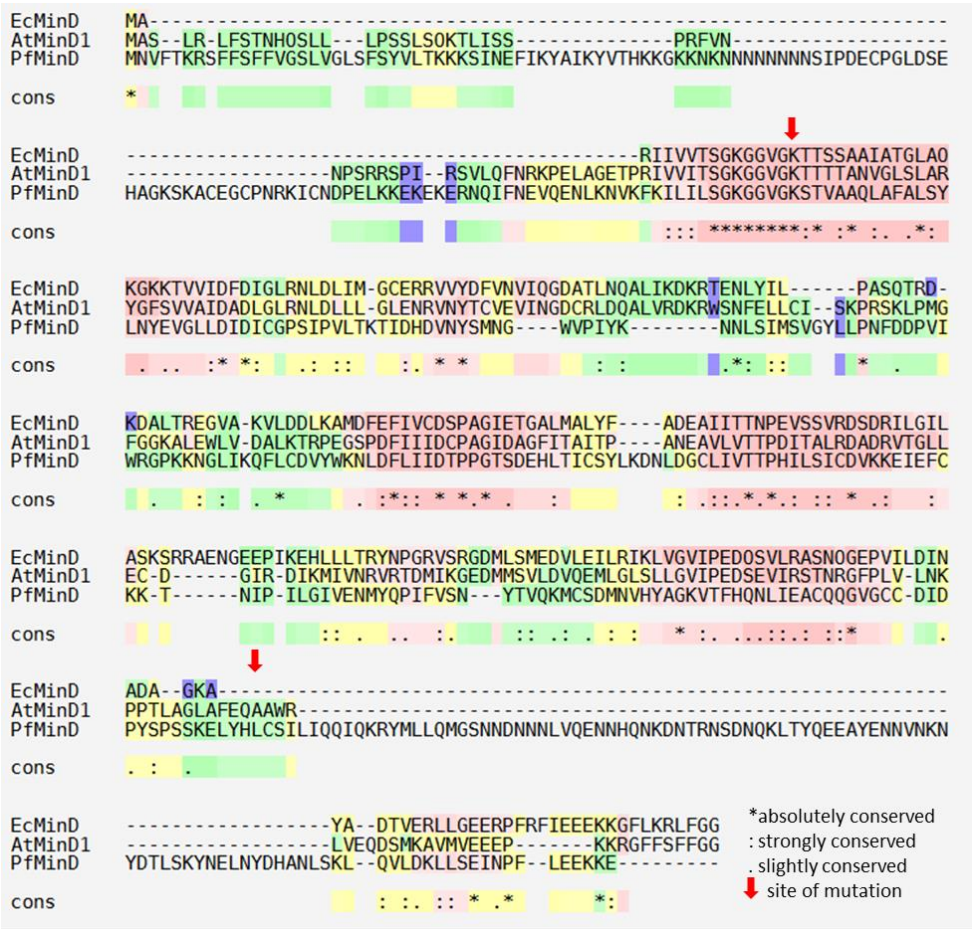

Figure 10: Sequence Alignment of different MinD proteins. The protein sequences of *Ec*MinD, *At*MinD1 and the possible MinD orthologue of *P. falciparum* have been analysed using T-coffee. Highly conserved regions are marked in red. The created mutations are marked by the red arrow.

via SDS-PAGE demonstrated several bands with the most prominent bands at a molecular weight of around 50kDa corresponding to the predicted size of *Pf*MinD and at around 60kDa. Western Blot analysis against the C-terminal Strep-Tag was performed to verify which band presents the recombinant protein (Figure 11B). The band at 50kDa shows a clear signal in the Western Blot, however, the band at 60kDa demonstrated also a weak signal. It is to be assumed that by the higher band is a chaperone which binds to the recombinant protein due to problems of *E. coli* with the protein folding of the protein. However, chaperones are displaying ATPase activity which would interfere with the

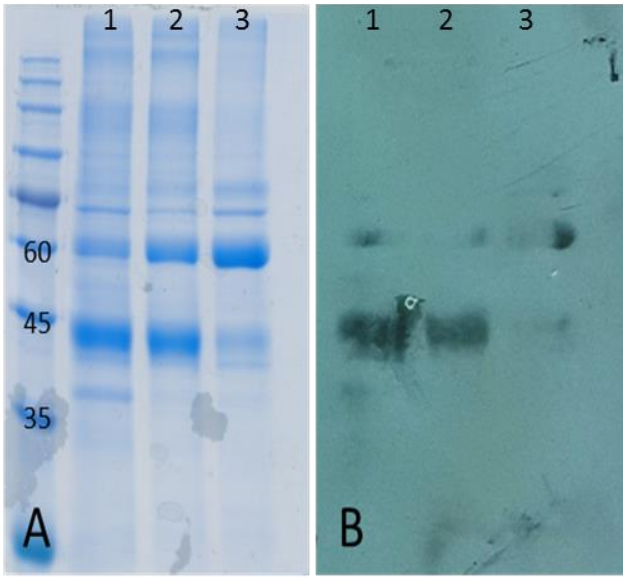

Figure 11: Strep Purification of *Pf*MinD and its mutants. The cloned constructs of *Pf*MinD and its mutated version *Pf*MinD K131A and *Pf*MinD L348G were expressed in *E. coli* BLR(DE3) cells for 4h at 37°C. The protein was purified via strep-tag and analysed by SDS-PAGE stained with Coomassie (A) and Western Blot revealed by the primary antibody anti-strep and secondary antibody anti-mouse labelled with HRP. The chemiluminescence signal was revealed by X-ray film. Lane 1 *Pf*MinD WT, Lane 2 *Pf*MinD K131A, Lane 3 *Pf*MinD L348G.

subsequent ATPase activity assay for the recombinant MinD. Further purification steps like Anion Exchange Chromatography (AEX) and Size Exclusion Chromatography (SEC) were performed with different buffers. Also, other expression strains of *E. coli* like BL21 star (DE3) or Rosetta (DE3) failed to express the protein without chaperone or to express the protein at all (data not shown). The genome of *P. falciparum* is rich on A/T content with genes being made up to 80% of A/T in contrary to the more even base pairs content in *E. coli*. It was assumed that *E. coli* displays these difficulties in expression due to the codon bias of the plasmodial gene. Thus, a codon-optimised version of the truncated *minD* construct was ordered to circumvent this problem.

The codon optimized construct was ordered from GeneScript, USA and recloned into the pASK-IBA3 vector. The protein was expressed in *E. coli* BLR(DE3) cells and was purified by its C-terminal 6xHis-tag.

Although the codon optimisation was supposed to help the *E. coli* cell to better express and fold the protein, the protein eluted with a similar contamination pattern after His-purification (Figure 12A). Western Blot analysis detected the C-terminal 6xHis-tag of the protein and confirmed its presence at the molecular weight of 50kDa (Figure 12B).

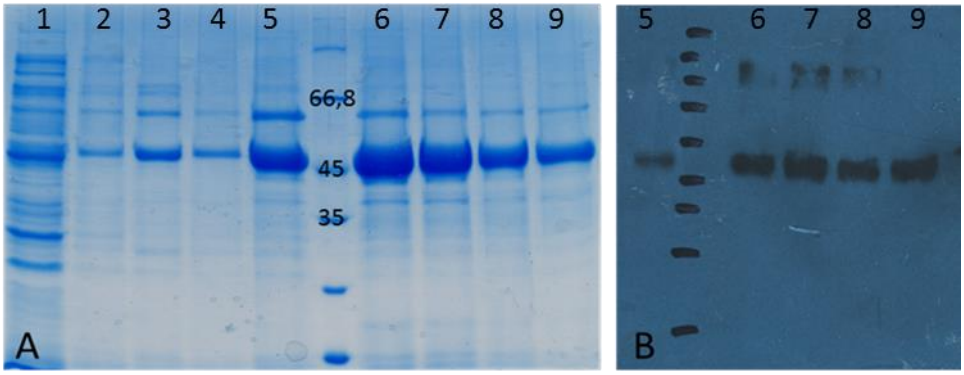

Figure 12: SDS-PAGE and Western Blot of the codon-optimized MinD. Due to the high A/T content in the gene, a construct with codon optimization for E. coli was ordered. The construct was expressed and purified via His-Tag with increasing concentrations Imidazole. Expression was tested on SDS-PAGE (A) stained with Coomassie and Western Blot (B) by using antibody against the C-terminal His-Tag. Lane 1 Pellet, Lane 2 flowthrough, Lane 3 25mM, Lane 4 50mM, Lane 5 100mM, Lane 6 to 8 250mM, Lane 9 500mM Imidazole.

Next, Size Exclusion and Anion Exchange Chromatography were tested in order to enhance the purification process. Size Exclusion is a technique which separates protein by their native size. Different buffers which were determined by differential scanning fluorimetry (DSF) were tested for SEC. Lowering the pH to 6.5 and addition of 10mM DTT as reducing agent succeeded to separate the protein from its contaminations (Figure 13). The histogram showed one dominant peak at an elution volume of 80ml which corresponds to a molecular weight of 50kDa, the size for monomeric *Pf*MinD. Smaller peaks were also observed during the run, but their protein content was not detectable during the SDS-PAGE analysis (Figure 13B). Sections of the dominant peak containing the pure recombinant protein were pooled and analysed by dynamic light scattering (DLS) to verify the dispersity of the sample (Figure 13C). DLS measurement revealed three different size distribution of the recombinant protein with the dominant peak calculation to a size of 14nm. This implies that the protein, although eluting into a single peak during SEC, is not stable in its oligomeric conformation in the used buffer.

As second method, AEX was tested to purify the protein further. Therefore, the recombinant protein had to be diluted in the AEX Buffer A to reduce the salt concentration and pH to 7.5 which was higher than the calculated pI of 5.5 of the recombinant protein. The diluted protein was applied to the column, washed and eluted using a gradient of NaCl (Figure

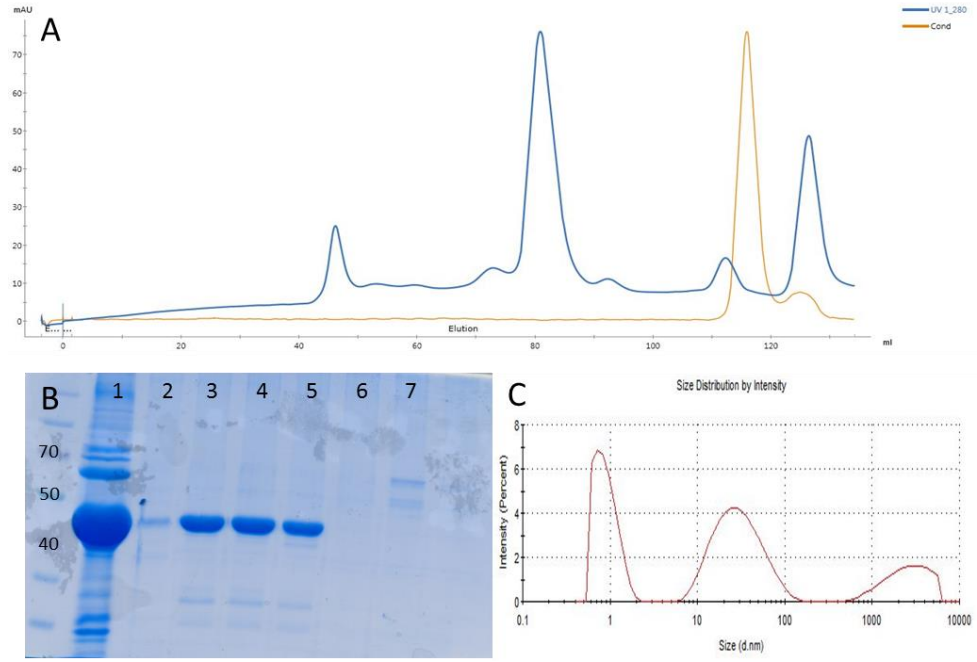

Figure 13: Size Exclusion Chromatography of *Pf*MinD. The codon-optimised construct was expressed and purified by His-purification. After His-purification the protein was applied to SEC by using the pre-equilibrated HiLoad 16/600 Superdex 200pg. (A) Histogram of the SEC demonstrating the UV signal at 280nm (in mAU) and the conductivity (in mS/cm) during the run. (B) SDS-PAGE of the obtained peaks during SEC. Lane 1 shows the His Elution which was applied to the column. lane 2 represents the first peak. Lanes 3-5 represent the second peak. Lane 6 represent the third peak and lane 7 shows the last peak. (C) Pooled fractions of the second peaks (lanes 3-5) were applied to DLS measurements and show three separate size population of *Pf*MinD.

14A). The histogram showed one dominant peak at a concentration of around 140mM NaCl which contained the recombinant protein (Figure 14B). Two smaller peaks were visible at NaCl concentrations of 50mM and 1M which were also revealed to contain the recombinant protein by SDS-PAGE. The peak at 50mM NaCl occurred during the washing of the column and might relate to overloading of the column and hence, not tightly bound protein. The peak at 1M NaCl elutes additional the chaperone and might represent the unfolded recombinant protein which is still bound to the chaperone. The fractions of the dominant peak were pooled and its dispersity was tested by DLS (Figure 14C). The measurement showed a single peak at a size of around 14nm, indicating that the protein was monodisperse in its confirmation. However, DLS measurements after 24 hours at 4°C revealed another

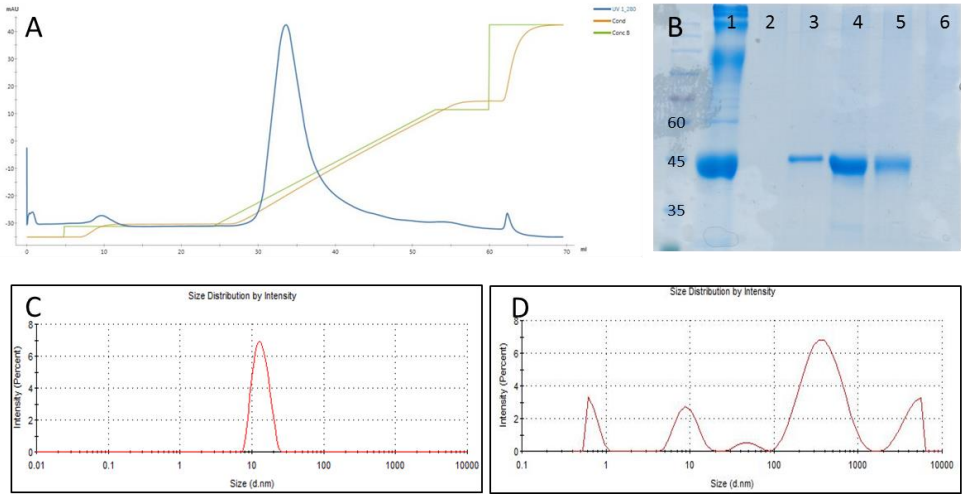

Figure 14: Anion Exchange Chromatography of *Pf*MinD. The protein was expressed and purified via His purification. The elution of His purification was diluted down to a NaCl concentration of 40mM and applied to the HiTrap Q column (A). The protein was eluted from the column by NaCl gradient. (B) Obtained fractions were applied to SDS-PAGE stained with Coomassie. The lane 1 represents the His Elution which was applied to the column. The lane 2 shows the first peak obtained at 5% Buffer B. Lane 3-5 represent the second peak obtained at 15% Buffer B. Lane 6 shows the last peak obtained at 100% Buffer B. (C-D) Pooled fractions of the second peak (lanes 3-5) were applied to the DLS directly after the concentration (C) and the following day after kept at 4°C (D).

size distribution with several peaks, hinting agglomeration of the sample. Thus, all subsequent analysis with the recombinant protein were performed directly after purification of the sample to get a more accurate picture of the behaviour of *Pf*MinD.

4.3. *Pf*MinD polymerises and binds to ATP

The mechanism of polymerisation and ATP hydrolysis by MinD was thoroughly studied for *Ec*MinD and *At*MinD1 (157,177). In short, MinD binds to ATP and forms a complex at the inner cell membrane together with MinC (or ARC3 in case of the chloroplast). This complex oscillates along the inner cell membrane until it comes in contact with MinE. MinE competes for binding to MinD with bound MinC and enhances the ATPase activity of MinD to hydrolyse the bound ATP. Following this, the complex is released from the inner cell membrane.

According to this mechanism, the plasmodial MinD orthologue should display ATP induced polymerisation and a weak ATPase activity which can be enhanced by its binding partner MinE. To verify the effect of ATP on polymerisation, the size distribution of the protein over time was measured by dynamic light scattering (DLS). The protein was observed for 20 min at a stable temperature of 22°C. Divalent metals ($MgCl_2$, $CaCl_2$ and $MnCl_2$) were added and the behaviour was observed without and with different concentrations of ATP (100µM, 1mM and 10mM). As a negative control, EDTA, a known chelator for divalent metals, was used in the reaction to remove possible contaminating metals. Size and its distribution are analysed by the Zetasizer software and demonstrated as value and peak distribution.

The size determination was plotted against the time to visualise the behaviour of *Pf*MinD upon induction with ATP (Figure 15). As controls, the size distribution of the protein was observed over 20 min in its normal buffer and with addition of the divalent metals or EDTA to exclude any possible aggregation effect during the measurement. Addition of 10mM ATP to the protein containing no metals or containing EDTA had a minor effect on the polymerisation by increasing the sizes of the complexes to 114nm in the case of no metals in solution and 178nm in case of EDTA while lower concentrations of ATP did not induce a response from *Pf*MinD (Figure 15A,B).

However, addition of the divalent metals $MgCl_2$, $CaCl_2$ and $MnCl_2$ showed a strong increase in the size upon interaction with ATP. Addition of $MgCl_2$ lead to a minor increase in size at low concentrations of ATP, but addition of 10mM ATP increased the size of the complex up to 6400nm (Figure 15C). Interestingly, the size reduces after 20min from 6400nm to 3500nm which might be due to hydrolysis of ATP by the protein or instability of the complex. Addition of $CaCl_2$ demonstrated an interesting effect on the size of MinD (Figure 15D). Without addition of ATP, the size is reduced by $CaCl_2$ to around 3nm in comparison to the size of around 12nm of the protein in its normal buffer. Upon addition of ATP, the size increases corresponding to the ATP concentration used. The size increases up to 220nm at 100µM ATP, 1950nm at 1mM ATP and up to 7900nm at a concentration of 10mM ATP. Like already observed with $MgCl_2$ the size distribution upon addition of 10mM ATP decreases at the last time point of 20min; seemingly reaching a maximum size beforehand. Addition of $MnCl_2$ induced polymerisation of the protein according to the ATP

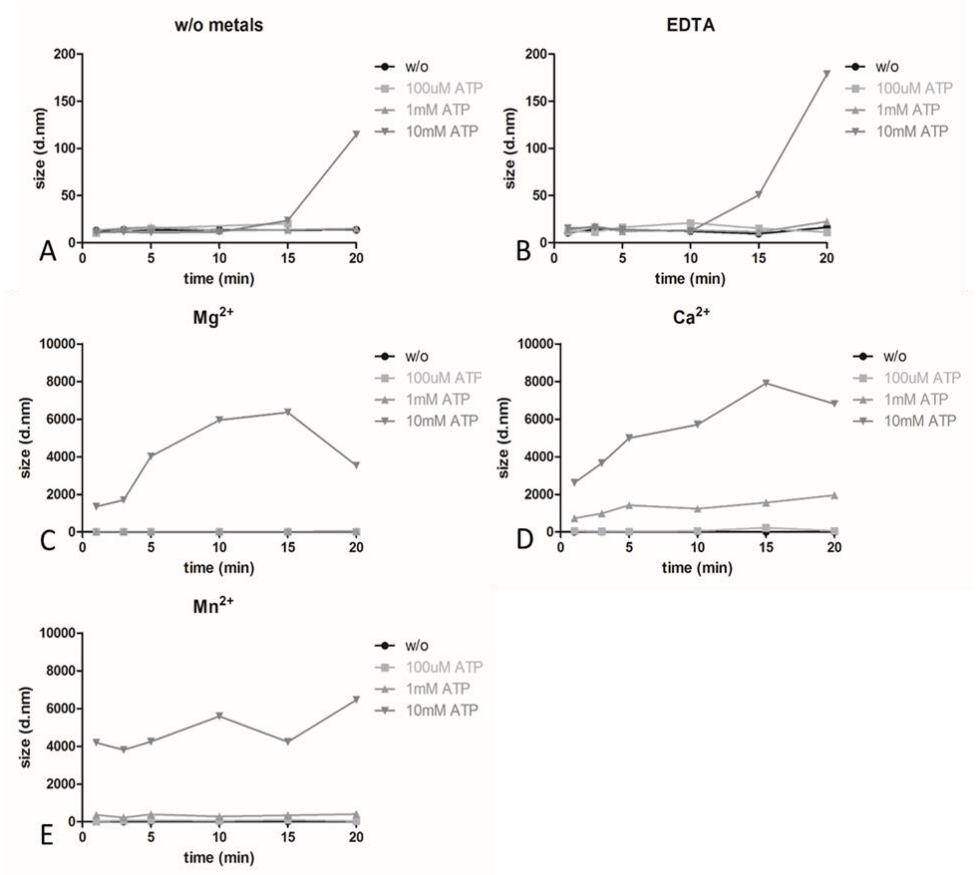

Figure 15: Polymerisation studies of *Pf*MinD by dynamic light scattering. *Pf*MinD was incubated for 20min without metals (A) or 10mM EDTA as control (B) or addition of 5mM $MgCl_2$ (C), $CaCl_2$ (D) or $MnCl_2$ (E) at different concentrations of ATP (100µM, 1mM and 10mM) and the size was monitored by DLS. Note that the y axis is scaled differently in A and B.

concentration used, with a minor increase to 39nm at 100µM ATP, to 400nm at 1mM ATP and up to 6400nm at the highest ATP concentration (Figure 15E).

ATP was shown to have strong effect in combinations with $CaCl_2$ on the polymerisation of *Pf*MinD. To show that *Pf*MinD is also able to hydrolyse ATP with help of divalent metals, the Malachite Green Assay was performed. The reagent malachite green forms a complex with molybdate and free inorganic phosphate under acidic conditions. The resulting colour shift can be measured at an absorbance of 640nm. Different concentrations of protein (0.5µM and 1µM) and ATP (100µM, 1mM and 10mM) as well as different time point

(5min, 10min and 30 min) and reaction temperatures (RT and 37°C) were tested in combination with 5mM $MgCl_2$, $CaCl_2$, $MnCl_2$ and EDTA. However, no activity was observed with the assay. Standard curves using KH_2PO_4 showed that the assay was not sensitive at low concentrations. Changes of the composition of the malachite green reagent lead to no improvement of sensitivity.

Assuming that the Malachite Green assay was not sensitive enough to detect the ATPase activity of MinD, we looked for other possibilities to measure the activity. We decided to test for the ATP-Glo assay from Biotium. The assay is constructed for the detection of ATP level in cells by coupling ATP to a luciferase reaction that produces a light signal which corresponds to the amount of ATP present in solution. The assay has a detection limit of 0.01 picomole of ATP and is highly sensitive and easy to perform. The MinD ATPase reaction was carried out with 5µM protein, 5mM of the respective divalent metal and 10µM of ATP for 30 min at 37°C. Since the luciferase reaction is dependent of Mg^{2+} the reaction was stopped by heat denaturation of the protein mixture and addition of a final concentration of 10mM EDTA to all the reactions to chelate the added metal ions. Therefore, 12mM $MgCl_2$ were added to the luciferase reaction to circumvent the effects of EDTA. As control we used 10µM ATP in the protein buffer to account for spontaneous hydrolysis of ATP. The values were calculated for amount of ATP in percentage with the ATP only control being 100% of ATP present (Figure 16). Mg^{2+} and Ca^{2+} showed similar activity in the assay with a reduction of the supplied ATP of around 60%. Mn^{2+} activates also the ATPase activity but just leads to a reduction of around 40% compared to the no enzyme control.

In conclusion, the possible *Pf*MinD orthologue displayed characteristic features of the already described MinD proteins of *E. coli* and *A. thaliana*. Upon addition of ATP and divalent metals, it was shown to polymerise and form a complex. Also, it was demonstrated that it binds to ATP upon interaction with divalent metals. The binding and polymerisation effect is furthermore depended on the divalent metal.

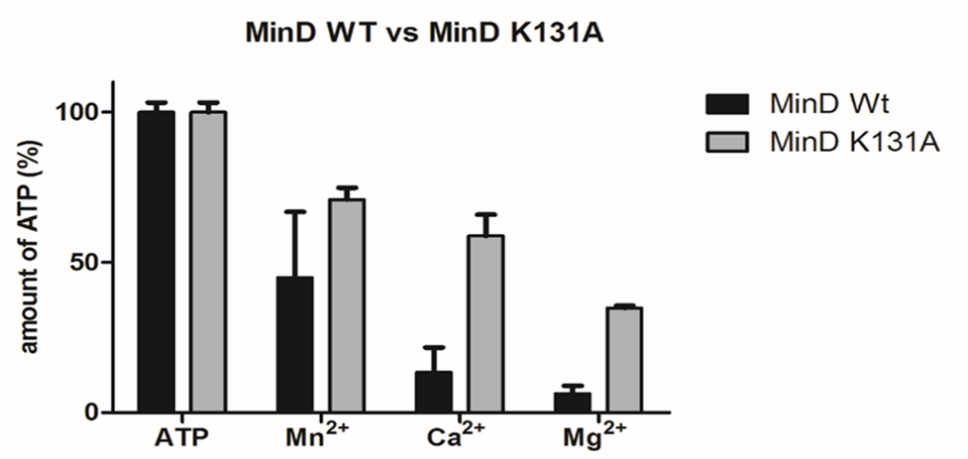

Figure 16: ATP-Glo Assay of *Pf*MinD WT and K131A. For analysing the ATPase activity of *Pf*MinD, the ATP-Glo Cell Viability Assay was used which measures ATP concentration by bioluminescence. The ATPase reaction was carried out with 5mM $MgCl_2$, $CaCl_2$ or $MnCl_2$ and 10µM ATP. As control the reaction was carried out without protein (ATP). The reaction was stopped after 30 min at 37°C. The concentration of ATP was measured by luciferase reaction. The no enzyme reaction was calculated as 100% ATP and the other reactions have been calculated regardingly. The amount of ATP in percentage is plotted.

4.4. Mutation of the Walker A motif leads to change in the ATP depending polymerisation

Several studies have focused on analysing the function and structure of MinD of different organism and thus, have identified which domains are responsible for which function of MinD. Mutation of the Walker A motif in *At*MinD1, more specific the lysine at position 72 to an alanine (K72A), lead to impairment of binding to the substrate ATP and interaction with *At*MinE1 but did not affect the dimerization of the protein (177). Another study which sequenced the genome of several recessive mutation of *A. thaliana* that resulted in altered morphology of the chloroplast could identify the responsible mutation in the *At*MinD1 protein (161). There, the alanine at position 296 is changed to a glycine (A296G) which impairs the polymerisation of *At*MinD1.

We aimed to replicate these two mutations described for *At*MinD1 and characterise their effect on the function of *Pf*MinD. Therefore, the lysine at position 131 was mutated to an alanine (*Pf*MinD K131A) to disrupt the Walker A motif. The polymerisation mutation was

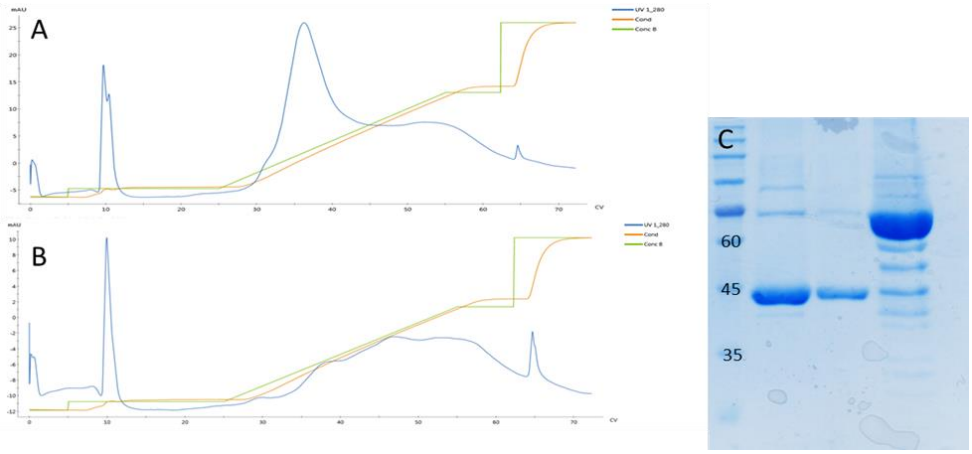

Figure 17: Anion Exchange Chromatography of *Pf*MinD K131A and *Pf*MinD L348G. The mutations were created by site directed mutagenesis and expressed and purified like the wildtype. The histogram of K131 (A) elutes similar to the wildtype while the L348G (B) generates three overlapping peaks. The pooled fractions were analysed by SDS-PAGE stained with Coomassie (C). First line represents *Pf*MinD WT, followed by K131A and L348G. Main part of the L348G fractions contains the chaperone.

created by changing the leucine at position 348 to a glycine (*Pf*MinD L348G). Both mutations were created by site directed mutagenesis using the construct *Pf*MinD-strep in the expression vector pASK-IBA3 as template. The recombinant proteins were expressed and purified as the wildtype protein and verified by Western Blot analysis against the C-terminal Strep-Tag (Figure 11). While MinD K131A expressed similar to the wildtype, the L348G mutation showed reduced expression but therefore a higher expression of the presumably chaperone. Western Blot confirmed the presence of the recombinant proteins at a molecular weight of 50kDa but also detected a weak signal at molecular weight of around 60kDa which matches the purification results obtained for the wildtype MinD-Strep construct.

Since the two mutated recombinant proteins were not able to be further purified like their wildtype counterpart, site direct mutagenesis was performed on the codon-optimised construct of MinD in the pASK-IBA3 vector. Again, the mutated constructs were expressed and purified as described for the wildtype, namely by His-purification followed by AEX (Figure 17). While the K131A mutation expressed and purified similarly to the wildtype construct, the L348G mutation showed again reduced expression. Changing the expression temperature from 37°C for 4 hours to 20°C overnight, slightly increased the expression of

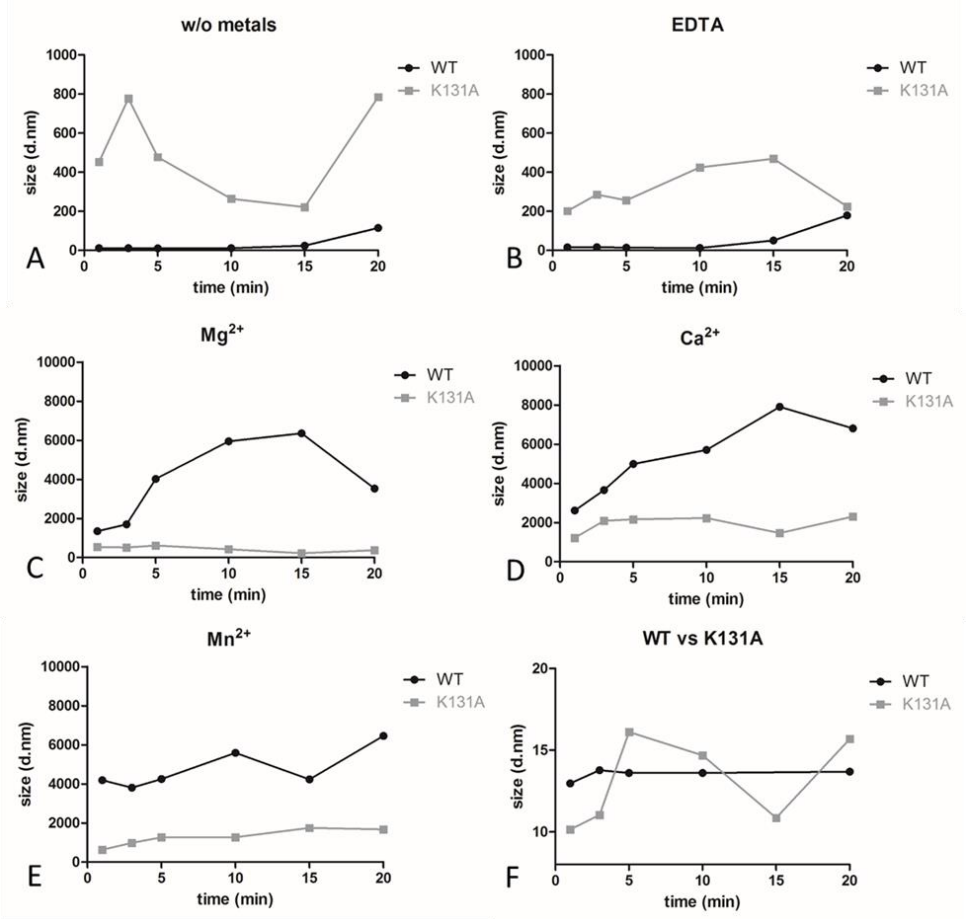

Figure 18: Polymerisation studies of *Pf*MinD K131A by dynamic light scattering. *Pf*MinD K131A was incubated for 20min without metals (A) or 10mM EDTA as control (B) or addition of 5mM $MgCl_2$(C), $CaCl_2$ (D) or $MnCl_2$ at an ATP concentration of 10mM or without any additives (F) and the size was monitored by DLS. Size distribution was plotted against the wildtype. Note that the y axis is scaled differently in A, B and F.

the protein. However, the L348G mutation was not amenable to purification by anion exchange and eluted in three overlapping peaks during the AEX chromatography (Figure 17B). Thus, further analyses were just performed for the K131A mutation.

To analyse the behaviour of the Walker A motif mutant, the purified recombinant MinD K131A protein was analysed by DLS and ATP-Glo Assay.

For polymerisation studies using DLS, the protein was incubated for 20 min without or with 5mM of one of the divalent metals $MgCl_2$, $CaCl_2$ or $MnCl_2$, 10mM EDTA and 10mM ATP

and its size distribution was observed. The highest amount of ATP was chosen because this induced the highest rate of polymerisation in the wildtype protein. The size distribution was plotted against the wildtype for direct comparison (Figure 18). Additionally, the protein was observed without additives over 20 min to check for possible agglomeration of the sample (Figure 18F). Compared to the wildtype, MinD K131A fluctuated slightly more without additives but the size still ranged in between 11nm up to 17nm. No agglomeration was observed; thus the sample was stable in the used conditions. Addition of 10mM ATP induces a stronger polymerisation reaction compared to MinD WT even after addition of EDTA as chelator (Figure 18A,B). Without addition of metals, a size of up to 800nm was observed compared to the size of 160nm of the wildtype. Addition of EDTA reduced polymerisation to a size of around 400nm which was still higher than the observed size of 200nm of the wildtype. It might be that MinD K131A already interacted with metals during expression or purification of the recombinant protein and thus, showed a stronger response towards addition of ATP. EDTA as chelator reduced the polymerisation but could not completely inhibit it. Another option is that MinD K131A is more unstable and tends to aggregate faster than MinD WT. Upon addition of the divalent metals, MinD K131A was able to polymerise, reaching sizes up to 2000nm (Figure 18C-E). However, polymerisation was not as strong as observed for MinD WT which reached sizes up to 7000nm.

The ATP-Glo Assay was performed as described for the wildtype and plotted against it for comparison (Figure 16). MinD K131A was still able to bind to ATP which can be seen by the reduction of ATP from the solution. However, the affinity to ATP is strongly reduced compared to the wildtype, with a reduction of ATP upon addition of $MgCl_2$ of 65% compared to the reduction through the wildtype of 94%. The affinity towards the metals is the same between the mutant and the wildtype with the least reduction achieved by addition of $MnCl_2$, followed by $CaCl_2$ and $MgCl_2$. In conclusion, the mutation of the Walker A motif reduced the affinity towards ATP but the recombinant protein is still able to polymerise and bind to ATP.

4.5. *Pf*MinD localises to the apicoplast within the parasite

The *Pf*MinD orthologue is described in PlasmoDB as the putative cytosolic Fe-S cluster assembly factor NBP35, although sequence analyses predict the bi-partite leader sequence

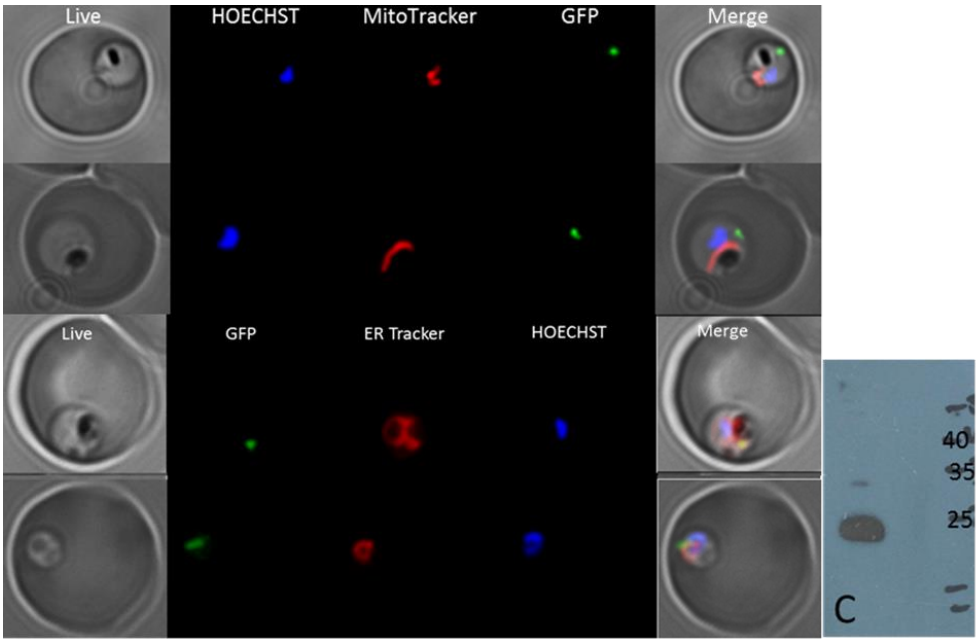

Figure 19: Localisation Studies of a GFP-Chimera with the bipartite leader sequence of MinD. The first four hundred basepairs of the MinD gene were cloned into the pARL 1+ GFP vector and transfected into *P. falciparum* parasites. The GFP signal was detected via fluorescence microscopy and co-localisation with the mitochondrion, endoplasmatic reticulum and nucleus were detected using the respective fluorescence dyes (A and B). Successful transfection was verified by Western Blot of parasites using an antibody against the C-terminal GFP (C).

for targeting into the apicoplast. To verify the exact localisation of MinD within the *P. falciparum* parasite the first four hundred base pairs of the *minD* ORF were cloned into the transfection vector pARL 1a+ which contains a C-terminal GFP and the plasmid was transfected into *P. falciparum* 3D7 ring stage (Table 3). Transgenic parasites were detected after 3 weeks after transfection. The episomal expression of the MinD-GFP chimera was confirmed via Western Blot Analysis (Figure 19C). Two signals have been detected at a molecular mass of about 25 kDa and at 35 kDa. The signal at a molecular mass of 35 kDa presents the GFP chimera of the apicoplast targeting sequence which has been predicted to have a molecular mass of 35 kDa. The signal at 25kDa likely corresponds to the size of GFP which is a common artefact during Western Blot utilizing GFP chimera constructs and GFP antibody.

Localisation studies were performed via live cell fluorescence microscopy using the dyes HOECHST 33342, MitoTracker Red CMX Ros and ER-Tracker Red for co-localisation with the nucleus, mitochondrion and endoplasmic reticulum, respectively (Figure 19). The GFP signal shows no co-localisation with the used markers. Also, it appears as a very well-defined signal which is a characteristic for the apicoplast as described in the literature (113,178,179). In conclusion, the protein seems to be trafficked into the apicoplast of the parasite which is in agreement with the prediction of the protein by applying bioinformatics tools (PlasmoAP).

4.6. MinD overexpression leads to a growth inhibition of the transgenic parasite

To analyse the effect of MinD on the morphology of the apicoplast, transgenic parasites overexpressing MinD wildtype or its mutants were created. Therefore, the ORF of *minD* was cloned into the transfection vector pARL 1a+ containing the *bsd* resistance cassette for selection with blasticidin (BSD). The created constructs were transfected into 3D7 ring stage via electroporation. Transgenic parasites expressing *Pf*MinD Wt and *Pf*MinD L348G were detected after 6 weeks after transfection while transfection with the construct *Pf*MinD K131A failed to recover parasites after blasticidin selection.

Correct expression of the proteins was verified by Western Blot analysis and quantitative real-time PCR (qRT-PCR). Western Blot analysis were performed against the C-terminal myc-Tag of the transgenic parasite using the transgenic parasite line BSD mock which contains the empty pARL 1a+ with the *bsd* resistance cassette as a control.

The effect on the proliferation of overexpression of *Pf*MinD and *Pf*Mind L348G has been tested by growth analysis in comparison to the BSD mock transgenic parasite line as control for blasticidine drug pressure (Figure 20). The growth of the transgenic parasite lines was observed for nine days at was repeated in three biological replicates. Parasitemia was determined daily by flow cytometry using the DNA intercalating dye ethidium bromide. At

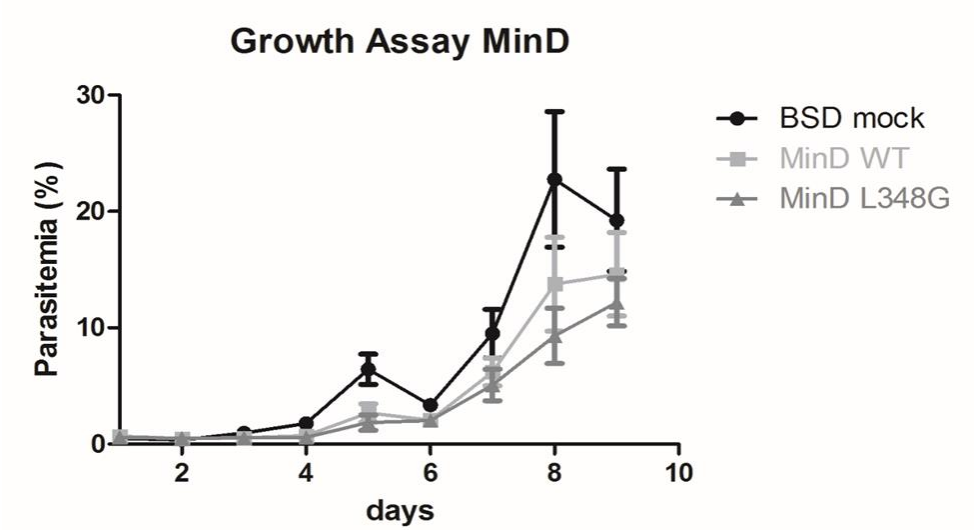

Figure 20: Growth Assay of *Pf*MinD. To study the effect of *Pf*MinD and *Pf*MinD L348G on the proliferation of *P. falciparum* the growth was analysed over the course of nine days. A simple was taken daily and the parasitemia was determined by flow cytometry using the DNA intercalating dye ethidium bromide. The assay was repeated three times with each three technical replicates. As control served the BSD mock line which contains the empty pARL 1a+ vector.

a parasitemia higher than 5%, the cultures were diluted to enable optimal growth. The dilution factor was calculated for each experiments accordingly. Overexpression of *Pf*MinD WT and *Pf*MinD L348G showed minor inhibition of the growth compared to the BSD mock line which were however not significant. After 9 days, the BSD mock line reached a parasitemia of 19% while *Pf*MinD Wt reached 14% and *Pf*MinD L348G reached 12%. Thus, overexpression of *Pf*MinD seems to have an effect on the vitality of the parasite leading to inhibition in growth. However, what exactly *Pf*MinD is influencing is not clear yet.

4.7. The apotome technique as tool for apicoplast visualisation

The aim of the project was also to determine the effect of *Pf*MinD on the morphology of the apicoplast. Thus, small changes in morphology and volume of this small organelle have to be visualised by sensitive techniques of fluorescence microscopy. Additionally, we aimed to follow the apicoplast over the entire erythrocytic life cycle which can be achieved by live

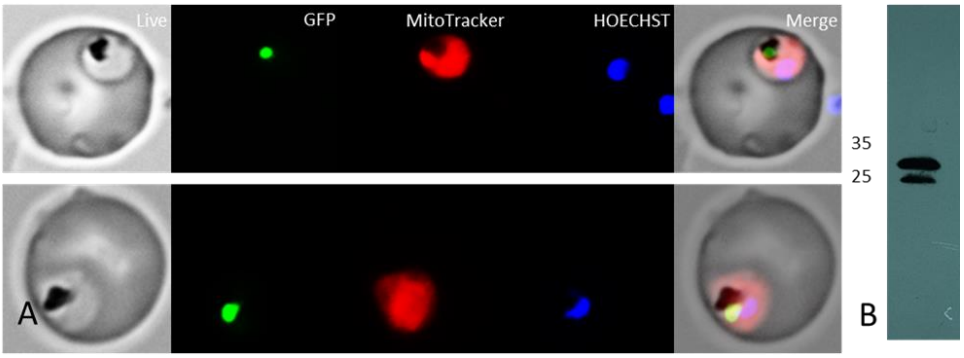

Figure 21: Fluorescence Images and Western Blot of the reference line PDH E1α. As reference line for the analysis of the apicoplast morphology the construct PDH E1α was tagged with GFP and transfected into *the P. falciparum* 3D7 parasite. (A) Localisation for the GFP signal was performed by live cell fluorescence microscopy by co-localisation with the MitoTracker and Hoechst. Presence of PDH E1α was verified by Western Blot analysis using antibody against the C-terminal GFP (B).

cell fluorescence imaging. No dye is available to stain the apicoplast yet and techniques to visualise the apicoplast relate to immunofluorescence or electron microscopy with the use of specific antibodies. These techniques depend on the fixation of the parasite which is known to be difficult for *Plasmodium* because it might destroy structures within the parasite. For live cell imaging, GFP has to be targeted to the apicoplast by tagging it to a protein targeted to the apicoplast. *Pf*MinD has been shown to be localised to the apicoplast, however, GFP might interfere with the polymerisation and association of *Pf*MinD to the inner organelle membrane. Hence, another transgenic parasite line had to be utilised for visualisation of the apicoplast which will be then transfected additionally with the *Pf*MinD transfection constructs.

The transgenic parasite line of the pyruvate dehydrogenase (PDH) E1α subunit was chosen as reference line for apicoplast morphology. The transgenic parasite line has been previously described to target PDH E1α to the apicoplast (178). The transfection construct, consisting of the PDH E1α subunit tagged with a C-terminal GFP in the transfection vector pARL 1a+ containing the *hDHFR* resistance cassette for selection with the WR99210 drug, was provided for this study. The plasmid was transfected into *P. falciparum* 3D7 ring stage and transgenic parasites appeared after 3 weeks of transfection (Table 3). The episomal expression of the PDH E1α-GFP chimera was confirmed via Western Blot Analysis against the C-terminal GFP-Tag (Figure 21B) and corresponds with the signals detected and

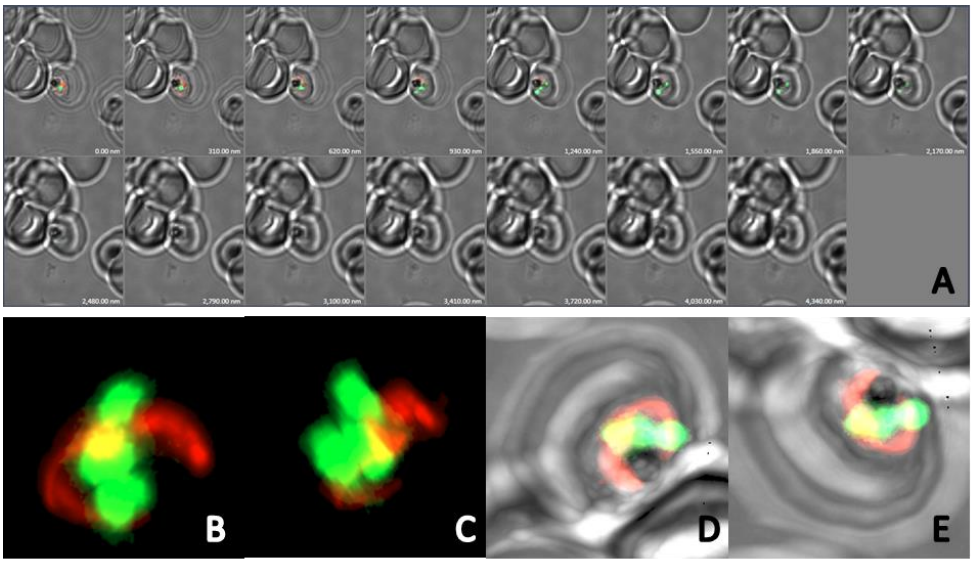

Figure 22: : Z-Stack and 3D images of PDH E1α. With the reference line PDH E1α fluorescence images were taken using the Apotome.2 technique and the Z-stack to create 3D images. (A) The Z-stack was chosen to span 8µm in the interval of 0.3µm for GFP. MitoTracker and Brightfield. (B-E) From these pictures a 3D model was created which can be visualised in different angles and also just for specific channels, like just GFP and MitoTracker (B and C) or all channels combined (D and E).

published in the previous study of Chan *et al.* (2013)(178) . Localisation studies for PDH E1α using live cell fluorescence microscopy with the markers HOECHST 33342 and MitoTracker Red CMX Ros for the nucleus and mitochondrion, respectively were performed to further verify the correct targeting to the apicoplast (Figure 21A). The images show no co-localisation for PDH E1α with the stained organelles and the well-defined GFP signal confirmed localisation in the apicoplast like described before (178). Thus, PDH E1α was a suitable reference line for the visualisation of the apicoplast morphology during the erythrocytic life cycle.

With the reference line chosen, the visualisation method had to be established which was performed with the Zeiss Axio Observer Z1 equipped with Apotome technique. This technique reduces greatly the background of three dimensional specimens by a specific illumination pattern (Figure 9). In combination with Z-stacking, where several photos in different Z-dimension are taken, a three dimensional model of the apicoplast could be achieved. The technique was established using the PDH E1α line (Figure 22). Z-stacks were

chosen to span 8µm which corresponds to the size of the erythrocyte in intervals of 0.3µm, and five photos were taken per plane by Apotome to greatly enhance the resolution of the observed signal. Additional to the GFP signal of the reference line, MitoTracker Red CMX Ros and Brightfield were visualised. By applying the Zeiss Zen 2.6 software, the three dimensional model was created (Figure 22B-E).

HOECHST turned out to be problematic for the Apotome technique. Upon use of Apotome, the fluorescence signal is greatly reduced due to the specific illumination pattern in use. Hence, the exposure time had to be increased. Upon repetitive illumination of the specimen, HOECHST started to leak from the nucleus which was strongly visible in the 3D model. When the exposure time was reduced, the HOECHST signal was difficult to observe and created a high background for the model. This problem was not observed for the MitoTracker which generated a stronger and sharper signal than HOECHST and was longer photostable. The same applies to the GFP signal of the reference line. Upon creation of the 3D model, the shape and connection between the apicoplast and mitochondrion were visible and clearly defined. However, further rendering of the 3D model and the determination of the volume of the apicoplast were not possible since the correct software was not available in time. Nevertheless, the equipment was sufficient to accomplish the task of visualising and analysing subtle changes in the morphology of even small compartments of the parasite.

DISCUSSION

The fast and coordinated treatment of malaria with antimalarial drugs have reduced the global malaria burden of 40% in the last seven years (2). Unfortunately, full or partial resistance have been reported for all current antimalarial drugs and new drugs are not excepted to hit the market before 2020. Upon its discovery, the chloroplast-like organelle of the *Plasmodium* parasite, called apicoplast, became an oasis for new possible drug targets and the focus for drug discovery. The apicoplast-localised metabolic pathways have been shown to be essential during different stages of the complex life cycle of *Plasmodium*. Due to its prokaryotic origins, these metabolic pathways differ considerably from the human host and thus, can be exploited for drug discovery.

Like the chloroplast, the apicoplast cannot be created *de novo*, but rather have to be evenly distributed between daughter cells. The *Plasmodium* parasite replicates by schizogony in its asexual stage of the life cycle, undergoing multiple fission of the nucleus before distribution of its organelles and the formation of the newly formed merozoites. How the parasite is distributing their organelles evenly during schizogony remains an open question in malaria research.

Visualisation of the apicoplast by live cell fluorescence imaging has shed some light on the morphological changes during the erythrocytic stage of *Plasmodium* and its close connection to the mitochondrion (113) but not on the molecular mechanism behind it. Studies in *Toxoplasma gondii*, another closely related Apicomplexan, have tried to answer this question (180,181). By means of fluorescence microscopy and electron microscopy, the studies reported an undefined structure localised with the apicoplast during the division. However, the conclusion of the nature of this structure differs in both studies. While the first study suggests an association of the nucleoid of the apicoplast with the centrosome and the division by the mitotic spindle (180), the other group postulates that the force generated by the mitotic spindle is not strong enough for division of the apicoplast and postulate the structure as a plastid-dividing ring similar to the one found in the chloroplast (181). Further elucidation of the structure by microscopy was not possible and has also been proven to be difficult for the division machinery of bacteria. Conventional fluorescence microscopy depicts the Z-ring as a continuous ring by uniform density (182,183). This was proven wrong by *in vitro* studies which demonstrate that FtsZ forms bundles of protofilaments. For visualization of the dynamic behaviour between FtsZ and the Min system *in vivo*, the spatial

resolution of conventional fluoresecene microscopy is not sufficient. Thus, reconstruction of this dynamic system was performed *in vitro* on articifical lipid mono- or bilayers or lipid vesicles (184,185). However, advances in microscopy techniques have shown first successful attempts to visualise Z-ring formation *in vivo* (186).

Thus, microscopy was not able to define the true nature of the structure observed in *T. gondii*. Also, none of the main components of the chloroplast division machinery have been discovered yet in either *Toxoplasma gondii* or *Plasmodium falciparum*.

This study aimed to describe a possible MinD orthologue of *Plasmodium falciparum*. This protein is listed as putative cytosolic Fe/s assembly factor NBP35 in the PlasmoDB. The protein displays the characteristic Walker A motif which indicates it as an ATPase and the C-terminal polymerisation site and the membrane-targeting sequence (MTS) described for the MinD protein. Furthermore, the N-terminal bipartite leader sequence for trafficking into the apicoplast has been predicted by the bioinformatics tool PlasmoAP.

5.1. PF3D7_0910800 - Could it be *Pf*MinD?

The role of MinD is to enhance the activity of MinC and transport it along the inner cell membrane (187,188). Therefore, it binds to ATP, changing its conformation, associating to the cell membrane and forming a complex with MinC. We were able to show that *Pf*MinD polymerise upon addition of ATP, an effect, which was correlated to the ATP concentration used and enhanced by addition of Ca^{2+}. Unlike most ATPases, *At*MinD1 evolved to be stimulated by Ca^{2+} which is abundant in the chloroplast of plants (177). ATPase activity has been shown to be enhanced by Ca^{2+} in comparison to other divalent metals in *At*MinD1 showing a ~5fold increase of activity compared to Mg^{2+}. Polymerisation studies of *Pf*MinD with Ca^{2+}, Mg^{2+} and Mn^{2+} showed strong polymerisation compared to the protein without any addition of metals or with EDTA as chelators for metals in solution.

*At*MinD1 has been described as a weak ATPase which is enhanced by *At*MinE1 by ~3fold (177). Thw Malachite Green Assay which is a standard assay for detection of free inorganic phosphate showed no activity for *Pf*MinD. Reducing the ATP concentration during the assay reached the detection limit and proved to be too insensitive to measure at such low concentrations of ATP. Instead, the ATP-Glo Assay was used which is a cell viability assay

for detection of ATP in cells. The assay is highly sensitive (down to 0.01 picomole of ATP) and thus can be used at low concentrations of ATP. The assay showed ATPase activity of *Pf*MinD in comparison to the no enzyme control containing only ATP. The results reflected the findings of the polymerisation study. Mg^{2+} and Ca^{2+} are both enhancing the activity of MinD leading to a reduction of supplied ATP of 94% and 87%, respectively. Mn^{2+} also shows an effect which is weaker compared to the other divalent metals tested. Thus, we demonstrated that *Pf*MinD is able to bind to ATP and polymerise into a complex upon addition of ATP and divalent metals.

However, the ATP-Glo assay is not optimal for detection of hydrolysis of ATP since it only measures its presence in the reaction. What the *Pf*MinD exactly does with its substrates remains unclear. Does the protein bind the ATP in its high energy state? Or does it hydrolyse it to form the complex? Upon hydrolysis, does it release ADP, AMP, PPi or free phosphate? The ATP-Glo simply cannot answer all these questions. Again, the Malachite Green Assay and ADP detection Kits showed no activity at all. Unfortunately, we could not identify a possible MinE orthologue in *P. falciparum* so far. Thus, enhancing the ATPase activity by its natural partner is impossible by now. It is also possible that *Pf*MinE does not exist and that *Pf*MinD functions alone.

Polymerisation studies have demonstrated an increase in size upon addition of ATP and divalent metals. However, the nature of the size increase cannot be visualised by dynamic light scattering. Thus, we do not know if the recombinant protein simply agglomerates or creates filamentous complex like described for *Ec*MinD and *Ec*MinC (189). Electron microscopy revealed the building complex of these two Min proteins upon interaction with ATP and phospholipids. So, it would be interesting to visualise the forming complex of *Pf*MinD which reaches sizes up to 7000nm and also observe its interaction with phospholipids.

Mutational studies of *At*MinD1 revealed two mutations which impair their behaviour toward ATP (161,177). We aimed to recreate these two mutation for *Pf*MinD and characterise the change in their behaviour. The K131A mutation aimed to impair the Walker A motif and hence, the hydrolysis of the substrate ATP. The second mutation L348G was aimed to disrupt the polymerisation site. While the Walker A motif is highly conserved in *Pf*MinD, the polymerisation site was more difficult to identify and the site of mutation was

chosen by using different alignment tools. Both mutations were successfully created, however, the L348G failed to purify without the chaperone. Additional purification steps and *E. coli* expression cell lines have to be tested to express and purify the mutation successfully.

Surprisingly, the K131A mutation did not lead to disruption of the Walker A motif as described for *At*MinD1 and *Ec*MinD (190,191) but only decreased its function. The mutated protein reacted to addition of ATP but in a lesser response than the wildtype protein. Mutation analysis of *Ec*MinD reported a total loss of activity for the K16Q mutation (191). However, mutation of the glycine at positions 15 to a serine (G15S) was reported to have less activity than the wildtype *Ec*MinD (191) which reflects the results obtained in this study. It is possible that the single point mutation was not sufficient to disrupt the Walker A motif of *Pf*MinD due to structural differences of the two orthologues. Unfortunately, *Pf*MinD was too unstable to be crystallised to compare and identify structural differences. Additional mutational analysis or mutation of several amino acids of the Walker A motif as done for *Ec*MinD might identify the responsible site for ATP interaction.

In conclusion, the studied *Pf*MinD displays characteristic behaviour attributed to MinD. The protein polymerises upon addition of its substrate ATP which is enhanced by the addition of divalent metals. It is able to bind ATP, although hydrolysis of ATP could not be shown. Lastly, it is targeted to the apicoplast inside the *Plasmodium* parasite.

5.2. The protein interference assay as evaluation tool for the effect of *Pf*MinD

Evaluation of the effect of *Pf*MinD inside the parasite were performed by protein interference assay (PIA) (192). This technique takes advantage of the oligomeric conformation of the targeted protein. In theory, upon overexpression of a mutated version of the studied protein, the native protein within the parasite interacts with the overexpressed mutated version, forming heteropolymers and rendering the complex inactive. Thus, the PIA can achieve a downregulation of the native protein. This technique has been successfully established and verified for use in *P. falciparum* (193). In this study, we aimed for downregulation of the native MinD by interaction with the two mutations K131A and

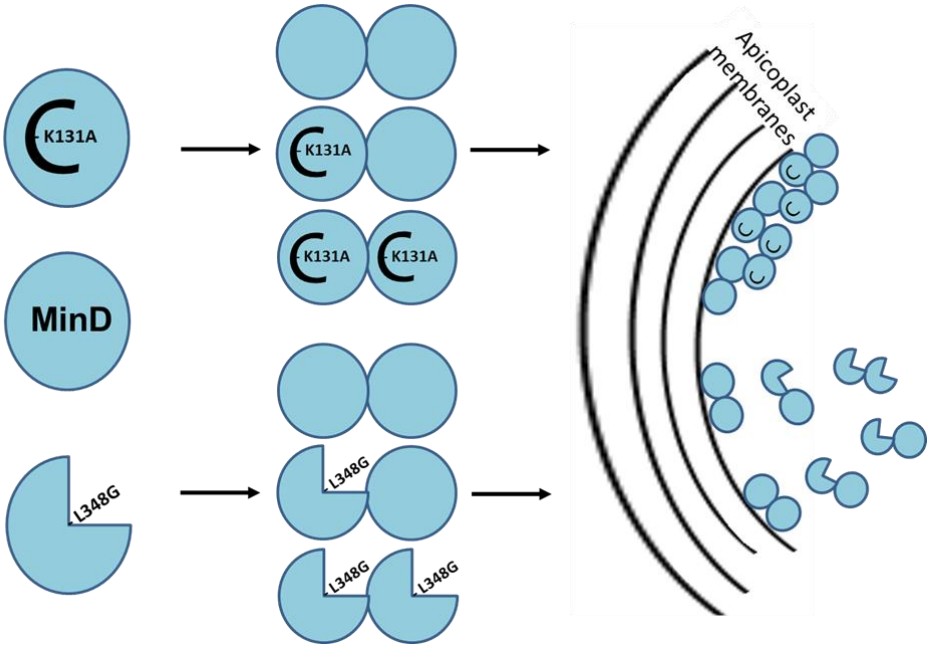

Figure 23: Protein Interference Assay of *Pf*MinD. The PIA makes use of the oligomeric state of a protein for downregulation on the protein level. In the case of MinD, the mutated versión K131A and L348G can interact with the native wildtype protein produced from the parasite. The formed complex is rendered inactive and thus, the native level of active protein in *P. falciparum* is downregulated. In case of K131A, the ATPase activity should be impaired. Mutation L348G impairs the association to the membrane.

L348G (Figure 23). Interaction with the K131A mutation should form a complex which is supposed to be unable to hydrolyse ATP and thus, be removed from the inner organelle membrane which produces an enlarged apicoplast who fails to divide. Interaction with the L348G mutation renders the complex unable to polymerise and associate to the inner organelle membrane and creating a minicell phenotype for the apicoplast. Overexpression of MinD WT should result in an enlarged apicoplast as described for overexpression of *At*MinD1 leads to enlarged chloroplasts (149).

Transgenic parasite lines expressing either *Pf*MinD WT, K131A and L348G conferring blasticidin resistance were generated for the study. Transfection was standardly performed into ring stage parasites by electroporation and drug pressure, in this case with 1µg/ml blasticidin, is applied after 24 hours after transfection. With this method, transgenic parasites appear after three to four weeks after transfection. However, transgenic parasites

carrying the MinD constructs only appeared after 7 weeks while the MinD K131A failed to appear at all even after repeated attempts of transfection. The observed time and voltage during the electroporation was concurrent with what is considered normal in the literature (194). Thus, we can only speculate why the MinD K131A failed to produce transgenic parasites. It might be that the PIA effect on the parasite was so strong that transgenic parasites were not viable. Also, the other MinD constructs appeared rather late after transfection. Plasmid preparation for transfection was performed with Qiagen Plasmid Kit, so the preparation was of sufficient quality and quantity.It was even demonstrated that transfection of Plasmodium is possible with plasmids prepaired by non-commerically means and Mini preparations (195). Blasticidin has already been used successfully as selection marker for transgenic parasite and thus, should not contribute to the difficulties in transfection (193).

Due to these difficulties in transfection, we suspected an effect of *Pf*MinD on the proliferation of the parasite. And in fact, the transgenic parasite lines demonstrated a slower growth of the parasite compared to the BSD mock line. Although the inhibitory effect was not significant, it was visible under normal culture conditions and might explain the late appearance of these transgenic parasite lines after transfection.

5.3. How to successfully visualise the apicoplast of *P. falciparum*

Imaging of the parasite plays an important role in malaria research. Up to date, the common method for the diagnostic detection of malaria is by light microscopy of a thick blood smear stained by Giemsa staining. The use of transgenic parasite lines expressing GFP have greatly contributed to understanding the cellular compartments and metabolic pathways of the parasite. As with other protozoans, imaging of *Plasmodium* does not come without its difficulties. Resolution after fixation of the parasite for immunofluorescence or electron microscopy is known to be poor and might destroy the intracellular structures under study. Fluorescent protein encoding genes like GFP have to be introduced into the parasite or even integrated into its genome which is still a time-consuming and inefficient process (196). In the case of visualisation of the apicoplast, there is no choice but to use either fluorescent

proteins or antibodies directed against protein targeted to the apicoplast because no dye is available yet.

We chose to not tag the MinD directly with GFP which might interfere with its function as reported for other division components. Fusion of the FtsZ protein with GFP does not impair the formation of protofilaments but the anchoring to the membrane by the FtszA and ZipA in *E. coli* (197) *At*FtsZ2-1 fused to GFP failed to produce a fluorescence signal in the chloroplast or plant cell but this can be related to problems in the identification of the exact open reading frame of this protein (182). N-terminal fusion of GFP to MinD did not effect its binding to MinC in *E. coli* (198). However, in the chloroplast and also apicoplast, the N-terminus is definied by the leader sequence for targeting into the respective organelle. Fusion to fluorescence proteins to *At*MinD1 was performed for localisation studies, but for overexpression studies smaller tags were chosen (199,200). So, a reference line had to be used to mark the apicoplast. The line chosen was the pyruvate dehydrogenase (PDH) E1α subunit tagged with GFP. PDH is part of the pathway for synthesis of fatty acids and although expressed during the erythrocytic stage, it is not essential in it (97). Thus, expression of (PDH) E1α subunit tagged with GFP should not interfere with the behaviour of *P. falciparum* in the blood stage.

Visualisation using the verified reference line and the newly established Apotome technique proved to be successful. The fluorescence signal of the apicoplast was rendered into a 3D model which demonstrated the size and shape of the organelle. Co-imaging of the mitochondrion by MitoTracker showed its close proximity to the apicoplast. However, imaging of the nucleus by HOECHST proved difficult due to the long exposure time and the low photostability of the dye inside the parasite. To visualise the nucleus would have served as a good control to differentiate between the forms of the blood stages, namely ring, trophozoite and schizont for the later analysis of the volume of the apicoplast. Nevertheless, the mitochondrion could be utilised as control as well, because it is the last organelle to be divided in the schizont (113). Also, it was shown that the mitochondrion behaves similar to the apicoplast during the development in the blood stage. In conclusion, we demonstrated that the Apotome technique is strong enough to generate highly resolution images of the apicoplast which is necessary to the study its morphology upon influence of *Pf*MinD.

CONCLUSION

In this study, we aimed to characterise a possible MinD orthologue of *Plasmodium falciparum*. We aimed to characterise its function by recombinant protein, the localisation inside the parasite and its effect on the morphology and division of the apicoplast.

We showed that the protein displayed typical behaviour of MinD by studying its affinity towards the substrate ATP. The recombinant protein was able to bind ATP and form large complexes upon binding. Also, the function could be disturbed by targeted mutation of the responsible domains. Sadly, the recombinant was rather unstable and tended to aggregate at high concentrations which made crystallisation studies unsuccessful. The MinD orthologue localised to the apicoplast in *P. falciparum* and resulted in an inhibitory effect on the growth of the parasite. The reference line which targets the fluorescence protein GFP to the apicoplast and techniques for visualisation of the organelle have been successfully established for analysis of its morphology. Thus, analysation of the morphology can be performed in the future.

BIBLIOGRAPHY

1. Cox FE. History of the discovery of the malaria parasites and their vectors. Parasit. Vectors 2010;3:5.

2. Anon. WHO | World malaria report 2018. WHO 2018.

3. Ta TH, Hisam S, Lanza M, Jiram AI, Ismail N, Rubio JM. First case of a naturally acquired human infection with Plasmodium cynomolgi. Malar. J. 2014;13:68.

4. Lacerda MVG, Fragoso SCP, Alecrim MGC, Alexandre MAA, Magalhães BML, Siqueira AM, Ferreira LCL, Araújo JR, Mourão MPG, Ferrer M, Castillo P, Martin-Jaular L, Fernandez-Becerra C, del Portillo H, Ordi J, Alonso PL, Bassat Q. Postmortem Characterization of Patients With Clinical Diagnosis of Plasmodium vivax Malaria: To What Extent Does This Parasite Kill? Clin. Infect. Dis. 2012;55:e67–e74.

5. Douglas NM, Pontororing GJ, Lampah DA, Yeo TW, Kenangalem E, Poespoprodjo JR, Ralph AP, Bangs MJ, Sugiarto P, Anstey NM, Price RN. Mortality attributable to Plasmodium vivax malaria: a clinical audit from Papua, Indonesia. BMC Med. 2014;12:217.

6. Carter R, Mendis KN. Evolutionary and historical aspects of the burden of malaria. Clin. Microbiol. Rev. 2002;15:564–94.

7. Roberts L, Enserink M. MALARIA: Did They Really Say ... Eradication? Science (80-.). 2007;318:1544–1545.

8. Amino R, Thiberge S, Martin B, Celli S, Shorte S, Frischknecht F, Ménard R. Quantitative imaging of Plasmodium transmission from mosquito to mammal. Nat. Med. 2006;12:220–224.

9. Jones MK, Good MF. Malaria parasites up close. Nat. Med. 2006;12:170–171.

10. Tavares J, Formaglio P, Thiberge S, Mordelet E, Van Rooijen N, Medvinsky A, Ménard R, Amino R. Role of host cell traversal by the malaria sporozoite during liver infection. J. Exp. Med. 2013;210:905–915.

11. Ejigiri I, Sinnis P. Plasmodium sporozoite–host interactions from the dermis to the hepatocyte. Curr. Opin. Microbiol. 2009;12:401–407.

12. Sturm A, Amino R, van de Sand C, Regen T, Retzlaff S, Rennenberg A, Krueger A, Pollok J-M, Menard R, Heussler VT. Manipulation of Host Hepatocytes by the Malaria Parasite for Delivery into Liver Sinusoids. Science (80-.). 2006;313:1287–1290.

13. Adams JH, Mueller I. The Biology of Plasmodium vivax. Cold Spring Harb. Perspect.

Med. 2017;7:a025585.
14. Weiss GE, Gilson PR, Taechalertpaisarn T, Tham W-H, de Jong NWM, Harvey KL, Fowkes FJI, Barlow PN, Rayner JC, Wright GJ, Cowman AF, Crabb BS. Revealing the Sequence and Resulting Cellular Morphology of Receptor-Ligand Interactions during Plasmodium falciparum Invasion of Erythrocytes Blackman MJ, editor. PLOS Pathog. 2015;11:e1004670.
15. Chitnis CE. Molecular insights into receptors used by malaria parasites for erythrocyte invasion. Curr. Opin. Hematol. 2001;8:85–91.
16. Cowman AF, Healer J, Marapana D, Marsh K. Malaria: Biology and Disease. Cell 2016;167:610–624.
17. Malleret B, Li A, Zhang R, Tan KSW, Suwanarusk R, Claser C, Cho JS, Koh EGL, Chu CS, Pukrittayakamee S, Ng ML, Ginhoux F, Ng LG, Lim CT, Nosten F, Snounou G, Rénia L, Russell B. Plasmodium vivax: restricted tropism and rapid remodeling of CD71-positive reticulocytes. Blood 2015;125:1314–24.
18. Langhi DM, Orlando Bordin J. Duffy blood group and malaria. Hematology 2006;11:389–398.
19. Josling GA, Williamson KC, Llinás M. Regulation of Sexual Commitment and Gametocytogenesis in Malaria Parasites. Annu. Rev. Microbiol. 2018;72:501–519.
20. Brancucci NMB, Gerdt JP, Wang C, De Niz M, Philip N, Adapa SR, Zhang M, Hitz E, Niederwieser I, Boltryk SD, Laffitte M-C, Clark MA, Grüring C, Ravel D, Blancke Soares A, Demas A, Bopp S, Rubio-Ruiz B, Conejo-Garcia A, Wirth DF, Gendaszewska-Darmach E, Duraisingh MT, Adams JH, Voss TS, Waters AP, Jiang RHY, Clardy J, Marti M. Lysophosphatidylcholine Regulates Sexual Stage Differentiation in the Human Malaria Parasite Plasmodium falciparum. Cell 2017;171:1532-1544.e15.
21. Joice R, Nilsson SK, Montgomery J, Dankwa S, Egan E, Morahan B, Seydel KB, Bertuccini L, Alano P, Williamson KC, Duraisingh MT, Taylor TE, Milner DA, Marti M. Plasmodium falciparum transmission stages accumulate in the human bone marrow. Sci. Transl. Med. 2014;6:244re5-244re5.
22. Ikemoto T. Tropical malaria does not mean hot environments. J. Med. Entomol. 2008;45:963–9.
23. Ilunga-Ilunga F, Levêque A, Dramaix M. Influence de l'âge et du niveau de transmission

sur l'expression clinique et biologique du paludisme grave de l'enfant. Arch. Pédiatrie 2016;23:455–460.
24. Idro R, Aloyo J, Mayende L, Bitarakwate E, John CC, Kivumbi GW. Severe malaria in children in areas with low, moderate and high transmission intensity in Uganda. Trop. Med. Int. Heal. 2006;11:115–124.
25. DOBBS KR, DENT AE. Plasmodium malaria and antimalarial antibodies in the first year of life. Parasitology 2016;143:129–138.
26. Luxemburger C, Ricci F, Nosten F, Raimond D, Bathet S, White NJ. The epidemiology of severe malaria in an area of low transmission in Thailand. Trans. R. Soc. Trop. Med. Hyg. 91:256–62.
27. Wassmer SC, Grau GER. Severe malaria: what's new on the pathogenesis front? Int. J. Parasitol. 2017;47:145–152.
28. Newbold C, Craig A, Kyes S, Rowe A, Fernandez-Reyes D, Fagan T. Cytoadherence, pathogenesis and the infected red cell surface in Plasmodium falciparum. Int. J. Parasitol. 1999;29:927–37.
29. Baruch DI. Adhesive receptors on malaria-parasitized red cells. Baillieres. Best Pract. Res. Clin. Haematol. 1999;12:747–61.
30. Chen Q, Schlichtherle M, Wahlgren M. Molecular Aspects of Severe Malaria. Clin. Microbiol. Rev. 2000;13:439–450.
31. Baruch DI, Pasloske BL, Singh HB, Bi X, Ma XC, Feldman M, Taraschi TF, Howard RJ. Cloning the P. falciparum gene encoding PfEMP1, a malarial variant antigen and adherence receptor on the surface of parasitized human erythrocytes. Cell 1995;82:77–87.
32. Smith JD, Chitnis CE, Craig AG, Roberts DJ, Hudson-Taylor DE, Peterson DS, Pinches R, Newbold CI, Miller LH. Switches in expression of plasmodium falciparum var genes correlate with changes in antigenic and cytoadherent phenotypes of infected erythrocytes. Cell 1995;82:101–110.
33. Su XZ, Heatwole VM, Wertheimer SP, Guinet F, Herrfeldt JA, Peterson DS, Ravetch JA, Wellems TE. The large diverse gene family var encodes proteins involved in cytoadherence and antigenic variation of Plasmodium falciparum-infected erythrocytes. Cell 1995;82:89–100.
34. Recker M, Buckee CO, Serazin A, Kyes S, Pinches R, Christodoulou Z, Springer AL,

Gupta S, Newbold CI. Antigenic variation in Plasmodium falciparum malaria involves a highly structured switching pattern. PLoS Pathog. 2011;7:e1001306.
35. Ukaegbu UE, Zhang X, Heinberg AR, Wele M, Chen Q, Deitsch KW. A Unique Virulence Gene Occupies a Principal Position in Immune Evasion by the Malaria Parasite Plasmodium falciparum Wahlgren M, editor. PLOS Genet. 2015;11:e1005234.
36. Taylor TE, Molyneux ME. The pathogenesis of pediatric cerebral malaria: eye exams, autopsies, and neuroimaging. Ann. N. Y. Acad. Sci. 2015;1342:44–52.
37. Finney CAM, Lu Z, Hawkes M, Yeh W-C, Liles WC, Kain KC. Divergent roles of IRAK4-mediated innate immune responses in two experimental models of severe malaria. Am. J. Trop. Med. Hyg. 2010;83:69–74.
38. Brabin BJ. An analysis of malaria in pregnancy in Africa. Bull. World Health Organ. 1983;61:1005–16.
39. Walker PGT, Griffin JT, Cairns M, Rogerson SJ, van Eijk AM, ter Kuile F, Ghani AC. A model of parity-dependent immunity to placental malaria. Nat. Commun. 2013;4:1609.
40. King LS. Mosquitoes, Malaria and Man: A History of the Hostilities Since 1880. JAMA J. Am. Med. Assoc. 1978;240:2331.
41. Breman JG, Mills A, Snow RW, Mulligan J-A, Lengeler C, Mendis K, Sharp B, Morel C, Marchesini P, White NJ, Steketee RW, Doumbo OK. Conquering Malaria. 2006.
42. Teutsch SM, Liu S, Choi HW, Breman JG, Hightower AW, Sexton JD. The Effectiveness of Insecticide-Impregnated Bed Nets in Reducing Cases of Malaria Infection: A Meta-Analysis of Published Results. Am. J. Trop. Med. Hyg. 1995;52:377–382.
43. Hassall KA. The chemistry of pesticides: their metabolism, mode of action and uses in crop protection. Chem. Pestic. their Metab. mode action uses Crop Prot. 1982.
44. Anon. WHO | WHO gives indoor use of DDT a clean bill of health for controlling malaria. WHO 2010.
45. Andrews KT, Fisher G, Skinner-Adams TS. Drug repurposing and human parasitic protozoan diseases. Int. J. Parasitol. Drugs Drug Resist. 2014;4:95–111.
46. Foley M, Tilley L. Quinoline antimalarials: mechanisms of action and resistance and prospects for new agents. Pharmacol. Ther. 1998;79:55–87.
47. Jana S, Paliwal J. Novel molecular targets for antimalarial chemotherapy. Int. J. Antimicrob. Agents 2007;30:4–10.

48. Sharma A, Mishra NC. Inhibition of a protein tyrosine kinase activity in Plasmodium falciparum by chloroquine. Indian J. Biochem. Biophys. 1999;36:299–304.
49. Olliaro P, Taylor WR, Rigal J. Controlling malaria: challenges and solutions. Trop. Med. Int. Health 2001;6:922–7.
50. Petersen I, Eastman R, Lanzer M. Drug-resistant malaria: Molecular mechanisms and implications for public health. FEBS Lett. 2011;585:1551–1562.
51. Ecker A, Lehane AM, Clain J, Fidock DA. PfCRT and its role in antimalarial drug resistance. Trends Parasitol. 2012;28:504–514.
52. Gregson A, Plowe C V. Mechanisms of Resistance of Malaria Parasites to Antifolates. Pharmacol. Rev. 2005;57:117–145.
53. Gamo F-J. Antimalarial drug resistance: new treatments options for Plasmodium. Drug Discov. Today Technol. 2014;11:81–88.
54. Severini C, Menegon M. Resistance to antimalarial drugs: An endless world war against Plasmodium that we risk losing. J. Glob. Antimicrob. Resist. 2015;3:58–63.
55. Graves PM, Gelband H, Garner P. Primaquine or other 8-aminoquinoline for reducing *P. falciparum* transmission. In: Graves PM, editor Cochrane Database Syst. Rev. Chichester, UK: John Wiley & Sons, Ltd; 2014. p CD008152.
56. Wongsrichanalai C, Sibley CH. Fighting drug-resistant Plasmodium falciparum: the challenge of artemisinin resistance. Clin. Microbiol. Infect. 2013;19:908–16.
57. Kaur K, Jain M, Reddy RP, Jain R. Quinolines and structurally related heterocycles as antimalarials. Eur. J. Med. Chem. 2010;45:3245–3264.
58. Tilley L, Straimer J, Gnädig NF, Ralph SA, Fidock DA. Artemisinin Action and Resistance in Plasmodium falciparum. Trends Parasitol. 2016;32:682–696.
59. Wells TNC, van Huijsduijnen RH, Van Voorhis WC. Malaria medicines: a glass half full? Nat. Rev. Drug Discov. 2015;14:424–442.
60. Noedl H, Se Y, Schaecher K, Smith BL, Socheat D, Fukuda MM, Artemisinin Resistance in Cambodia 1 (ARC1) Study Consortium. Evidence of Artemisinin-Resistant Malaria in Western Cambodia. N. Engl. J. Med. 2008;359:2619–2620.
61. Dondorp AM, Nosten F, Yi P, Das D, Phyo AP, Tarning J, Lwin KM, Ariey F, Hanpithakpong W, Lee SJ, Ringwald P, Silamut K, Imwong M, Chotivanich K, Lim P, Herdman T, An SS, Yeung S, Singhasivanon P, Day NPJ, Lindegardh N, Socheat D, White

NJ. Artemisinin Resistance in *Plasmodium falciparum* Malaria. N. Engl. J. Med. 2009;361:455–467.

62. Djimde AA, Makanga M, Kuhen K, Hamed K. The emerging threat of artemisinin resistance in malaria: focus on artemether-lumefantrine. Expert Rev. Anti. Infect. Ther. 2015;13:1031–1045.

63. Mbengue A, Bhattacharjee S, Pandharkar T, Liu H, Estiu G, Stahelin R V., Rizk SS, Njimoh DL, Ryan Y, Chotivanich K, Nguon C, Ghorbal M, Lopez-Rubio J-J, Pfrender M, Emrich S, Mohandas N, Dondorp AM, Wiest O, Haldar K. A molecular mechanism of artemisinin resistance in Plasmodium falciparum malaria. Nature 2015;520:683–687.

64. Mita T, Culleton R, Takahashi N, Nakamura M, Tsukahara T, Hunja CW, Win ZZ, Htike WW, Marma AS, Dysoley L, Ndounga M, Dzodzomenyo M, Akhwale WS, Kobayashi J, Uemura H, Kaneko A, Hombhanje F, Ferreira MU, Björkman A, Endo H, Ohashi J. Little Polymorphism at the K13 Propeller Locus in Worldwide Plasmodium falciparum Populations Prior to the Introduction of Artemisinin Combination Therapies. Antimicrob. Agents Chemother. 2016;60:3340–3347.

65. Straimer J, Gnädig NF, Stokes BH, Ehrenberger M, Crane AA, Fidock DA. *Plasmodium falciparum* K13 Mutations Differentially Impact Ozonide Susceptibility and Parasite Fitness *In Vitro* Miller LH, editor. MBio 2017;8.

66. Menard D, Dondorp A. Antimalarial Drug Resistance: A Threat to Malaria Elimination. Cold Spring Harb. Perspect. Med. 2017;7:a025619.

67. Haldar K, Bhattacharjee S, Safeukui I. Drug resistance in Plasmodium. Nat. Rev. Microbiol. 2018;16:156–170.

68. Blasco B, Leroy D, Fidock DA. Antimalarial drug resistance: linking Plasmodium falciparum parasite biology to the clinic. Nat. Med. 2017;23:917–928.

69. Adepoju P. RTS,S malaria vaccine pilots in three African countries. Lancet 2019;393:1685.

70. Kilejian A. Circular mitochondrial DNA from the avian malarial parasite Plasmodium lophurae. Biochim. Biophys. Acta - Nucleic Acids Protein Synth. 1975;390:276–284.

71. Gardner MJ, Bates PA, Ling IT, Moore DJ, McCready S, Gunasekera MBR, Wilson RJM, Williamson DH. Mitochondrial DNA of the human malarial parasite Plasmodium falciparum. Mol. Biochem. Parasitol. 1988;31:11–17.

72. Williamson DH, Wilson RJ, Bates PA, McCready S, Perler F, Qiang BU. Nuclear and mitochondrial DNA of the primate malarial parasite Plasmodium knowlesi. Mol. Biochem. Parasitol. 1985;14:199–209.
73. Suplick K, Akella R, Saul A, Vaidya AB. Molecular cloning and partial sequence of a 5.8 kilobase pair repetitive DNA from Plasmodium falciparum. Mol. Biochem. Parasitol. 1988;30:289–90.
74. Aldritt SM, Joseph JT, Wirth DF. Sequence identification of cytochrome b in Plasmodium gallinaceum. Mol. Cell. Biol. 1989;9:3614–20.
75. Vaidya AB, Akella R, Suplick K. Sequences similar to genes for two mitochondrial proteins and portions of ribosomal RNA in tandemly arrayed 6-kilobase-pair DNA of a malarial parasite. Mol. Biochem. Parasitol. 1989;35:97–107.
76. Feagin JE. The 6-kb element of Plasmodium falciparum encodes mitochondrial cytochrome genes. Mol. Biochem. Parasitol. 1992;52:145–8.
77. Gardner MJ, Williamson DH, Wilson RJ. A circular DNA in malaria parasites encodes an RNA polymerase like that of prokaryotes and chloroplasts. Mol. Biochem. Parasitol. 1991;44:115–23.
78. Gardner MJ, Feagin JE, Moore DJ, Rangachari K, Williamson DH, Wilson RJM. Sequence and organization of large subunit rRNA genes from the extrachromosomal 35 kb circular DNA of the malaria parasite *Plasmodium falciparum*. Nucleic Acids Res. 1993;21:1067–1071.
79. Gardner MJ, Preiser P, Rangachari K, Moore D, Feagin JE, Williamson DH, Wilson RJM. Nine duplicated tRNA genes on the plastid-like DNA of the malaria parasite Plasmodium falciparum. Gene 1994;144:307–308.
80. Wilson (Iain) R.J.M., Denny PW, Preiser PR, Rangachari K, Roberts K, Roy A, Whyte A, Strath M, Moore DJ, Moore PW, Williamson DH. Complete Gene Map of the Plastid-like DNA of the Malaria ParasitePlasmodium falciparum. J. Mol. Biol. 1996;261:155–172.
81. Kohler S, Delwiche CF, Denny PW, Tilney LG, Webster P, Wilson RJ, Palmer JD, Roos DS. A Plastid of Probable Green Algal Origin in Apicomplexan Parasites. Science (80-.). 1997;275:1485–1489.
82. Gould SB, Waller RF, McFadden GI. Plastid Evolution. Annu. Rev. Plant Biol. 2008;59:491–517.

83. Moore RB, Oborník M, Janouškovec J, Chrudimský T, Vancová M, Green DH, Wright SW, Davies NW, Bolch CJS, Heimann K, Šlapeta J, Hoegh-Guldberg O, Logsdon JM, Carter DA. A photosynthetic alveolate closely related to apicomplexan parasites. Nature 2008;451:959–963.

84. McFadden GI. Mergers and acquisitions: malaria and the great chloroplast heist. Genome Biol. 2000;1:reviews1026.1.

85. Ramya TNC, Mishra S, Karmodiya K, Surolia N, Surolia A. Inhibitors of nonhousekeeping functions of the apicoplast defy delayed death in Plasmodium falciparum. Antimicrob. Agents Chemother. 2007;51:307–16.

86. Waller RF, Keeling PJ, Donald RG, Striepen B, Handman E, Lang-Unnasch N, Cowman AF, Besra GS, Roos DS, McFadden GI. Nuclear-encoded proteins target to the plastid in Toxoplasma gondii and Plasmodium falciparum. Proc. Natl. Acad. Sci. U. S. A. 1998;95:12352–7.

87. Waller RF, Reed MB, Cowman AF, McFadden GI. Protein trafficking to the plastid of Plasmodium falciparum is via the secretory pathway. EMBO J. 2000;19:1794–1802.

88. Foth BJ, Ralph SA, Tonkin CJ, Struck NS, Fraunholz M, Roos DS, Cowman AF, McFadden GI. Dissecting Apicoplast Targeting in the Malaria Parasite Plasmodium falciparum. Science (80-.). 2003;299:705–708.

89. Tonkin CJ, Roos DS, McFadden GI. N-terminal positively charged amino acids, but not their exact position, are important for apicoplast transit peptide fidelity in Toxoplasma gondii. Mol. Biochem. Parasitol. 2006;150:192–200.

90. Tonkin CJ, Kalanon M, McFadden GI. Protein targeting to the malaria parasite plastid. Traffic 2008;9:166–75.

91. Zuegge J, Ralph S, Schmuker M, McFadden GI, Schneider G. Deciphering apicoplast targeting signals--feature extraction from nuclear-encoded precursors of Plasmodium falciparum apicoplast proteins. Gene 2001;280:19–26.

92. Ralph SA, van Dooren GG, Waller RF, Crawford MJ, Fraunholz MJ, Foth BJ, Tonkin CJ, Roos DS, McFadden GI. Metabolic maps and functions of the Plasmodium falciparum apicoplast. Nat. Rev. Microbiol. 2004;2:203–216.

93. Yu M, Kumar TRS, Nkrumah LJ, Coppi A, Retzlaff S, Li CD, Kelly BJ, Moura PA, Lakshmanan V, Freundlich JS, Valderramos J-C, Vilcheze C, Siedner M, Tsai JH-C,

Falkard B, Sidhu ABS, Purcell LA, Gratraud P, Kremer L, Waters AP, Schiehser G, Jacobus DP, Janse CJ, Ager A, Jacobs WR, Sacchettini JC, Heussler V, Sinnis P, Fidock DA. The fatty acid biosynthesis enzyme FabI plays a key role in the development of liver-stage malarial parasites. Cell Host Microbe 2008;4:567–78.

94. Vaughan AM, O'Neill MT, Tarun AS, Camargo N, Phuong TM, Aly ASI, Cowman AF, Kappe SHI. Type II fatty acid synthesis is essential only for malaria parasite late liver stage development. Cell. Microbiol. 2009;11:506–520.

95. Lindner SE, Sartain MJ, Hayes K, Harupa A, Moritz RL, Kappe SHI, Vaughan AM. Enzymes involved in plastid-targeted phosphatidic acid synthesis are essential for Plasmodium yoelii liver-stage development. Mol. Microbiol. 2014;91:679–93.

96. van Schaijk BCL, Kumar TRS, Vos MW, Richman A, van Gemert G-J, Li T, Eappen AG, Williamson KC, Morahan BJ, Fishbaugher M, Kennedy M, Camargo N, Khan SM, Janse CJ, Sim KL, Hoffman SL, Kappe SHI, Sauerwein RW, Fidock DA, Vaughan AM. Type II fatty acid biosynthesis is essential for Plasmodium falciparum sporozoite development in the midgut of Anopheles mosquitoes. Eukaryot. Cell 2014;13:550–9.

97. Pei Y, Tarun AS, Vaughan AM, Herman RW, Soliman JMB, Erickson-Wayman A, Kappe SHI. *Plasmodium* pyruvate dehydrogenase activity is only essential for the parasite's progression from liver infection to blood infection. Mol. Microbiol. 2010;75:957–971.

98. Toler S. The plasmodial apicoplast was retained under evolutionary selective pressure to assuage blood stage oxidative stress. Med. Hypotheses 2005;65:683–90.

99. Seeber F. Biogenesis of iron-sulphur clusters in amitochondriate and apicomplexan protists. Int. J. Parasitol. 2002;32:1207–17.

100. van Dooren GG, Stimmler LM, McFadden GI. Metabolic maps and functions of the *Plasmodium* mitochondrion. FEMS Microbiol. Rev. 2006;30:596–630.

101. Nagaraj VA, Sundaram B, Varadarajan NM, Subramani PA, Kalappa DM, Ghosh SK, Padmanaban G. Malaria parasite-synthesized heme is essential in the mosquito and liver stages and complements host heme in the blood stages of infection. Mota MM, editor. PLoS Pathog. 2013;9:e1003522.

102. Ke H, Sigala PA, Miura K, Morrisey JM, Mather MW, Crowley JR, Henderson JP, Goldberg DE, Long CA, Vaidya AB. The Heme Biosynthesis Pathway Is Essential for *Plasmodium falciparum* Development in Mosquito Stage but Not in Blood Stages. J. Biol.

Chem. 2014;289:34827–34837.
103. Sigala PA, Goldberg DE. The Peculiarities and Paradoxes of *Plasmodium* Heme Metabolism. Annu. Rev. Microbiol. 2014;68:259–278.
104. Sullivan DJ, Gluzman IY, Goldberg DE. Plasmodium Hemozoin Formation Mediated by Histidine-Rich Proteins. Science (80-.). 1996;271:219–222.
105. Yeh E, DeRisi JL. Chemical rescue of malaria parasites lacking an apicoplast defines organelle function in blood-stage Plasmodium falciparum. Striepen B, editor. PLoS Biol. 2011;9:e1001138.
106. Jomaa H, Wiesner J, Sanderbrand S, Altincicek B, Weidemeyer C, Hintz M, Türbachova I, Eberl M, Zeidler J, Lichtenthaler HK, Soldati D, Beck E. Inhibitors of the nonmevalonate pathway of isoprenoid biosynthesis as antimalarial drugs. Science 1999;285:1573–6.
107. Borrmann S, Adegnika AA, Matsiegui P, Issifou S, Schindler A, Mawili-Mboumba DP, Baranek T, Wiesner J, Jomaa H, Kremsner PG. Fosmidomycin-Clindamycin for *Plasmodium falciparum* Infections in African Children. J. Infect. Dis. 2004;189:901–908.
108. Borrmann S, Issifou S, Esser G, Adegnika AA, Ramharter M, Matsiegui P, Oyakhirome S, Mawili-Mboumba DP, Missinou MA, Kun JFJ, Jomaa H, Kremsner PG. Fosmidomycin-Clindamycin for the Treatment of *Plasmodium falciparum* Malaria. J. Infect. Dis. 2004;190:1534–1540.
109. Borrmann S, Lundgren I, Oyakhirome S, Impouma B, Matsiegui P-B, Adegnika AA, Issifou S, Kun JFJ, Hutchinson D, Wiesner J, Jomaa H, Kremsner PG. Fosmidomycin plus Clindamycin for Treatment of Pediatric Patients Aged 1 to 14 Years with Plasmodium falciparum Malaria. Antimicrob. Agents Chemother. 2006;50:2713–2718.
110. Borrmann S, Adegnika AA, Moussavou F, Oyakhirome S, Esser G, Matsiegui P-B, Ramharter M, Lundgren I, Kombila M, Issifou S, Hutchinson D, Wiesner J, Jomaa H, Kremsner PG. Short-Course Regimens of Artesunate-Fosmidomycin in Treatment of Uncomplicated Plasmodium falciparum Malaria. Antimicrob. Agents Chemother. 2005;49:3749–3754.
111. Okamoto N, Spurck TP, Goodman CD, McFadden GI. Apicoplast and mitochondrion in gametocytogenesis of Plasmodium falciparum. Eukaryot. Cell 2009;8:128–32.
112. Stanway RR, Witt T, Zobiak B, Aepfelbacher M, Heussler VT. GFP-targeting allows

visualization of the apicoplast throughout the life cycle of live malaria parasites. Biol. Cell 2009;101:415–435.

113. Van Dooren GG, Marti M, Tonkin CJ, Stimmler LM, Cowman AF, McFadden GI. Development of the endoplasmic reticulum, mitochondrion and apicoplast during the asexual life cycle of Plasmodium falciparum. Mol. Microbiol. 2005;57:405–419.

114. Lim L, McFadden GI. The evolution, metabolism and functions of the apicoplast. Philos. Trans. R. Soc. Lond. B. Biol. Sci. 2010;365:749–63.

115. Sinden RE, Canning EU, Spain B. Gametogenesis and fertilization in *Plasmodium yoelii nigeriensis* : a transmission electron microscope study. Proc. R. Soc. London. Ser. B. Biol. Sci. 1976;193:55–76.

116. Creasey A, Mendis K, Carlton J, Williamson D, Wilson I, Carter R. Maternal inheritance of extrachromosomal DNA in malaria parasites. Mol. Biochem. Parasitol. 1994;65:95–8.

117. Rowlett VW, Margolin W. The bacterial Min system. Curr. Biol. 2013;23:R553–R556.

118. Haeusser DP, Margolin W. Splitsville: structural and functional insights into the dynamic bacterial Z ring. Nat. Rev. Microbiol. 2016;14:305–19.

119. den Blaauwen T, Hamoen LW, Levin PA. The divisome at 25: the road ahead. Curr. Opin. Microbiol. 2017;36:85–94.

120. Matsui T, Han X, Yu J, Yao M, Tanaka I. Structural Change in FtsZ Induced by Intermolecular Interactions between Bound GTP and the T7 Loop. J. Biol. Chem. 2014;289:3501–3509.

121. Huecas S, Ramírez-Aportela E, Vergoñós A, Núñez-Ramírez R, Llorca O, Díaz JF, Juan-Rodríguez D, Oliva MA, Castellen P, Andreu JM. Self-Organization of FtsZ Polymers in Solution Reveals Spacer Role of the Disordered C-Terminal Tail. Biophys. J. 2017;113:1831–1844.

122. Ruiz-Martínez Á, Bartol TM, Sejnowski TJ, Tartakovsky DM. Efficient models of polymerization applied to FtsZ ring assembly in *Escherichia coli*. Proc. Natl. Acad. Sci. 2018;115:4933–4938.

123. Low HH, Moncrieffe MC, Löwe J. The Crystal Structure of ZapA and its Modulation of FtsZ Polymerisation. J. Mol. Biol. 2004;341:839–852.

124. Schumacher MA, Zeng W. Structures of the nucleoid occlusion protein SlmA bound

to DNA and the C-terminal domain of the cytoskeletal protein FtsZ. Proc. Natl. Acad. Sci. 2016;113:4988–4993.
125. Durand-Heredia JM, Yu HH, De Carlo S, Lesser CF, Janakiraman A. Identification and characterization of ZapC, a stabilizer of the FtsZ ring in Escherichia coli. J. Bacteriol. 2011;193:1405–13.
126. Roach EJ, Wroblewski C, Seidel L, Berezuk AM, Brewer D, Kimber MS, Khursigara CM. Structure and Mutational Analyses of Escherichia coli ZapD Reveal Charged Residues Involved in FtsZ Filament Bundling. DiRita VJ, editor. J. Bacteriol. 2016;198:1683–1693.
127. Schumacher MA, Huang K-H, Zeng W, Janakiraman A. Structure of the Z Ring-associated Protein, ZapD, Bound to the C-terminal Domain of the Tubulin-like Protein, FtsZ, Suggests Mechanism of Z Ring Stabilization through FtsZ Cross-linking. J. Biol. Chem. 2017;292:3740–3750.
128. Söderström B, Daley DO. The bacterial divisome: more than a ring? Curr. Genet. 2017;63:161–164.
129. Krupka M, Sobrinos-Sanguino M, Jiménez M, Rivas G, Margolin W. Escherichia coli ZipA Organizes FtsZ Polymers into Dynamic Ring-Like Protofilament Structures. Losick R, editor. MBio 2018;9.
130. Pichoff S, Lutkenhaus J. Tethering the Z ring to the membrane through a conserved membrane targeting sequence in FtsA. Mol. Microbiol. 2005;55:1722–34.
131. Conti J, Viola MG, Camberg JL. FtsA reshapes membrane architecture and remodels the Z-ring in Escherichia coli. Mol. Microbiol. 2018;107:558–576.
132. Viola MG, LaBreck CJ, Conti J, Camberg JL. Proteolysis-Dependent Remodeling of the Tubulin Homolog FtsZ at the Division Septum in Escherichia coli Cascales E, editor. PLoS One 2017;12:e0170505.
133. Wang S, Wingreen NS. Cell shape can mediate the spatial organization of the bacterial cytoskeleton. Biophys. J. 2013;104:541–52.
134. Bisson-Filho AW, Hsu Y-P, Squyres GR, Kuru E, Wu F, Jukes C, Sun Y, Dekker C, Holden S, VanNieuwenhze MS, Brun Y V, Garner EC. Treadmilling by FtsZ filaments drives peptidoglycan synthesis and bacterial cell division. Science 2017;355:739–743.
135. Ramirez-Diaz DA, García-Soriano DA, Raso A, Mücksch J, Feingold M, Rivas G, Schwille P. Treadmilling analysis reveals new insights into dynamic FtsZ ring architecture.

Löwe J, editor. PLoS Biol. 2018;16:e2004845.
136. Bernhardt TG, de Boer PAJ. SlmA, a nucleoid-associated, FtsZ binding protein required for blocking septal ring assembly over Chromosomes in E. coli. Mol. Cell 2005;18:555–64.
137. Adler HI, Fisher WD, Cohen A, Hardigree AA. MINIATURE escherichia coli CELLS DEFICIENT IN DNA. Proc. Natl. Acad. Sci. U. S. A. 1967;57:321–6.
138. Davie E, Sydnor K, Rothfield LI. Genetic basis of minicell formation in Escherichia coli K-12. J. Bacteriol. 1984;158:1202–3.
139. de Boer PAJ, Crossley RE, Rothfield LI. A division inhibitor and a topological specificity factor coded for by the minicell locus determine proper placement of the division septum in E. coli. Cell 1989;56:641–649.
140. Wu W, Park K-T, Holyoak T, Lutkenhaus J. Determination of the structure of the MinD-ATP complex reveals the orientation of MinD on the membrane and the relative location of the binding sites for MinE and MinC. Mol. Microbiol. 2011;79:1515–28.
141. Zhou H, Schulze R, Cox S, Saez C, Hu Z, Lutkenhaus J. Analysis of MinD mutations reveals residues required for MinE stimulation of the MinD ATPase and residues required for MinC interaction. J. Bacteriol. 2005;187:629–38.
142. Ramm B, Glock P, Mücksch J, Blumhardt P, García-Soriano DA, Heymann M, Schwille P. The MinDE system is a generic spatial cue for membrane protein distribution in vitro. Nat. Commun. 2018;9:3942.
143. Szeto TH, Rowland SL, Habrukowich CL, King GF. The MinD membrane targeting sequence is a transplantable lipid-binding helix. J. Biol. Chem. 2003;278:40050–6.
144. Park K-T, Wu W, Lovell S, Lutkenhaus J. Mechanism of the asymmetric activation of the MinD ATPase by MinE. Mol. Microbiol. 2012;85:271–81.
145. Renner LD, Weibel DB. MinD and MinE interact with anionic phospholipids and regulate division plane formation in Escherichia coli. J. Biol. Chem. 2012;287:38835–44.
146. Park K-T, Wu W, Battaile KP, Lovell S, Holyoak T, Lutkenhaus J. The Min Oscillator Uses MinD-Dependent Conformational Changes in MinE to Spatially Regulate Cytokinesis. Cell 2011;146:396–407.
147. Raskin DM, de Boer PA. Rapid pole-to-pole oscillation of a protein required for directing division to the middle of Escherichia coli. Proc. Natl. Acad. Sci. U. S. A.

1999;96:4971–6.
148. Ma L-Y, King G, Rothfield L. Mapping the MinE Site Involved in Interaction with the MinD Division Site Selection Protein of Escherichia coli. J. Bacteriol. 2003;185:4948–4955.
149. Dinkins R, Reddy MS, Leng M, Collins GB. Overexpression of the Arabidopsis thaliana MinD1 gene alters chloroplast size and number in transgenic tobacco plants. Planta 2001;214:180–8.
150. Hu Z, Mukherjee A, Pichoff S, Lutkenhaus J. The MinC component of the division site selection system in Escherichia coli interacts with FtsZ to prevent polymerization. Proc. Natl. Acad. Sci. U. S. A. 1999;96:14819–24.
151. Dajkovic A, Lan G, Sun SX, Wirtz D, Lutkenhaus J. MinC spatially controls bacterial cytokinesis by antagonizing the scaffolding function of FtsZ. Curr. Biol. 2008;18:235–44.
152. Shen B, Lutkenhaus J. Examination of the interaction between FtsZ and MinCN in E. coli suggests how MinC disrupts Z rings. Mol. Microbiol. 2010;75:1285–98.
153. Hernández-Rocamora VM, García-Montañés C, Reija B, Monterroso B, Margolin W, Alfonso C, Zorrilla S, Rivas G. MinC protein shortens FtsZ protofilaments by preferentially interacting with GDP-bound subunits. J. Biol. Chem. 2013;288:24625–35.
154. Arumugam S, Petrašek Z, Schwille P. MinCDE exploits the dynamic nature of FtsZ filaments for its spatial regulation. Proc. Natl. Acad. Sci. U. S. A. 2014;111:E1192-200.
155. Hu Z, Lutkenhaus J. Topological regulation of cell division in Escherichia coli involves rapid pole to pole oscillation of the division inhibitor MinC under the control of MinD and MinE. Mol. Microbiol. 1999;34:82–90.
156. Raskin DM, de Boer PA. MinDE-dependent pole-to-pole oscillation of division inhibitor MinC in Escherichia coli. J. Bacteriol. 1999;181:6419–24.
157. de Boer PA, Crossley RE, Rothfield LI. Roles of MinC and MinD in the site-specific septation block mediated by the MinCDE system of Escherichia coli. J. Bacteriol. 1992;174:63–70.
158. Johnson JE, Lackner LL, Hale CA, de Boer PAJ. ZipA is required for targeting of DMinC/DicB, but not DMinC/MinD, complexes to septal ring assemblies in Escherichia coli. J. Bacteriol. 2004;186:2418–29.
159. Colletti KS, Tattersall EA, Pyke KA, Froelich JE, Stokes KD, Osteryoung KW. A

homologue of the bacterial cell division site-determining factor MinD mediates placement of the chloroplast division apparatus. Curr. Biol. 2000;10:507–16.
160. Maple J, Chua N-H, Møller SG. The topological specificity factor AtMinE1 is essential for correct plastid division site placement in Arabidopsis. Plant J. 2002;31:269–77.
161. Fujiwara MT, Nakamura A, Itoh R, Shimada Y, Yoshida S, Møller SG. Chloroplast division site placement requires dimerization of the ARC11/AtMinD1 protein in Arabidopsis. J. Cell Sci. 2004;117:2399–410.
162. Shaik RS, Sung MW, Vitha S, Holzenburg A. Chloroplast division protein ARC3 acts on FtsZ2 by preventing filament bundling and enhancing GTPase activity. Biochem. J. 2018;475:99–115.
163. Anon. PlasmoDB: An integrative database of the Plasmodium falciparum genome. Tools for accessing and analyzing finished and unfinished sequence data. The Plasmodium Genome Database Collaborative. Nucleic Acids Res. 2001;29:66–9.
164. Nielsen H, Engelbrecht J, Brunak S, von Heijne G. A neural network method for identification of prokaryotic and eukaryotic signal peptides and prediction of their cleavage sites. Int. J. Neural Syst. 8:581–99.
165. Thompson JD, Higgins DG, Gibson TJ. CLUSTAL W: improving the sensitivity of progressive multiple sequence alignment through sequence weighting, position-specific gap penalties and weight matrix choice. Nucleic Acids Res. 1994;22:4673–80.
166. Di Tommaso P, Moretti S, Xenarios I, Orobitg M, Montanyola A, Chang J-M, Taly J-F, Notredame C. T-Coffee: a web server for the multiple sequence alignment of protein and RNA sequences using structural information and homology extension. Nucleic Acids Res. 2011;39:W13-7.
167. Green MR, Sambrook J. Molecular Cloning: A Laboratory Manual. Fourth Edi. Cold Spring Harbor Laboratory Press; 2012. 2,028 p.
168. Reinhard L, Mayerhofer H, Geerlof A, Mueller-Dieckmann J, Weiss MS. Optimization of protein buffer cocktails using Thermofluor. Acta Crystallogr. Sect. F. Struct. Biol. Cryst. Commun. 2013;69:209–14.
169. Wrenger C, Müller IB, Schifferdecker AJ, Jain R, Jordanova R, Groves MR. Specific inhibition of the aspartate aminotransferase of Plasmodium falciparum. J. Mol. Biol. 2011;405:956–71.

170. Waterkeyn JG, Crabb BS, Cowman AF. Transfection of the human malaria parasite Plasmodium falciparum. Int. J. Parasitol. 1999;29:945–55.
171. Trager W, Jensen JB. Human malaria parasites in continuous culture. Science 1976;193:673–5.
172. Das Gupta R, Krause-Ihle T, Bergmann B, Muller IB, Khomutov AR, Muller S, Walter RD, Luersen K. 3-Aminooxy-1-Aminopropane and Derivatives Have an Antiproliferative Effect on Cultured Plasmodium falciparum by Decreasing Intracellular Polyamine Concentrations. Antimicrob. Agents Chemother. 2005;49:2857–2864.
173. Lambros C, Vanderberg JP. Synchronization of Plasmodium falciparum erythrocytic stages in culture. J. Parasitol. 1979;65:418–20.
174. Wu Y, Sifri CD, Lei HH, Su XZ, Wellems TE. Transfection of Plasmodium falciparum within human red blood cells. Proc. Natl. Acad. Sci. U. S. A. 1995;92:973–7.
175. Ménard R (Ed. . Malaria - Methods and Protocols. Springer; 2013.
176. Salanti A, Staalsoe T, Lavstsen T, Jensen ATR, Sowa MPK, Arnot DE, Hviid L, Theander TG. Selective upregulation of a single distinctly structured var gene in chondroitin sulphate A-adhering Plasmodium falciparum involved in pregnancy-associated malaria. Mol. Microbiol. 2003;49:179–191.
177. Aldridge C, Møller SG. The plastid division protein AtMinD1 is a Ca2+-ATPase stimulated by AtMinE1. J. Biol. Chem. 2005;280:31673–8.
178. Chan XWA, Wrenger C, Stahl K, Bergmann B, Winterberg M, Müller IB, Saliba KJ. Chemical and genetic validation of thiamine utilization as an antimalarial drug target. Nat. Commun. 2013;4:2060.
179. Wrenger C, Müller S. The human malaria parasite Plasmodium falciparum has distinct organelle-specific lipoylation pathways. Mol. Microbiol. 2004;53:103–13.
180. Striepen B, Crawford MJ, Shaw MK, Tilney LG, Seeber F, Roos DS. The Plastid of *Toxoplasma gondii* Is Divided by Association with the Centrosomes. J. Cell Biol. 2000;151:1423–1434.
181. Matsuzaki M, Kikuchi T, Kita K, Kojima S, Kuroiwa T. Large amounts of apicoplast nucleoid DNA and its segregation in Toxoplasma gondii. Protoplasma 2001;218:180–91.
182. Vitha S, McAndrew RS, Osteryoung KW. FtsZ ring formation at the chloroplast division site in plants. J. Cell Biol. 2001;153:111–20.

183. Si F, Busiek K, Margolin W, Sun SX. Organization of FtsZ filaments in the bacterial division ring measured from polarized fluorescence microscopy. Biophys. J. 2013;105:1976–86.
184. Kretschmer S, Ganzinger KA, Franquelim HG, Schwille P. Synthetic cell division via membrane-transforming molecular assemblies. BMC Biol. 2019;17:43.
185. Zieske K, Chwastek G, Schwille P. Protein Patterns and Oscillations on Lipid Monolayers and in Microdroplets. Angew. Chem. Int. Ed. Engl. 2016;55:13455–13459.
186. Strauss MP, Liew ATF, Turnbull L, Whitchurch CB, Monahan LG, Harry EJ. 3D-SIM Super Resolution Microscopy Reveals a Bead-Like Arrangement for FtsZ and the Division Machinery: Implications for Triggering Cytokinesis Amos L, editor. PLoS Biol. 2012;10:e1001389.
187. Lutkenhaus J, Sundaramoorthy M. MinD and role of the deviant Walker A motif, dimerization and membrane binding in oscillation. Mol. Microbiol. 2003;48:295–303.
188. Szeto TH, Rowland SL, Rothfield LI, King GF. Membrane localization of MinD is mediated by a C-terminal motif that is conserved across eubacteria, archaea, and chloroplasts. Proc. Natl. Acad. Sci. U. S. A. 2002;99:15693–8.
189. Conti J, Viola MG, Camberg JL. The bacterial cell division regulators MinD and MinC form polymers in the presence of nucleotide. FEBS Lett. 2015;589:201–206.
190. Aldridge C, Møller SG. The Plastid Division Protein AtMinD1 Is a Ca^{2+} -ATPase Stimulated by AtMinE1. J. Biol. Chem. 2005;280:31673–31678.
191. de Boer PA, Crossley RE, Hand AR, Rothfield LI. The MinD protein is a membrane ATPase required for the correct placement of the Escherichia coli division site. EMBO J. 1991;10:4371–80.
192. Meissner KA, Lunev S, Wang Y-Z, Linzke M, Batista F de A, Wrenger C, Groves MR. Drug Target Validation Methods in Malaria - Protein Interference Assay (PIA) as a Tool for Highly Specific Drug Target Validation. Curr. Drug Targets 2017;18:1069–1085.
193. Batista FA, Bosch SS, Butzloff S, Lunev S, Meissner KA, Linzke M, Romero AR, Wang C, Müller IB, Dömling ASS, Groves MR, Wrenger C. Oligomeric protein interference validates druggability of aspartate interconversion in *Plasmodium falciparum*. Microbiologyopen 2019;8:e00779.
194. Hasenkamp S, Russell KT, Horrocks P. Comparison of the absolute and relative

efficiencies of electroporation-based transfection protocols for Plasmodium falciparum. Malar. J. 2012;11:210.

195. Spielmann T, Dixon MWA, Hernandez-Valladares M, Hannemann M, Trenholme KR, Gardiner DL. Reliable transfection of Plasmodium falciparum using non-commercial plasmid mini preparations. Int. J. Parasitol. 2006;36:1245–1248.

196. Webster WAJ, McFadden GI. From the genome to the phenome: tools to understand the basic biology of Plasmodium falciparum. J. Eukaryot. Microbiol. 2014;61:655–71.

197. Fu G, Huang T, Buss J, Coltharp C, Hensel Z, Xiao J. In Vivo Structure of the E. coli FtsZ-ring Revealed by Photoactivated Localization Microscopy (PALM) Polymenis M, editor. PLoS One 2010;5:e12680.

198. Rowland SL, Fu X, Sayed MA, Zhang Y, Cook WR, Rothfield LI. Membrane redistribution of the Escherichia coli MinD protein induced by MinE. J. Bacteriol. 2000;182:613–9.

199. FUJIWARA MT, LI D, KAZAMA Y, ABE T, UNO T, YAMAGATA H, KANAMARU K, ITOH RD. Further Evaluation of the Localization and Functionality of Hemagglutinin Epitope- and Fluorescent Protein-Tagged AtMinD1 in *Arabidopsis thaliana*. Biosci. Biotechnol. Biochem. 2009;73:1693–1697.

200. Kanamaru K, Fujiwara M, Kim M, Nagashima A, Nakazato E, Tanaka K, Takahashi H. Chloroplast Targeting, Distribution and Transcriptional Fluctuation of AtMinD1, a Eubacteria-Type Factor Critical for Chloroplast Division. Plant Cell Physiol. 2000;41:1119–1128.

APPENDIX

List of publications

Meissner KA, Lunev S, Wang YZ, **Linzke M**, de Assis Batista F, Wrenger C, Groves MR. (2017) Drug Target Validation Methods in Malaria - Protein Interference Assay (PIA) as a Tool for Highly Specific Drug Target Validation. Curr Drug Targets. DOI: 10.2174/1389450117666160201115003.

Lunev S, Bosch SS, Batista FA, Wang C, Li J, **Linzke M**, Kruithof P, Chamoun G, Dömling ASS, Wrenger C, Groves MR. (2018) Identification of a non-competitive inhibitor of *Plasmodium falciparum* aspartate transcarbamoylase. Biochem Biophys Res Commun. DOI: 10.1016/j.bbrc.2018.02.112.

Lunev S, Butzloff S, Romero AR, **Linzke M**, Batista FA, Meissner KA, Müller IB, Adawy A, Wrenger C, Groves MR. (2018) Oligomeric interfaces as a tool in drug discovery: Specific interference with activity of malate dehydrogenase of *Plasmodium falciparum in vitro*. PLoS One. DOI: 10.1371/journal.pone.0195011.

Batista FA, Bosch SS, Butzloff S, Lunev S, Meissner KA, **Linzke M**, Romero AR, Wang C, Müller IB, Dömling ASS, Groves MR, Wrenger C. (2019) Oligomeric protein interference validates druggability of aspartate interconversion in *Plasmodium falciparum*. Microbiologyopen. DOI: 10.1002/mbo3.779.

Linzke M, Yan SLR, Tarnok A, Ulrich H, Groves MR, Wrenger C. (2019) Live and let dye: visualising the malarial parasite *Plasmodium falciparum* cellular compartments. (in press)

Bosch SS, Lunev S, Batista FA, **Linzke M**, Groves MR, Wrenger C (2019). Drug target validation of aspartate transcarbamoylase from *Plasmodium falciparum*. (submitted)

Batista FA, Bosch SS, **Linzke M**, Lunev S, Wrenger C, Groves MR. Ribose-phosphate diphosphokinase from *Plasmodium falciparum* targeted by the compound Torin 2. (in preparation)

Acknowledgment

First of all, I want to thank my supervisor Prof. Carsten Wrenger for giving me the possibilities to perform my PhD thesis in your group. You invited me to study and live in Brazil and leave my comfort zone, which made me grow into a stronger person and created a lot of experience and memories I do not want to miss. Thanks to your support I feel like I became a proper scientist. When I felt lost in São Paulo, you always tried to help me the best you can. And thank you for trusting me enough to enlist me into the double degree program between the USP and the RUG.

I also would like to thank my second supervisor Prof. Alexander Dömling and my co-supervisor Prof. Matthew Groves from the University of Groningen. Thanks for letting me join the group during my stay in the Netherlands. Thank you Matthew for listening to all my problems, be it work related or not and always trying to help me. Your always open door was very appreciated.

Furthermore, I want to thank all the past and current members of the UDD group. I know it was not always easy but I am happy to have you people in my life. A big thanks to Prof. Gerhard Wunderlich for joining the lab. Your comments and suggestions were always helpful. *Danke* to Kamila and Jasmin for teaching me how to work in cell culture and help me organise my life here in São Paulo. A big *obrigada* to Thales, for showing me the city, help me in the lab and make me feel more at home. *Gracias* to Sory for helping me with my thesis and all the formalities of the double degree program. *Obrigada* to Sun whom I already met in the Netherlands and then again here in the lab in São Paulo. You brought back with you the good vibes from the Netherlands. Another *obrigada* to Felipe for being this weirdly funny person who you simply are. And of course a big *Danke* to Arne, it was great working with you. Your input and help was always appreciated. I had a lot of fun around you although I spent a lot of time simply waiting for you.

I want to thank Prof. Claudio Marinho and his group where I was allowed to work in the cell culture. I always felt welcomed in your lab and the small talk with André, Erika and Jamille very often made my day. *Obrigada* to you guys for all the help and fun.

Another big thank you to all the former and current members of the Drug Design group. Thank you all for this fun year I was allowed to spend with you. The weekly drinks, the many visits to different restaurants and our daily coffee breaks were the starting point of so many great conversations and memories. I want to thank the former postdocs from the lab, Eshwar and Niels for helping me to crack this abstract concept of crystallography. *Dhanyavaad* and *dank je wel*! Then a big *bedankt* to the two technicians of the lab, André and Robin who helped me with the organization and technical issues of the lab. And a very big thank you goes to Fernando, Rick and Kai. You three made my life there so much more enjoyable and I miss the time spent with you dearly. Kai, *xièxiè* for trying to teach me your language and watching me completely failing in it. Rick, *dank je wel* for showing and explaining me the magic behind computers and programming and always disturbing my work when I needed it the most. You are the best lab mate I could wish for. And of course *muito obrigada* to Fernando. You were my life savior in the Netherlands starting with picking up the key to my new room and ending with becoming one of my best friends. I am so grateful for all your help inside and outside of the lab and you are still the person I feel most comfortable talking Portuguese to. *Tenho saudades de você!*

A big thank you also for the support of the organisation of this study by the two secretaries Silvia and Jolanda, and the one responsible for the double degree system Cathy.

A big thank you for all the people I met on the way. My students which allowed me to be their teacher and to guide them during their studies. The German exchange students from my former university which brought me a little bit home to São Paulo. Especially a *Danke* to Lena, Wiebke and Paul for coming to our lab and office and *blagodarya* to Vessi for staying in São Paulo with me for my last months. A big *danke je wel* goes to my crazy group of PhD students from Groningen for our funny conversations and drunken calls. And *Danke* to my German friends who haven´t forgotten about me although I am not the best person in responding to messages.

My biggest thanks goes to my family for the constant support and love I received from them. Leaving to the other side of the world was not easy but they never stopped believing in me. Without you guys, I could not have done that. Danke an meine beiden Schwestern Mimi und Ina und an meine beiden Brüder Maik und Nico für die Unterstützung. Ich weiß, ich habe viele Dinge verpasst, während ich weg war, aber wenn immer wir uns gesehen

haben, habt ihr mir neue Kraft gegeben. Ich freu mich unfassbar, euch bald alle wiederzusehen. Und natürlich mein größter Dank geht an dich Mutti. Obwohl die Trennung für dich am schwersten war, hast du mich in allen meinen Entscheidung unterstützt und mich immer wieder ermutigt, meinen Weg zu Ende zu gehen. Ohne dich hätte ich es nicht geschafft.

About the author

Marleen Linzke was born at the 17th of January 1991 in Grevesmühlen, a small town in the state of Mecklenburg-Vorpommern, Germany. After finishing school in the year 2009, she started her Bachelor of Science in Bioscience at the University of Münster (WWU). She decided to stay at the WWU for her master studies where she focused on infection biology, undergoing different courses in microbiology, virology and parasitology. She started her master thesis with the title "Surface associated proteins of parasites" in the laboratory of Prof. Eva Liebau who gave her the opportunity to conduct part of her study in the laboratory of Prof. Carsten Wrenger at the University of São Paulo (USP) in Brazil. Following successful graduation of her Master, she returned to Brazil to pursue her doctoral degree at the department of parasitology, USP under the supervision of Prof. Carsten Wrenger. Shortly after initiating her studies, she entered the established double degree program between the University of São Paulo and the University of Groningen in the Netherlands built by Prof. Carsten Wrenger and Prof. Matthew R. Groves through the CAPES/Nuffic MALAR-ASP network. With her doctoral thesis entitled "Morphological Analysis of the Apicoplast Formation in *Plasmodium falciparum*" she aimed to uncover the mechanism behind the correct division of an essential organelle of this deadly parasite to open up the road for new drug targets.